

2013-12-20

# Evaluation of a Novel Electrospun Polymer Dermal Regeneration Composite Matrix

Jennifer Elizabeth Molignano

Follow this and additional works at: <https://digitalcommons.wpi.edu/etd-theses>

---

## Repository Citation

Molignano, Jennifer Elizabeth, "Evaluation of a Novel Electrospun Polymer Dermal Regeneration Composite Matrix" (2013). *Masters Theses (All Theses, All Years)*. 1324.

<https://digitalcommons.wpi.edu/etd-theses/1324>

This thesis is brought to you for free and open access by Digital WPI. It has been accepted for inclusion in Masters Theses (All Theses, All Years) by an authorized administrator of Digital WPI. For more information, please contact [wpi-etd@wpi.edu](mailto:wpi-etd@wpi.edu).

# Evaluation of a Novel Electrospun Polymer Composite Matrix for Dermal Regeneration



Jennifer Elizabeth Mollignano

A thesis to be submitted to the faculty of Worcester Polytechnic Institute in partial fulfillment of the requirements for the Degree of Master of Science

Submitted by:

Jennifer Mollignano

Department of Biomedical Engineering

A handwritten signature in black ink that reads "Jennifer E. Mollignano" is written over a horizontal line.

Approved by:

George Pins, PhD, Advisor

Associate Professor

Department of Biomedical Engineering

A handwritten signature in black ink that reads "George Pins" is written over a horizontal line.

Matt Phaneuf  
President and CTO  
BioSurfaces, Inc.

A handwritten signature in blue ink is written over a horizontal line.

Raymond Dunn, MD  
Affiliated Faculty, WPI  
Professor and Chief of Plastic Surgery, UMMS

A handwritten signature in black ink that reads "Raymond M. Dunn" is written over a horizontal line.

November 4, 2013

## Acknowledgements

I am eternally grateful to the many people who contributed to this research, thank you for being a part of this project and a part of my life. It's been fun!

Special thanks to:

Jason Forte  
Jon Grasman  
Tom Moutinho  
Cara Ting  
Melanie Wiater

My committee members: Matt Phaneuf and Dr. Raymond Dunn. Your insight, guidance, and feedback were instrumental for the completion of this project.

My advisor, Dr. George Pins, for your unwavering support, patience, guidance, and advice. Thank you for never giving up on me, and most importantly for never letting me give up on myself.

Everyone at BioSurfaces, Inc. especially Matt Phaneuf, Syed Ali, Jason Hu, Saif Pathan, and Dave Nelson for providing the electrospun materials used for this project as well as for your knowledge, support, and guidance.

My "lab best friend" Amanda Clement, for always being there for me, in the lab and in life.

My family and friends, especially my wonderful parents and my husband, Mike Molignano, I never could have made it through without your support and encouragement. I love you.

## Abstract

Bioengineered skin is a promising treatment for chronic skin wounds because of its ability to promptly promote wound healing at the injury site and to restore the skin's epidermal and dermal structures and functions. Despite some level of clinical success, commercially available bioengineered skin substitutes are still limited by a high incidence of infection, a lack of mechanical integrity, and a slow rate of tissue ingrowth from the surrounding wound margin. To address these challenges, we propose to engineer novel polymer composite matrices for dermal regeneration. These matrices consist of two different electrospun polymer layers which create a composite matrix made up of a highly porous three-dimensional fibrous network. Each composite matrix contains a biodegradable electrospun "dermal" layer which acts as a scaffold for dermal cell ingrowth and tissue regeneration and a non-degradable electrospun "epidermal" layer that serves as a provisional barrier to protect the wound from environmental insult. To evaluate the success of our designs, we performed quantitative analyses of the physical properties of our electrospun scaffolds including fiber diameter and angle analyses and mechanical properties. We found our electrospun scaffolds are comprised of a random network of fibers ranging from approximately 0.2 – 5 $\mu$ m in diameter. They exhibit several mechanical properties that are similar to those measured in native skin tissue, including tangent elastic modulus and strain at failure. We have also found the proposed nanofibrous scaffolds to be capable of supporting normal human fibroblast attachment and migration. Our scaffolds show similar attachment to tissue culture polystyrene controls and better attachment than collagen-GAG sponge controls. The dermal layer of our scaffolds show fibroblast outgrowth rates between 185 - 206 $\mu$ m/day, which is similar to rates observed by others in collagen-GAG sponges and wounds. The promising findings from these *in vitro* studies warrant that our novel electrospun dermal regeneration matrix be further developed.

## Table of Contents

Acknowledgements.....	2
Abstract.....	3
Table of Figures.....	7
Table of Tables.....	8
Chapter 1: Introduction.....	9
Chapter 2: Background.....	12
2.1 Skin Structure and Function.....	12
2.1.1 Native Skin Wound Healing.....	14
2.1.2 Growth Factors in Wound Healing.....	16
2.1.3 Wound healing in severe skin injuries.....	19
2.2 Motivation for Bioengineered Skin Substitutes.....	19
2.2.1 Clinical Treatments for Severe Skin Injuries.....	20
2.3 Bioengineered Skin Substitutes.....	21
2.3.1 Design Considerations for Tissue Engineered Skin.....	21
2.3.2 Current Methods and Limitations.....	30
2.4 Electrospinning.....	45
2.4.1 The Electrospinning Process.....	45
2.4.2 Electrospinning for Skin Regeneration.....	49
2.5 Summary.....	58
Chapter 3: Hypothesis and Specific Aims.....	59
Specific Aim 1.....	61
Specific Aim 2.....	61
Chapter 4: Materials and Methods.....	63
4.1 Electrospun Polymer Composite Matrices.....	63
4.2 Physical and Mechanical Properties of Electrospun Scaffolds.....	64

4.2.1 Scaffold Morphology.....	64
4.2.2 Specific Surface Area.....	68
4.2.3 Mechanical Properties .....	68
4.3 Biologic Activity of Electrospun Scaffolds .....	70
4.3.1 Cell Culture.....	70
4.3.2 Quantifying Cell Attachment by MTT Assay.....	71
4.3.3 Cell Outgrowth .....	73
4.4 Statistics .....	76
Chapter 5: Results.....	77
5.1 Physical and Mechanical Properties of Electrospun Scaffolds.....	77
5.1.1. Characterization of scaffold morphology by measurement of fiber diameter and angle .....	77
5.1.2 Mechanical properties measured using uniaxial tensile testing.....	82
5.2 Biologic Activity of Electrospun Scaffolds .....	87
5.2.1 In Vitro Analysis of Cell Attachment .....	88
5.2.2 In Vitro Analysis of Cellular Outgrowth.....	89
Chapter 6: Discussion.....	93
6.1 Physical and Mechanical Properties of Electrospun Scaffolds.....	94
6.1.1. Characterization of scaffold morphology by measurement of fiber diameter and orientation .....	94
6.1.2. Mechanical properties measured by uniaxial tensile testing .....	95
6.2. Biologic Activity of Electrospun Scaffolds .....	97
6.2.1. <i>In Vitro</i> Analysis of Cell Attachment .....	97
6.2.2. <i>In Vitro</i> Analysis of Cellular Outgrowth.....	99
Chapter 7: Future Work and Recommendations.....	102
7.1 Additional <i>In Vitro</i> Characterizations .....	103
7.1.1 Pore size and porosity .....	103

7.1.2 <i>In vitro</i> scaffold degradation .....	104
7.1.3 <i>In vitro</i> scaffold permeability .....	105
7.1.4 Long term <i>in vitro</i> cell viability and proliferation.....	105
7.1.5 Three-dimensional <i>in vitro</i> cell distribution and movement .....	106
7.1.6 <i>In vitro</i> barrier function.....	107
7.2 <i>In Vivo</i> Animal Model.....	108
7.2.1 <i>In vivo</i> biocompatibility and degradation .....	108
7.2.2 <i>In vivo</i> wound healing model .....	108
7.3 Scaffold Modifications .....	109
7.3.1 Polymer composition .....	109
7.3.2 Scaffold thickness.....	109
7.3.3 Development of a pro-angiogenic, antimicrobial composite scaffold.....	110
Chapter 8: Conclusions .....	111
References .....	112
Appendix A: Mechanical Testing Data Analysis .....	117
Appendix A.1 Mechanical Testing Raw Data .....	117
Appendix A.2: Modulus Calculations .....	118
Appendix B: Cell Attachment .....	127
Appendix B.1: Standard curve data (7/25/12).....	127
Appendix B.2: Standard curve data (7/26/12).....	129
Appendix B.3: Cell Attachment Raw Data.....	131
Appendix C: Cellular Outgrowth Data.....	133
Appendix C.1: Cellular Outgrowth Raw Data – Blend A.....	133
Appendix C.2: Cellular Outgrowth Raw Data – Blend B.....	136
Appendix C.3: Individual Outgrowth Traces .....	139

## Table of Figures

Figure 1: Anatomy of human skin .....	13
Figure 2: Scanning electron microscopy (SEM) images of human dermal tissue. ....	14
Figure 3: Growth factors that play a key role in cutaneous wound healing.....	18
Figure 4: Physiochemical and mechanical requirements in bioengineered skin design .....	25
Figure 5: Schematic of the basic electrospinning setup. ....	47
Figure 6: Schematic showing two different blends of electrospun polymer composite matrix .....	60
Figure 7: Schematic showing two different blends of electrospun polymer composite matrix. ....	63
Figure 8: Scanning electron microscopy sample preparation .....	65
Figure 9: Method for quantifying the distribution of fiber diameter in electrospun scaffolds.....	66
Figure 10: Method for quantifying the distribution of fiber angle in electrospun scaffolds.....	67
Figure 11: Dimensions of dog bone shaped scaffolds for uniaxial tensile testing.....	68
Figure 12: Sample cutting orientation for uniaxial tensile testing.....	69
Figure 13: Using the stress-strain curve to define mechanical properties .....	70
Figure 14: Scaffold seeding method for quantification of cell viability with MTT assay. ....	72
Figure 15: Use of standard curve to create linear regression relating absorbance to number of cells. ....	73
Figure 16: Experimental method for measuring cellular outgrowth .....	75
Figure 17: Representative SEM images .....	78
Figure 18: Histograms showing the distribution of fiber diameter .....	79
Figure 19: Histograms showing the distribution of fiber angle. ....	80
Figure 20: Characteristic plots of tensile stress vs. strain for electrospun scaffolds.....	83
Figure 21: Ultimate tensile strength (UTS) of electrospun scaffolds.....	84
Figure 22: Strain at failure of electrospun scaffolds.....	84
Figure 23: Tangent elastic modulus of electrospun scaffolds .....	85
Figure 24: SEM images of mechanically failed electrospun scaffolds .....	87
Figure 25: Cell viability on electrospun scaffolds.....	88
Figure 26: Representative images of cellular outgrowth on electrospun scaffolds .....	90
Figure 27: Representative plots of distance to leading cell over time on electrospun scaffolds. ....	91
Figure 28: Average distance to leading cell over time on dermal layer of electrospun scaffolds.....	92
Figure 29: Linear curve fit graph from standard curve on 7/25/12.....	128
Figure 30: Linear curve fit graph from standard curve on 7/26/12.....	130



## Table of Tables

Table 1: Important growth factors and their sources and effects in cutaneous wound healing .....	19
Table 2: Summary of Stage 1 in Artificial Skin Design.....	22
Table 3: Summary of Stage 2 in Artificial Skin Design.....	24
Table 4: Tensile properties of native skin tissue.....	29
Table 5: Commercially available epidermal skin substitutes.....	34
Table 6: Commercially available dermal skin substitutes .....	39
Table 7: Commercially available composite skin substitutes .....	43
Table 8: Effect of process parameters and material properties on electrospun nanofibers.....	48
Table 9: Electrospun strategies for skin regeneration.....	55
Table 10: Summary of fiber diameter measurements made on electrospun scaffolds .....	79
Table 11: Summary of fiber angle measurements made on electrospun scaffolds .....	81
Table 12: Summary of measured tensile properties and published values for native skin tissue. ....	82
Table 13: Summary of cell attachment (4 hours post seeding) on electrospun scaffolds.....	89
Table 14: Mechanical properties of electrospun scaffolds.....	117
Table 15: Tensile stress vs. strain data for each sample blend and direction.. ....	118
Table 16: Cell attachment on electrospun scaffolds measured by MTT on 7/25/12. ....	127
Table 17: Cell attachment on electrospun scaffolds measured by MTT on 7/26/12 .....	129

## Chapter 1: Introduction

Annually in the United States, millions of individuals are impacted by chronic skin ulcers. These wounds pose a significant medical problem due to their diminished wound healing capacity which results from impaired blood circulation or prolonged pressure. The individuals affected by chronic ulcers include more than 500,000 whose wounds are secondary to venous insufficiency and 3 million who suffer from pressure ulcers as a result of immobility [1]. Additionally, up to 10% of the estimated 25 million people suffering from diabetes suffer from chronic diabetic foot ulcers [1, 2].

The current “gold-standard” treatment for chronic skin ulcers is the split-thickness autograft. Split-thickness autografts are harvested from healthy areas of the patient’s own skin tissue and are applied to the wound to induce a native wound healing response. Autografts provide the wound with intact cells, extracellular matrix, and signaling molecules, but their use is often limited by a high incidence of infection and a lack of appropriate donor sites due to high wound surface area or compromised native wound healing. Autografts are also associated with tissue morbidity at the donor sites and severe scarring in both the application and donor sites [3-6]. These limitations have led to the development of bioengineered skin substitutes, which have achieved some clinical success in restoring damaged skin, but continue to be limited by sub-optimal wound healing, prolonged healing times, limited mechanical stability, and high incidences of infection and scarring [3-5, 7-9]. As such, there is a continued need to develop a skin substitute that promotes rapid tissue regeneration, maintains the mechanical stability of the tissue, and provides immediate barrier function for the wound site [9, 10].

**We hypothesize that an electrospun polymer composite scaffold will support human dermal fibroblast attachment and outgrowth and provide an appropriate structural and mechanical matrix for dermal tissue regeneration.** Electrospinning produces highly porous, nanofibrous scaffolds with finely tuned physical properties and can be used to create scaffolds from a variety of different natural and

synthetic polymers. This study seeks to evaluate two composite electrospun matrices made of different synthetic polymer blends which each incorporate a biodegradable dermal layer to support tissue ingrowth and a non-degradable barrier layer to provide immediate and provisional wound protection.

The goals of this study are to evaluate the following scaffold properties which have been identified as important for the success of our electrospun scaffolds as dermal regeneration matrices:

1. Evaluate the physical properties (fiber diameter, fiber orientation, specific surface area) of the scaffolds.
2. Evaluate the mechanical properties of the scaffolds and compare to native tissue and established design standards for tissue engineered skin devices.
3. Evaluate the cellular response (attachment, outgrowth) to the scaffolds.

We used scanning electron microscopy to visualize the nanofibrous structure of the various blends and layers and quantified the diameter and orientation using ImageJ analysis software. This analysis showed that our electrospun scaffolds have similar fiber diameters and fiber orientation distribution to the fibrillar extracellular matrix of native dermal tissue [11]. We also measured the mechanical properties of our full thickness composite scaffolds by loading them to failure under uniaxial tension. Our analyses revealed that in the mechanical properties we measured (tangent elastic modulus and strain at failure) in our scaffolds were comparable to results of published studies that tested the mechanical properties of native dermal tissue [12].

We also quantified the cellular response to our electrospun scaffolds by measuring cellular attachment and outgrowth. We used an MTT assay to quantify the initial attachment of dermal fibroblasts four hours after seeding on each of the unique layers of our proposed scaffolds. We found that overall our electrospun scaffolds showed similar initial fibroblast attachment when compared to tissue culture polystyrene and significantly better initial fibroblast attachment when compared to

collagen-glycosaminoglycan (collagen-GAG) sponges which are currently used as the dermal component of commercially available dermal scaffolds [13]. Our scaffold relies on the ingrowth of cells from the wound margins in order to regenerate dermal tissue. In order to quantify cell movement on our scaffolds *in vitro* we used a custom assay that allowed us to measure fibroblast outgrowth from a fibroblast populated collagen gel onto the dermal layer of our proposed scaffolds. We found that the outgrowth rate we observed was similar to published fibroblast migration rate for collagen-GAG sponges [14].

Overall, the results of the morphological, mechanical, and *in vitro* cellular response analyses performed on our proposed electrospun scaffold show strong correlation with properties of native dermal tissue and control scaffolds currently utilized for dermal regeneration. These promising outcomes warrant continued investigation of our composite blends as matrices for dermal regeneration including further studies of *in vitro* scaffold degradation and permeability, long term *in vitro* cell viability and, eventually, *in vivo* analyses of biocompatibility, degradation, and wound healing.

## Chapter 2: Background

This project investigates a novel scaffold for dermal regeneration that could be used as a provisional matrix in the treatment of chronic skin ulcers. The development of such a dermal regeneration matrix requires an understanding of skin function and anatomy, including the wound healing process that occurs naturally in injured skin. As a part of scaffold development it is important to consider properties of the graft itself as well as how the graft will interface with the surrounding wound bed. This section will also summarize the current approaches to treating chronic skin ulcers both with traditional surgical methods and bioengineered skin substitutes.

### 2.1 Skin Structure and Function

Skin, the body's largest organ, primarily functions as a barrier, protecting the body against external factors and providing sensing and temperature regulation. Human skin has two layers, the epidermis which is the outmost layer and the underlying dermis (Figure 1). The epidermis is primarily made up of cells called keratinocytes, which are constantly proliferating and differentiating to form a stratified squamous epithelium. The epidermis is avascular and is responsible for providing most of the skin's barrier functions including protecting the body against pathogens, UV irradiation, and excessive water loss.

The skin's innermost layer, the dermis, is comprised of a network of fibroelastic connective tissue which provides structural support to the skin and contains a variety of specialized structures including hair follicles, sebaceous and sweat glands, and arrector pili muscles (Figure 1). The dermis also contains nerve endings that function in sensing touch and registering temperature changes as well as lymphatic and blood vessels responsible for delivering nutrients to the body. The fibroelastic network of the dermis is comprised mostly of fibrils of collagen interspersed with elastin and reticular fibers.

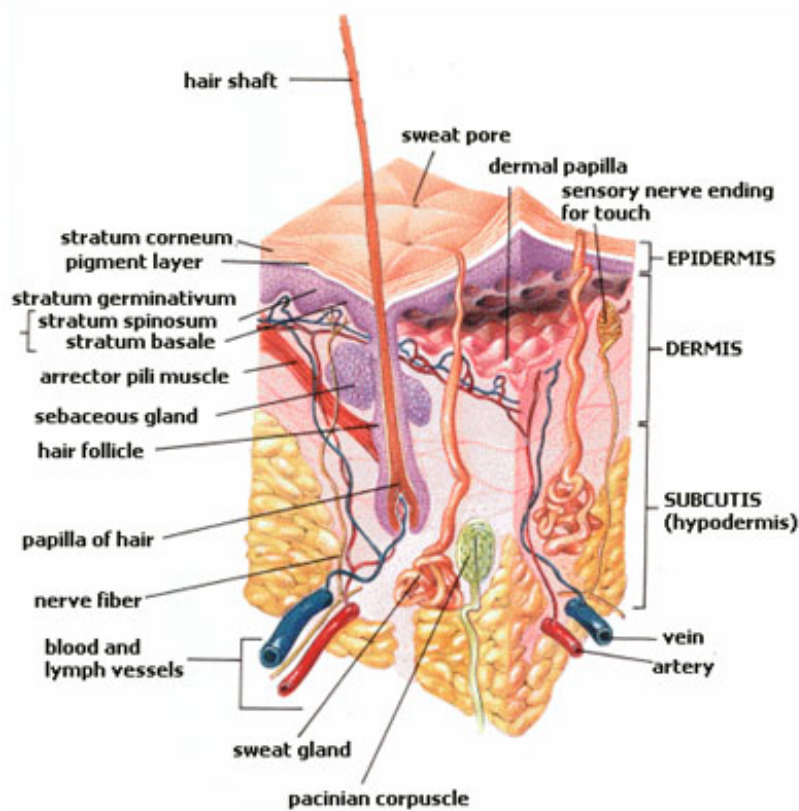
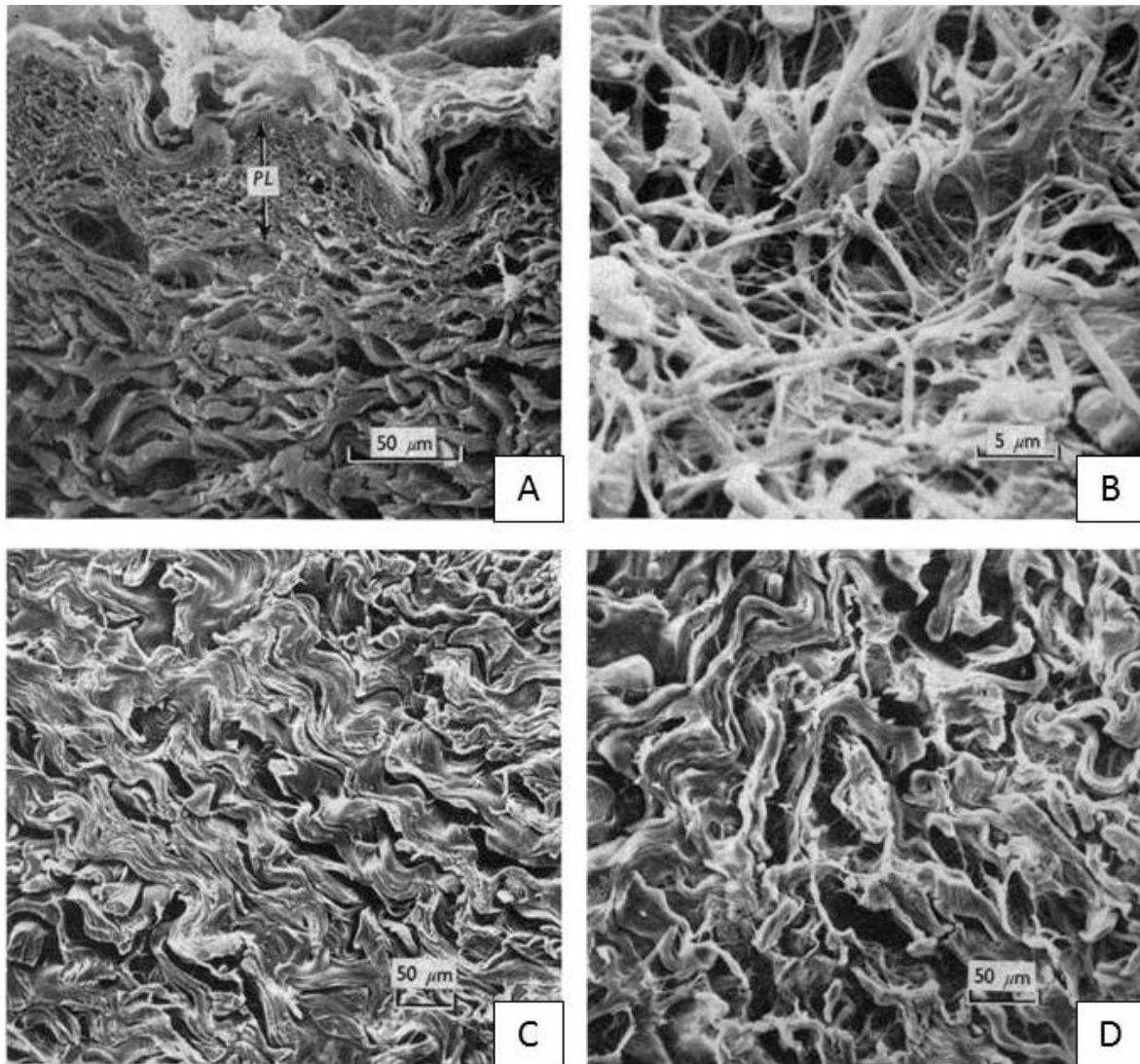


Figure 1: Anatomy of human skin [15]

The dermis can be further sub-divided into two layers: the papillary layer and the reticular layer (Figure 2A). The papillary layer, which is immediately underlying the epidermis, is composed of an open, porous network of thin fibers, ranging in diameter between 0.3 – 3  $\mu\text{m}$  (Figure 2B). The underlying reticular layer has two distinct regions, the mid-zone and deep zone, which are both characterized by densely intertwined coarse fibers with diameters in the 10 – 40  $\mu\text{m}$  range. The mid-zone has a more compact arrangement (Figure 2C) while the deep-zone has a looser arrangement (Figure 2D). The fibers of the dermal layers lie in a plane mostly parallel to the surface of the skin. Within this plane the fiber network is multi-directional and irregular in structure and shows no preferential fiber orientation [11]. The planar arrangement of collagen fibers and their interactions and attachments to elastic fibers in the reticular layer give the skin its ability to recoil and resist applied shear forces.



**Figure 2: Scanning electron microscopy (SEM) images of human dermal tissue. [A]: a cross section of skin showing the epidermis (top layer), papillary layer (middle, labeled "PL"), and the reticular layer (bottom). 300x. [B]: the thin fibers of the dermis' papillary layer form a relatively open network. 2200x. [C]: the mid-zone of the dermal reticular layer has densely packed coarse fibers. 175x. [D]: the deep zone of the dermal reticular layer has a looser arrangement of coarse fibers 185x. B, C, and D show sections cut parallel to the surface of the skin. Images reproduced with permission from Brown, 1972 [11].**

### 2.1.1 Native Skin Wound Healing

When tissues and organs are wounded the body begins a series of specific responses aimed at repairing damage and restoring physiologic function. As a primary function of the skin is serving as a protective barrier against the outside world, injured tissue must repair as quickly and efficiently as possible. In order to accomplish this, cutaneous wound healing has three overlapping phases:

inflammation, tissue formation, and tissue remodeling [1, 16]. The inflammatory phase begins with the formation of a fibrin clot at the wound site immediately following injury. This clot is formed by the extravasation of blood and its constituents from disrupted blood vessels, causing platelet aggregation and activation [1]. The clot, a meshwork of polymerized fibrinogen (fibrin), fibronectin, vitronectin, and thrombospondin, provides a provisional matrix that provides structure at the wound site and also serves as temporary wound coverage to ward off bacteria and stop bleeding [17]. Additionally, the clot acts as a reservoir of cytokines and growth factors secreted by activated platelets which act to recruit circulating inflammatory leukocytes such as neutrophils and monocytes, and macrophages [17]. Increased blood flow to the wound site following injury also aids in bringing an influx of leukocytes [1, 16]. As the inflammatory phase continues, these leukocytes begin to “clean-up” the wound site, recognizing healthy tissue, removing necrotic tissue, and acting as protectors from micro-organism colonization that could lead to infection. The resolution of the inflammatory phase is a wound bed that is stabilized, but still mechanically fragile. In order to complete wound healing, the fibrin clot must be replaced with new tissue [16, 17].

Replacement of the provisional fibrin matrix occurs in the tissue formation phase, also called the proliferation and repair phase because it requires the proliferation of several cell types to generate new tissue. The tissue formation phase in skin is characterized by three processes which occur simultaneously in the wound site: angiogenesis, formulation of granulation tissue, and reepithelialization [17]. Angiogenesis, or new blood vessel formation, is characterized by the migration and proliferation of vascular endothelial cells from existing blood vessels at the wound margins. These endothelial cells mature into a tubular network of new blood vessels that are necessary for re-supplying oxygen and other nutrients to maintain the new tissue [17]. These newly forming blood vessels are also a part of the granulation tissue that forms in the wound bed, named for its soft granular appearance. In addition to the new vasculature made up of endothelial cells, granulation tissue is rich in proteoglycans



and collagen deposited by dermal fibroblasts that proliferate and migrate into the wound bed. The collagen rich granulation tissue provides a more permanent support structure for the developing dermal tissue [1].

While angiogenesis and granulation tissue formation occur primarily in the skin's dermal layer, the epidermis undergoes its own proliferation and repair process called reepithelialization. During reepithelialization, which actually begins in the inflammatory phase, epidermal keratinocytes proliferate, migrate, and spread from the wound margins, as well as intact deep epidermal appendages, such as hair follicles and sweat glands, to bridge the wound and provide closure [16, 18].

While reepithelialization results in the restoration of the skin's barrier function, its conclusion is not the culmination of wound healing. The final phase of the wound healing pathway is the tissue remodeling phase. During this phase, which may take years to complete, the extracellular matrix (ECM) laid down during granulation tissue formation is reorganized and remodeled. Because skin is not a regenerative organ, reorganization of the dermis results in scar tissue, which is characterized by dense parallel bundles of collagen [19, 20]. While this fibrous scar tissue is effective in filling the voids left by skin injuries, it results in areas with compromised mechanics. In fact the mechanical properties of scar tissue are only about 60-70% of those of native tissue [16, 17].

### **2.1.2 Growth Factors in Wound Healing**

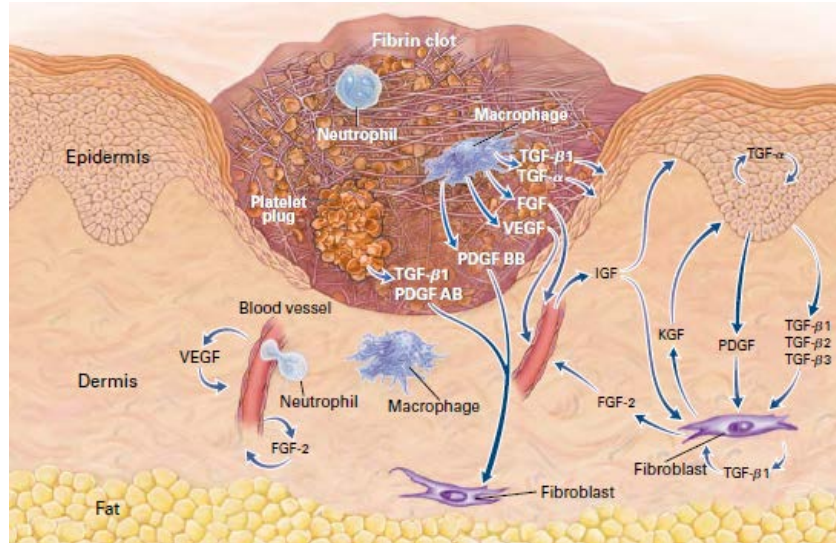
Growth factors, in conjunction with physical cues from the provisional wound matrix, play an important role in stimulating and regulating the cascade of events that occur in cutaneous wound healing [1, 16-18, 20].

Table 1 shows an overview of some important growth factors that stimulate and regulate cutaneous wound healing.

During the inflammatory phase wound healing relies on the presence of growth factors released by activated platelets such as platelet derived growth factor (PDGF), transforming growth factor-beta (TGF- $\beta$ ), epidermal growth factor (EGF), and transforming growth factor-alpha (TGF- $\alpha$ ). These growth factors, which appear in the wound bed shortly after injury, attract and activate inflammatory cells as well as fibroblasts [16, 17, 20, 21]. Attracted monocytes infiltrate the wound bed and become activated macrophages which continue to release PDGF, as well as vascular endothelial growth factor (VEGF) and acidic and basic fibroblast growth factor (FGF1 and FGF2 respectively) [1, 16, 20].

The synthesis of these growth factors helps to begin the tissue formation phase by initiating the formation of granulation tissue. PDGF, TGF- $\beta$ 1, and the FGFs along with extracellular matrix molecules from the wound bed stimulate fibroblasts to proliferate and migrate into the wound bed from the margins. These fibroblasts are then responsible for the synthesis, deposition, and remodeling of new extracellular matrix, gradually replacing the provisional fibrin matrix with a collagenous matrix, perhaps under the influence of TGF- $\beta$ 1 [16, 20]. Neovascularization of the new tissue requires FGF2 during the early stages of wound repair, but then relies on VEGF as well as appropriate extracellular matrix clues and endothelial receptors to promote angiogenesis during granulation tissue formation. VEGF comes from macrophages as well as epidermal cells which produce it in response to the hypoxia (low oxygen condition) of the tissue caused the disruption of the blood supply as a result of the original injury [16]. Macrophages also release TGF- $\beta$  and TGF- $\alpha$  which may help to stimulate the epidermal cells at the wound margins to mobilize into the wound and begin the process of reepithelialization. Epidermal cells

may also be stimulated by EGF produced by activated platelets, keratinocyte growth factor (KGF) secreted by fibroblasts, and their own local release of TGF- $\alpha$  [16].



**Figure 3: Growth factors play a key role in cutaneous wound healing. Representation of growth factor activity in early stage (inflammatory and tissue remodeling phases) cutaneous wound healing. . Reproduced with permission from Singer and Clark, 1999 [16], Copyright Massachusetts Medical Society.**

The wound contraction and remodeling phase of the wound healing process is orchestrated by the synchronized interactions of cytokines, extracellular matrix molecules, and cells. During this phase of wound healing, fibroblasts assume a myofibroblast phenotype (characterized by expression of  $\alpha$ -smooth muscle actin and the capacity to generate strong contractile forces [22]). This transformation is triggered by a combination of growth factors including TGF- $\beta$ 1 and mechanical signals from the ECM and results in contraction of the wound bed [16].

Table 1: Important growth factors and their sources and effects in cutaneous wound healing [16, 17, 20].

Growth Factor	Sources	Target cells/effects
<b>Platelet derived growth factor (PDGF)</b>	<ul style="list-style-type: none"> <li>• Platelets</li> <li>• Macrophages</li> <li>• Epidermal cells</li> </ul>	<ul style="list-style-type: none"> <li>• Macrophages – chemoattraction, activation</li> <li>• Fibroblasts – chemoattraction, proliferation</li> </ul>
<b>Transforming growth factor-alpha (TGF-<math>\alpha</math>)</b>	<ul style="list-style-type: none"> <li>• Macrophages</li> <li>• Epidermal cells</li> </ul>	<ul style="list-style-type: none"> <li>• Multiple – motility, proliferation</li> </ul>
<b>Transforming growth factor-beta (TGF-<math>\beta</math>)</b>	<ul style="list-style-type: none"> <li>• Platelets</li> <li>• Macrophages</li> </ul>	<ul style="list-style-type: none"> <li>• Epidermal cells – motility</li> <li>• Macrophages – chemotaxis</li> <li>• Fibroblasts – chemotaxis, ECM synthesis and remodeling</li> </ul>
<b>Epidermal growth factor (EGF)</b>	<ul style="list-style-type: none"> <li>• Platelets</li> </ul>	<ul style="list-style-type: none"> <li>• Multiple – motility, proliferation</li> </ul>
<b>Vascular endothelial growth factor (VEGF)</b>	<ul style="list-style-type: none"> <li>• Macrophages</li> <li>• Epidermal cells</li> </ul>	<ul style="list-style-type: none"> <li>• Angiogenesis</li> </ul>
<b>Fibroblast growth factor (FGF)</b>	<ul style="list-style-type: none"> <li>• Macrophages</li> <li>• Endothelial cells</li> </ul>	<ul style="list-style-type: none"> <li>• Fibroblasts – proliferation</li> <li>• Angiogenesis</li> </ul>
<b>Keratinocyte growth factor (KGF)</b>	<ul style="list-style-type: none"> <li>• Fibroblasts</li> </ul>	<ul style="list-style-type: none"> <li>• Epidermal cells – motility, proliferation</li> </ul>

### 2.1.3 Wound healing in severe skin injuries

In cases of chronic skin ulcers in which there may be significant tissue loss or physiologic and biochemical defects, the wound healing process may not occur in the linear fashion described above. Approximately 20% of wounds with significant tissue loss transition to a chronic state, often due to ischemia, or diminished blood supply, which is a common cause of chronic wounds in patients with conditions that affect blood circulation such as diabetes mellitus, venous insufficiency, and immobility are especially susceptible to chronic wounds. The completion of healing and restoration of skin function in chronic ulcers often requires advanced surgical intervention techniques, including auto-grafting and, more recently, the use of bioengineered skin substitutes [1].

## 2.2 Motivation for Bioengineered Skin Substitutes

Millions of individuals in the United States are impacted by chronic ulcers including more than 500,000 annually whose wounds are secondary to venous insufficiency and 3 million who suffer from

pressure ulcers as a result of immobility [1]. Additionally, up to 10% of the estimated 25 million people suffering from diabetes suffer from chronic diabetic foot ulcers [1, 2]. The cost of treating chronic wounds is estimated in excess of \$8 billion annually [1, 2].

Chronic skin ulcers present a significant challenge in wound management because they are often characterized by significant tissue loss and physiological or biochemical defects. As a result, the wound healing process in these wounds may not occur in the linear fashion described in the previous section. Skin ulcers are commonly caused by impaired blood circulation or prolonged pressure and often occur secondary to other health conditions such as venous insufficiency, peripheral arterial disease, diabetes, or other conditions that cause a patient to become immobile or bedridden [1, 2]. Chronic ulcers have diminished wound healing, often characterized by a prolonged inflammatory stage, which causes new matrix formed during the tissue formation phase to be digested almost immediately by inflammatory cells [23]. In fact, of all cutaneous wounds with significant tissue loss, approximately 20% have been found to transition to a non-healing or chronic state [1]. The completion of healing and restoration of skin function in chronic ulcers often requires advanced surgical intervention techniques, including auto-grafting and, more recently, the use of bioengineered skin substitutes.

### **2.2.1 Clinical Treatments for Severe Skin Injuries**

The “gold-standard” treatment for severe skin injuries is the split-thickness autograft. This procedure involves harvesting skin from a healthy part of the patient’s body, called a donor site, using a special reciprocating cutting tool called a dermatome. Split-thickness grafts are usually about 0.3 to 0.5 mm thick and include the epidermal layer and part of the skin’s dermal layer [6]. To cover large wounds, skin grafts may be “meshed”, a process which involves passing the graft through a mesher which makes small linear incisions in the autograft and allows it to be stretched to up to 9 times its original area.

Meshed grafts rely on normal wound healing and reepithelialization to close the gaps created by the meshing and stretching process [3-6].

While autografting is a very commonly used procedure in treating chronic skin ulcers and is often successful, it does have some specific limitations and disadvantages. First is the requirement for a second surgical procedure and site at the harvest location. This second surgical site adds to the potentials for infection and donor site morbidity may also occur. Additionally, in patients with very large wound areas there may be limited sites in which to harvest autografts from. Another limitation of using the split-thickness autograft is its potential for severe scarring. Because the autograft includes a portion of the dermis, which does not regenerate, patients often see scarring not only at the wound site, but at the harvest site as well. In meshed autograft applications, there is also often additional scarring at the application site in which the mesh pattern may be visible for extended periods after application [3-6].

## **2.3 Bioengineered Skin Substitutes**

The limitations and challenges presented from the use of traditional autografting have led to the research and development of bioengineered skin substitutes. These skin substitutes seek to provide an immediate and provisional barrier at the wound site and ultimately regenerates the native anatomy and physiology of the damaged skin.

### **2.3.1 Design Considerations for Tissue Engineered Skin**

The design of a successful bioengineered skin substitute relies heavily on the fulfillment of several physiochemical, biochemical, and mechanical parameters to replace native tissue lost in skin injuries that affect the epidermal and dermal layers (full-thickness injuries). As described in the preceding sections, the most critical property of skin is its function as a barrier. Yannas and Burke [13] describe the restoration of barrier function as Stage 1 in artificial skin design. During this stage it is clinically imperative to restore the skin's ability to keep bacteria out of the wound while preventing

evaporation of water from the underlying tissues and organs. To accomplish the clinical functions of infection control and fluid loss control, Yannas and Burke identified and described specific critical properties of the graft, wound bed, and graft/wound bed interface that should be incorporated in artificial skin design (Table 2).

Table 2: Summary of Stage 1 in Artificial Skin Design (reproduced with permission from Yannas and Burke [13])

<b>Objective: Membrane for single-application closure of full-thickness skin wounds, leading to control of infection and fluid loss, and eventual contracture with scar formation</b>		
<b><i>Clinical functions</i></b>		
<b>Infection control</b>		
<b>Fluid loss control</b>		
<b><i>Critical graft properties</i></b>	<b><i>Critical woundbed property</i></b>	<b><i>Critical properties of the graft/wound interface</i></b>
<b>Bending rigidity</b>	Viable tissue	
<b>Surface energy</b>		Wetting
<b>Moisture flux rate</b>		Peel strength
<b>Blood compatibility</b>		
<b>Tear strength</b>		

Many of the critical physiochemical and mechanical properties associated with the restoration of barrier function center around the need to create robust contact between the wound bed and the artificial skin graft. In particular, the wettability, resistance to shearing and peeling forces, and moisture flux rate have significant impact on maintaining strong adherence of the graft to the wound bed. Figure 4 shows schematic representations of the impact of these properties on the artificial skin graft's ability to effectively close wounds.

While Stage 1 in the design of an artificial skin graft focuses on achieving prompt wound closure, Stage 2 (summarized in Table 3) shifts the design focus to long term regenerative functions and eventually, to metabolic degradation of the graft itself. Yannas and Burke [13] identified three unique possible design alternatives for this stage of skin wound treatment, as follows:

1. **Organotypic approach** – design a highly complex cellular and fully vascularized tissue that can be rapidly incorporated into the wound bed. The result is a true skin analog without risk of rejection and with negligible wound contracture and scarring. At the time of publishing, Yannas and Burke recognized that this approach required extensive parallel advancements in tissue and organ culture techniques. More recently, however, attempts have been made in the design of an organotypic skin substitute with limited success (see 2.3.2.3 Composite Skin Substitutes for a description of Apligraf).
2. **Temporary scaffold approach** – design a solid, non-degradable matrix that supports tissue ingrowth, but must then be surgically removed and replaced by an autograft. This approach was not ultimately investigated by Yannas and Burke, but has been used by several commercially available products which are effective at temporarily enhancing wound healing, but do not result in long term wound closure (see 2.3.2.2 Dermal Skin Substitutes for a description of Biobrane).
3. **Degradable scaffold approach** – design a solid, degradable matrix that supports tissue ingrowth while minimizing antigenic responses. Scaffolds of this type should allow for simultaneous enzymatic matrix degradation and replacement by neodermal tissue. This approach was utilized by Yannas and Burke and eventually resulted in the development of their commercially available Integra Dermal Regeneration Template (see 2.3.2.2 Dermal Skin Substitutes for a description). It is also the approach that was ultimately chosen for the scaffold material that is the subject of this project.

During Stage 2, the degradable graft must continue to function as a barrier against infection and fluid loss as it did in Stage 1, but also aims to accomplish the clinical functions of controlling wound contraction and minimizing scar formation, resulting in replacement of the artificial graft with neodermal tissue. The critical graft properties associated with this design stage are summarized in Table



3 and include specific levels of biodegradability, antigenicity, pore size, thickness, and blood compatibility. Successful optimization and inclusion of these properties would hopefully induce migration and infiltration of the graft with non-inflammatory cells, synthesis of neodermal tissue, and finally metabolic degradation of the graft, resulting in a fully healed wound with minimal wound contraction and scarring.

**Table 3: Summary of Stage 2 in Artificial Skin Design (reproduced with permission from Yannas and Burke, 1980)**

<b>Objective: Control infection and fluid loss and, in addition, control contracture and scarring</b>	
<b><i>Clinical functions</i></b>	
<b>Infection control</b>	
<b>Fluid loss control</b>	
<b>Contracture control</b>	
<b>Scar control</b>	
<b><i>Critical graft properties</i></b>	<b><i>Desired events in graft lifetime</i></b>
<b>Biodegradability rate</b>	Migration of non-inflammatory cells
<b>Antigenicity</b>	Synthesis of neo-dermal tissue
<b>Mean pore size</b>	Metabolic disposal of graft
<b>Thickness</b>	
<b>Blood compatibility</b>	

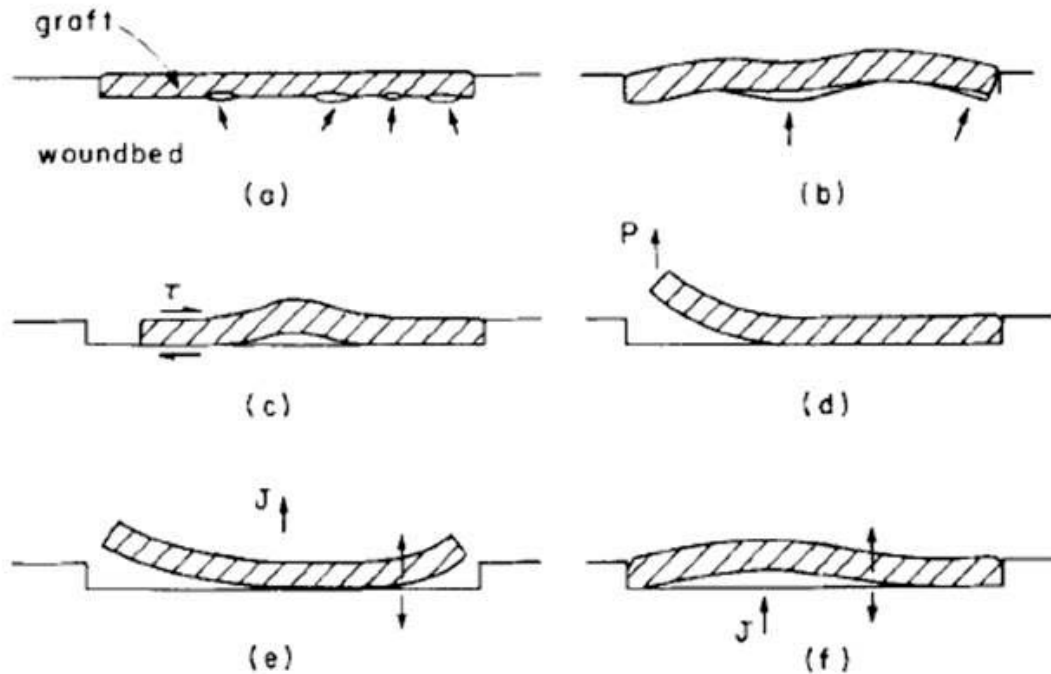


Figure 4: Schematic representation of certain physiochemical and mechanical requirements in the design of an effective wound closure (reproduced with permission from Yannas and Burke [13]). (a) and (b) show the effect of proper wetting on scaffold performance. In (a), the scaffold does not sufficiently wet the wound bed and air pockets result. In (b), the scaffold's flexural rigidity is too high resulting in an inability to sufficiently drape and make continuous contact with the wound bed. (c) and (d) show the effects of proper mechanical resistance. Scaffolds must resist the shear and peeling forces associated with normal movement and clinical manipulations. Failure to resist shear forces (c) and peeling forces (d) may result in scaffold displacement and lifting respectively. (e) and (f) show the effects of proper moisture flux rate through the scaffold. If the moisture flux rate is too high (e) dehydration and peeling occur. If the moisture flux rate is too low (f), fluid pools under the scaffold.

### Material Selection

A wide variety of materials are available for use in engineering scaffolds for skin regeneration. When selecting materials it is important to consider the properties of the material and how they may be manipulated to mimic properties of native tissue. In designing a biomaterial scaffold for skin regeneration, it is important to consider intrinsic properties of the material, such as wettability, which influence interactions between the material and the surrounding tissue, but also properties that can be manipulated through various processing methods such as mechanical properties, porosity, and biodegradability which influence the scaffold's ability to support wound healing. Properties such as

mechanical resistance and breathability (through maintenance of appropriate moisture flux rate) are important for protecting the healing wound and facilitating wound healing.

Scaffolds for skin regeneration can be made from a wide range of natural or synthetic bulk materials. Yannas and Burke chose a biological polymer, bovine collagen, for their dermal regeneration matrix, but there has also been a great deal of investigation into other biopolymers such as hyaluronan, fibrin, and alginate [5]. Synthetic polymers are also being investigated because they are easily processed with control over geometric morphology, mechanical properties, and biofunctionality. Some of the synthetic polymers being investigated for skin regeneration include poly(lactic-co-glycolic acid) (PLGA), polyurethane (PU), polycaprolactone (PCL), and polyvinyl alcohol (PVA) [5]. There is also much investigation and development in the use of composite materials in skin regeneration. Combining various synthetic and/or natural polymers allow for further tailoring of material properties that affect specific wound healing responses [1, 5, 24].

### ***Wettability***

Upon initial application, the bond between the graft and the wound bed is heavily influenced by the graft's ability to wet the wound on contact and spread over it, displacing air from the graft/wound interface. According to Yannas and Burke [13], this wetting is only effective if the wound bed has been properly prepared (residual eschar and scab are removed) and is enhanced by the use of a hydrophilic material to manufacture the graft. If the graft is not able to sufficiently wet the wound bed, air pockets may result and disrupt adhesion at the graft/wound interface as shown in Figure 4a. Efficient wetting is also influenced by the graft's flexural rigidity (the product of elastic modulus and moment of inertia), which must be low enough to sufficiently allow the membrane to drape intimately over the meticulously prepared wound bed, and the surface energy of the graft/wound interface, which must be lower than that of the air/wound bed in order for the graft to adequately displace air pockets. Figure 4b shows the

effect of a graft with an excessively high flexural rigidity which is not able to deform and make contact with the wound under its own weight.

### ***Mechanical Resistance***

Once the graft and wound bed have made sufficient contact, additional mechanical considerations include the graft's ability to resist shear forces and peeling forces. These forces, which could be applied accidentally during clinical manipulations of the wound site, such as bandaging, could cause graft displacement and result in air pockets (Figure 4c) or lifting of the graft away from the wound bed (Figure 4d). Suturing of the graft in place helps to minimize movement in these situations, but resistance is enhanced by prompt development of a strong bond between the apposed surfaces of the graft and wound bed [13].

### ***Moisture Flux Rate***

In order to effectively sustain long term wound closure, artificial skin grafts must maintain an appropriate moisture flux rate through the membrane. According to a study by Spruit and Malten in the 1960s [25], the physiological moisture flux rate in skin is about 0.5 mg/cm<sup>2</sup>/hr. If the moisture flux rate of the artificial skin graft is too high, water may evaporate and leave the wound bed too quickly, resulting in dehydration and alteration of the graft/wound interface. In this scenario, the graft loses its ability to sufficiently wet the wound bed and it may slough off or shrink and pull away from the wound (Figure 4e). By contrast, Yannas and Burke [13] note that if the moisture flux rate of the artificial skin graft is too low, the result is accumulation of excess fluid at the graft/wound interface. This edema may also disrupt the adhesive contact between the graft and the wound and diminishes barrier function.

### ***Biodegradability***

The design approach chosen by Yannas and Burke [13], and ultimately, by this project, is dependent on simultaneous biodegradation of the scaffold and its replacement by newly formed dermal

tissue synthesized by fibroblasts that migrate into the scaffold from the wound margins. In order for this approach to be successful, the relationship between the lifetime of the scaffold (expressed as  $t_b$ , the time constant of biodegradation) and the time constant for normal skin incision healing (expressed as  $t_h$  = about 25 days [26]), must be optimized. If the scaffold has a very rapid biodegradation rate and thus  $t_b \ll t_h$ , the membrane will be reduced to a liquid-like state within a few days. In this scenario, the scaffold becomes ineffective as a platform for cell migration and dermal synthesis and is also ineffective as a wound closure. By contrast, if the scaffold has an excessively long degradation time ( $t_b \gg t_h$ ) and hardly degrades at all within the normal healing time, the infiltrating fibroblasts are unable to produce ECM that replicates the native dermal structure and the result is the formation of a barrier of dense fibrotic tissue between the scaffold and the wound bed and necessitating surgical removal of the scaffold. Yannas and Burke [13] report that the optimized relationship between biodegradation and healing time is about proportional such that  $t_b \approx t_h$ . Biodegradation rate can be controlled through various means including chemical composition and crosslinking density.

### ***Porosity***

A porous scaffold is essential in this type of scaffold design because porosity promotes vascularization, nutrient exchange, and the infiltration of fibrovascular cells responsible for tissue ingrowth and neodermal formation. For skin regeneration the optimal pore size should be related not only the size of the epithelial and mesenchymal cells responsible for wound healing, but also to the nutrients they require to do so. Most of these cells, which are found in the wound bed, are on the order of 10  $\mu\text{m}$  in diameter, necessitating the development of a scaffold with pores that are at least as large in order to induce migration into the graft material. Smaller pores, those on the nanoscale, also have important functions in skin regeneration scaffolds. Nanopores are too small for cell migration and infiltration, but play a crucial role in enhancing the surface area for cell-biomaterial interactions and the diffusion of gases and nutrients essential for supporting cell survival [1, 24]. Yannas, et al. investigated

the relationship between pore size and rate of wound closure in collagen-GAG sponges and found that scaffolds with average pore sizes between 20 - 125 $\mu$ m regenerated tissue while maintaining an appropriately long degradation profile [27]. To date, there have been several strategies aimed at creating porous scaffolds including lyophilization, which was utilized by Yannas and Burke [13] in the creation of their porous collagen-GAG sponge dermal regeneration template, as well as others such as electrospinning, particulate leaching, gas infusion, and computer aided design and manufacturing via 3-D printing [24, 28]. Changing processing parameters can be used to control porosity and pore size in each of these strategies with varying degrees of success.

### ***Mechanical Properties***

The mechanical properties for an engineered tissue scaffold should mimic the properties of the tissue they seek to replace as closely as possible. For skin, the ideal scaffold should be flexible, elastic, and durable, with specific property values that resemble those of native skin. The tensile properties of native skin as reviewed by Edwards and Marks [12] is outlined in Table 4. The anisotropic nature of skin, especially around joints, leads to a wide range of measured values depending on measurement location and direction. Additionally, the degree of anisotropy varies from person to person as well as with age, gender and health. Thus it is difficult to pinpoint specific ideal values for engineered tissues. Related to both mechanical properties and mechanical resistance is the desire to create a scaffold with appropriate surgical handling properties. It is important that scaffolds maintain their structural integrity during sterilization and implantation.

**Table 4: Tensile properties of native skin tissue. Average values for children and elderly subjects are reported in addition to the full range of values measured in all subjects [12].**

	<b>Ultimate tensile strength (MPa)</b>	<b>Strain at failure (mm/mm)</b>	<b>Modulus (MPa)</b>
<b>Average – child</b>	21	0.75	70
<b>Average – elderly</b>	17	0.60	60
<b>Full range</b>	5-30	0.35 – 1.15	15-150

## 2.3.2 Current Methods and Limitations

The currently commercially available bioengineered skin substitutes can be divided into three categories based on the skin structure they seek to mimic: epidermal skin substitutes, dermal skin substitutes, and composite (epidermal and dermal) skin substitutes.

### 2.3.2.1 Epidermal Skin Substitutes

The ability to culture human keratinocytes *in vitro* was first demonstrated in the 1970s [29]. Soon after, this process was utilized in the development of constructs made up of cultured human epidermal cells that form sheets suitable for grafting onto burn wounds [30-33]. In 1988, this technology was used to develop a commercial product, Epicel® cultured epithelial autograft (CEA; Genzyme). Epicel® is made by initiating a culture of autologous keratinocytes which are enzymatically isolated from a 2–5 cm<sup>2</sup> biopsy taken from the patient along with initial wound debridement. These keratinocytes are then expanded in culture on a feeder layer of mitotically inactivated murine fibroblasts in a specially formulated culture medium. As they expand, single colonies of keratinocytes merge together and form a sheet with stratified epithelial layers within the tissue culture vessel. This sheet is then enzymatically detached from the culture flask, mounted to a backing support (paraffin gauze) and applied to the wound [5]. Since the 1980s, CEAs have been successful in providing permanent coverage for many types of severe skin wounds including large burns, acute wounds, chronic ulcers, and epidermolysis bullosa [31, 34]. Other commercially available CEAs include EPIBASE™, which like Epicel® consists of cells derived from a small skin biopsy and EpiDex® which consists of keratinocytes isolated from the outer root sheath of scalp hair follicles [5].

The advantages of using CEAs include their demonstrated ability to quickly and permanently provide wounds with a barrier against fluid loss and infection. The autologous nature of the cells in CEAs limits negative immune responses in patients. Additionally, CEAs have the capacity provide clinicians

with enough epithelial wound dressing to cover very large wound areas from a small biopsy. There are, several significant limitations associated with this type of bioengineered skin substitute. First is the two to three week delay in treatment while the autologous cells are grown into sheets that are suitable for grafting. During this time, doctors and nurses must take extra care to stabilize the wound and prevent infection. Second, there must be precise communication and coordination between the cell culture facility and the clinic during CEA manufacture. Once detached from the culture vessel Epicel® only has a shelf life of about 24 hours before it must be applied to the wound [5]. Upon arrival at the hospital great care must be taken in handling of CEAs. Third, they are thin, fragile, and expensive and require complicated surgical application.

After grafting, the success of CEAs is unpredictable. Graft take rates reported in the literature vary from 0-85% engraftment , and are usually associated with other complications such as poor keratinocyte attachment and blistering, which can occur months after application [33]. Several hypotheses have been proposed to explain the inconsistent and suboptimal graft take in CEAs including the disruption of keratinocyte-ECM substrate binding by the enzymatic treatment required to remove the CEA from the culture vessel. This may cause contraction of the CEAs as well as decreased mechanical stability and prevent their attachment to the wound bed [35]. Another possible explanation of inconsistent graft take is the theory that the quality of CEAs is heavily impacted by their clonal cellular composition. In human epidermal tissue there are three clonal types of keratinocytes, related to their spatial location within the epidermis [36]. Holoclones, made up of basal keratinocytes have the highest proliferative potential (less than 5% terminally differentiate) and are essential for long-term graft success and survival. Paraclones consist of committed keratinocytes and make up the majority of the epidermal tissue. Paraclones have a low proliferative potential and are only able to replicate a few times (not more than 15 cell generations) before terminal differentiation and senescence. Therefore, a CEA containing only paraclones would not be able to provide permanent wound closure. The final type is a



mixed population of transient amplifying cells and cells that have degraded to paraclone-formers called a meroclone. Meroclones have variable potential for proliferation and can provide only temporary wound closure [5, 36].

It is also possible that the culture strategy employed to manufacture CEAs is responsible for their unpredictable clinical outcome. Although thicker CEA sheets are easier to handle, as the confluent layers of cells build up in the culture vessels the basal cells may become isolated from the nutrients in the cell culture medium. This could result in the starving of the highly proliferative cells and impede the graft's ability to close wounds. This finding has led to exploration in the use of sub-confluent keratinocytes as a bioengineered skin substitute. CellSpray® (Avita Medical; Perth, Australia) is a product that delivers sub-confluent autologous keratinocytes suspended in culture medium to the wound bed as an aerosol spray. By aiming to harvest subconfluent keratinocytes at their most active proliferating state before application to the wound bed, CellSpray® allows for further *in vivo* proliferation and differentiation to complete wound closure[5]. In wounds treated with a fully expanded 3:1 meshed split-thickness autograft, wounds that were also sprayed keratinocyte cell suspension showed improved healing compared to control wounds treated with an autograft and sprayed with culture medium. Overall, the sprayed keratinocyte cell suspension treatment resulted in faster and better quality epithelialization compared to the control treatment [37].

Another approach to epidermal wound healing that utilizes subconfluent keratinocytes is Myskin™ (Altrika Ltd.; Sheffield, UK). Myskin™ is an epidermal wound dressing that consists of a medical grade silicone sheet with a special nanometer scale coating that allows for the growth of proliferative, sub-confluent, autologous keratinocytes cultured *in vitro*. The Myskin™ system has several distinct advantages over traditional CEA sheets including a shorter culture and preparation time and greater time flexibility for delivery to the wound site [38]. The substrate used to culture Myskin™ also adds

mechanical stability to the graft and improves and simplifies surgical handling and application. In terms of improving graft take, Myskin™ does not require enzymatic detachment of cells from the substrate, which may negatively affect anchoring fibrils responsible for graft attachment, as the substrate is applied directly to the wound with the subconfluent keratinocytes [38]. Additionally, subconfluent keratinocyte strategies have been shown to contribute to earlier basement membrane formation, resulting in a more mature and robust epidermal-dermal junction region in comparison to CEA sheets [5, 39].

Although still plagued by some inconsistencies, the epidermal skin substitute strategies presented in this section have been effective in providing permanent wound closure overall. They are particularly successful in treating chronic ulcers and provide those patients with improved healing and quality of life. There is however, some debate as to their effectiveness and efficiency in treating burn wounds, especially in the long-term [5]. Many of the shortcomings of epidermal skin substitutes may come from a need for a properly prepared wound bed. Engraftment rates of epidermal grafts have been shown to increase when grafted onto early granulation tissue or a freshly debrided wound bed over grafting onto chronic granulation tissue and infected wounds. Even higher engraftment success can be observed when epidermal skin substitutes are grafted onto wounds that already have a well vascularized dermal or neodermal wound bed in place[7]. These findings strongly advocate for the pregraftment of full thickness wounds with a dermal analog prior to treatment with cultured autologous keratinocytes [5].

Table 5: Commercially available epidermal skin substitutes. This table contains a subset of clinically used products with a description of the components, advantages, and disadvantages of each.

Skin Substitute Type/Name	Components	Advantages	Disadvantages
<b>Epidermal</b>			
<b>Epicel®</b>	<ul style="list-style-type: none"> <li>• <u>Cells</u> – an integrated sheet of autologous keratinocytes</li> </ul>	<ul style="list-style-type: none"> <li>• Permanent coverage for a variety of wound types</li> <li>• Coverage of large areas</li> <li>• Good cosmetic results</li> <li>• Limited negative immune response</li> </ul>	<ul style="list-style-type: none"> <li>• Biopsy needed for cell source</li> <li>• Delay to grow autologous cells (2-3 weeks)</li> <li>• Complicated handling and application procedures</li> <li>• Unpredictable clinical outcome (take rates between 15-85%) [40, 41]</li> <li>• Poor keratinocyte attachment can lead to delayed blistering [33]</li> <li>• Precise time coordination between cell culture and clinic</li> <li>• High cost</li> <li>• Short shelf life (~24 hrs.)</li> </ul>
<b>CellSpray®</b>	<ul style="list-style-type: none"> <li>• <u>Cells</u> – a subconfluent, autologous, keratinocyte suspension delivered to wounds as a spray</li> </ul>	<ul style="list-style-type: none"> <li>• Permanent coverage</li> <li>• Coverage of large areas</li> <li>• Good cosmetic results</li> <li>• Limited negative immune response</li> <li>• Decreased cell culture time</li> <li>• Earlier wound coverage [40]</li> <li>• Earlier basement membrane formation</li> <li>• More flexible application time</li> </ul>	<ul style="list-style-type: none"> <li>• Biopsy needed for cell source</li> <li>• Delay to grow autologous cells</li> <li>• Full thickness wounds require dermal element for functional permanent skin restoration [42]</li> </ul>

<b>MySkin™</b>	<ul style="list-style-type: none"> <li>• <u>Scaffold</u> – silicone support layer with specially formulated surface coating</li> <li>• <u>Cells</u> – subconfluent autologous keratinocytes</li> </ul>	<ul style="list-style-type: none"> <li>• Permanent coverage</li> <li>• Coverage of large areas</li> <li>• Good cosmetic results</li> <li>• Limited negative immune response</li> <li>• Easier handling and application</li> <li>• Decreased cell culture time</li> <li>• Longer shelf life than CEAs</li> </ul>	<ul style="list-style-type: none"> <li>• Biopsy needed for cell source</li> <li>• Delay to grow autologous cells</li> <li>• Cannot be used alone for deep wounds (requires dermal support)</li> </ul>
----------------	--	---	---

### 2.3.2.2 Dermal Skin Substitutes

While cultured epithelial sheets have been shown to enhance healing, they lack a component that recapitulates the collagen-rich ECM of the native dermis. In full-thickness wounds, a dermal component may prevent wound contraction and provide greater mechanical stability to the healing tissue [16]. This has led to the development of a number of commercially available dermal skin substitutes (for a subset see Table 6) that are mostly acellular and may be comprised of allogenic, xenogenic, or synthetic materials. An advantage of using acellular strategies for dermal skin substitutes is their ease in manufacturing. Acellular dermal constructs can be made in at low cost in large batches with a high level of quality control. Additionally, the processes for gaining licensing and approval for acellular products is much less rigorous than those for products that contain cells [5].

Among the first strategies utilized to create a bioengineered dermal matrix was the use of allogenic acellular human dermis. An example of these products is Alloderm® (LifeCell Corporation; Bridgewater, NJ), an acellular human cadaveric dermal construct. Alloderm® is decellularized through a proprietary lyophilization process that kills the donor’s cells, but preserves the extracellular matrix including growth factors, cytokines, and other signaling molecules that may help to promote wound healing [23]. The well conserved matrix of Alloderm® helps it to readily incorporate into the patient’s wound bed and the lack of a cellular component results in very little risk of rejection or immunogenic

response. Additionally, pre-grafting of full thickness wounds with Alloderm® provides a solid dermal replacement which can then be grafted by a very thin and widely meshed autograft. This pre-grafting approach minimizes the number of split-thickness autografts required and results in minimal undesirable scarring and wound contracture commonly associated with the use of thin, widely meshed autografts [43, 44].

Although Alloderm® was originally developed as a dermal replacement product and has been shown to successfully support fibroblast infiltration, neovascularization, and epithelialization [44], it has also exhibited some uncertainty in the rate of vascularization which is critically important in dermal replacement [18]. As such, Alloderm® has been investigated more recently in applications that do not rely heavily on revascularization such as abdominal wall hernia reconstruction, subcutaneous mastectomy, and periodontal surgery [5]. Another limitation of Alloderm® is that it does not provide the patient with an immediate barrier (epidermal) component and instead relies on the skin's native reepithelialization processes or on treatment with a split-thickness skin graft to provide full wound closure.

Integra® Dermal Regeneration Template (Integra®-DRT; Integra LifeSciences; Plainsboro, NJ) is a xenogenic dermal bioengineered skin substitute developed by Yannas and Burke in 1980 [13, 45]. Integra®-DRT incorporates a bovine type I collagen and shark chondroitin-6-sulphate glycosaminoglycan sponge dermal component bonded to a silicone barrier layer. The degradable natural polymer dermal component supports the ingrowth of host dermal cells, which begin to replace the scaffold with new dermal tissue. The silicone barrier provides a barrier immediately upon application that protects the healing wound from excessive water loss and bacterial contamination. Fifteen to twenty days after application, once Integra's dermal component is vascularized and neodermal formation is complete, the

silicone barrier layer is mechanically removed and the wound can be permanently closed with a split-thickness autograft [5].

Integra®-DRT has been successfully used clinically for full-thickness burn wound treatment since 1981 [46], and is widely considered to be the “gold standard” dermal substitute biomaterial. It has also been used to effectively treat chronic ulcers[47, 48] and other full-thickness non-thermal skin injuries as well as for reconstructive surgery applications [49]. Some of the advantages of the Integra®-DRT are that it is readily available, has a very long shelf life (2 years from date of manufacture), it is very easy to handle, and it can be manufactured in a variety of sizes. Integra®-DRT also has a low risks of immunogenic response and disease transmission and has been shown to have reduced rates of scarring and wound contraction leading to very good cosmetic outcomes overall [18]. There has been however, some issues with bacterial contamination when using Integra®-DRT [16, 18] and it cannot be used on wounds that are infected [5]. Additional disadvantages include prolonged wound healing times (10-14 days for vascularization) and the need for a second surgical procedure to close the wound with a split thickness skin graft. There is also some inconsistency in the material properties of Integra®-DRT due to the xenogenic sourcing of the collagen in the dermal component [50].

Dermal skin substitutes have also been made using synthetic materials. Biobrane® and Biobrane®-L (UDL Laboratories, Inc.; Rockford, IL) are both temporary dermal dressings that aid in speeding up the wound healing process. The Biobrane® products consist of a nylon fabric that is chemically bound with porcine dermal collagen and partially embedded into a semipermeable silicone film pseudo-epidermis. These dressings are intended to be applied to partial thickness burn wounds, the donor sites from split-thickness autografts, or over an applied meshed autograft [5]. They provide matrix proteins, growth factors, cytokines that reduce the time necessary for wound healing as well as controlling vapor loss and providing pain relief when compared to conventional dressings [51-53].

However, because the Biobrane® dressings are made up of synthetic, non-degradable materials, they must be removed 7-14 days after application and require another means of achieving permanent coverage.

Dermagraft® (Shire Regenerative Medicine, Inc.; La Jolla, CA) is a dermal skin substitute that is also manufactured using synthetic materials. The scaffold is comprised of a cryopreserved polyglactin mesh that is seeded with allogenic neonatal dermal fibroblasts [54] and is indicated for and primarily used in treating chronic diabetic foot ulcers and chronic venous ulcers [55]. Following application to the wound site Dermagraft® degrades over a period of 20-30 days by hydrolysis. During this time, the incorporated allogenic fibroblasts produce various growth factors and ECM components that encourage wound healing, including the recruitment of native fibroblasts and the reconstitution of a dermal layer [56]. Dermagraft® can be applied to the same wound multiple times until dermal healing is complete and the wound reepithelializes by keratinocyte migration from the wound margins or the wound can be closed with a split-thickness autograft [56]. There is a higher risk of disease transmission in Dermagraft® because of the use of an allogenic cell source and careful screening must take place to ensure the product's safety to the patient [5, 55]. Additionally, the incorporation of allogenic fibroblasts also contributes to a higher cost for treatment with Dermagraft® when compared to other treatment options [56].

Overall, dermal bioengineered skin substitutes are extremely effective in preparing the wound bed and at reconstituting the dermal layer. These steps are essential for effective graft take and may significantly improve wound healing and graft take when used in conjunction with thin meshed autografts or epidermal skin substitutes such as cultured epithelial autografts. Acellular dermal skin substitutes also have the advantage of being relatively easy and inexpensive to manufacture and in some cases have been shown to reduce treatment costs when compared to conventional dressings [51].

Restoration the dermal tissue alone does not however permanently close wounds and dermal skin substitutes must incorporate a pseudo-epidermis or other barrier to reduce the risk of bacterial contamination and control moisture loss.

**Table 6: Commercially available dermal skin substitutes. This table contains a subset of clinically used products with a description of the components, advantages, and disadvantages of each.**

Skin Substitute Type/Name	Components	Advantages	Disadvantages
<b>Dermal</b>			
<b>AlloDerm®</b>	<ul style="list-style-type: none"> <li>• <u>Scaffold</u> – Lyophilized acellular human dermis</li> </ul>	<ul style="list-style-type: none"> <li>• Readily incorporates into wound without rejection [5]</li> </ul>	<ul style="list-style-type: none"> <li>• Uncertain rates of vascularization</li> <li>• Variability in source material properties</li> <li>• Human-derived safety issues [5]</li> </ul>
<b>Integra®-DRT</b>	<ul style="list-style-type: none"> <li>• <u>Scaffold</u> – Bovine collagen and GAG sponge (dermal), polysiloxane membrane (barrier)</li> </ul>	<ul style="list-style-type: none"> <li>• Long shelf life</li> <li>• Simple handling</li> <li>• Low risk of immunogenic response and disease transmission</li> <li>• Good cosmetic outcomes [5, 56]</li> </ul>	<ul style="list-style-type: none"> <li>• High incidence of infection [5, 16]</li> <li>• Prolonged wound healing time/inconsistent graft take [5]</li> <li>• Meticulous surgical preparation [5]</li> <li>• Variability in source material properties [50]</li> </ul>
<b>Dermagraft®</b>	<ul style="list-style-type: none"> <li>• <u>Scaffold</u> – PGA/PLA, ECM</li> <li>• <u>Cells</u> – allogenic neonatal fibroblasts</li> </ul>	<ul style="list-style-type: none"> <li>• Degrades by hydrolysis in 20-30 days</li> <li>• Provides wound with growth factors and ECM components [5, 56]</li> </ul>	<ul style="list-style-type: none"> <li>• Meticulous surgical preparation [5]</li> <li>• Necessity for for multiple applications</li> <li>• High cost</li> <li>• Safety due to incorporation of allogenic cells [5, 56]</li> </ul>
<b>Transcyte™ (Dermagraft®-TC)</b>	<ul style="list-style-type: none"> <li>• <u>Scaffold</u> – silicone film, nylon mesh, porcine collagen</li> <li>• <u>Cells</u> – allogenic neonatal fibroblasts</li> </ul>	<ul style="list-style-type: none"> <li>• Provide matrix proteins, growth factors, and cytokines to enhance wound healing</li> <li>• Effective for vapor loss control</li> <li>• Reduced healing time when compared to conventional dressings [53]</li> </ul>	<ul style="list-style-type: none"> <li>• Meticulous surgical preparation [5]</li> <li>• Temporary and non-degradable, must be removed 7-14 days after application [5]</li> <li>• Safety considerations due to incorporation of allogenic cells [5]</li> </ul>



<b>Biobrane®</b>	<ul style="list-style-type: none"> <li>• Scaffold – silicone film, nylon fabric, porcine collagen</li> </ul>	<ul style="list-style-type: none"> <li>• Provide matrix proteins, growth factors, and cytokines to enhance wound healing</li> <li>• Effective for vapor loss control</li> <li>• Reduced healing time when compared to conventional dressings [53]</li> </ul>	<ul style="list-style-type: none"> <li>• Meticulous surgical preparation [5]</li> <li>• Temporary and non-degradable, must be removed 7-14 days after application [5]</li> </ul>
------------------	--	--	--

### 2.3.2.3 Composite Skin Substitutes

Concurrent repair of both the epidermal and dermal layers of skin has been investigated and utilized by several commercially available composite bioengineered skin substitutes (see Table 7 for a subset). Composite bioengineered skin substitutes are the most advanced and sophisticated of the tissue engineered skin products aiming to mimic the morphological structure of native skin as well as provide some of the function of each skin layer lost in a full-thickness injury. Most composite bioengineered skin products are comprised of allogenic skin cells integrated into a manufactured or native dermal matrix. There is some concern regarding the long-term viability of these allogenic cells following implantation in the wound bed. In many cases these cells, keratinocytes in particular, are rejected by the host 3-4 weeks after graft application [57].

The most simple allogenic composite skin substitute strategy for the treatment of full-thickness wounds is the use of an allograft from cadaveric donors. This approach provides a durable epidermal barrier and pain relief to the wound site and is readily revascularized from the wound bed [5, 58]. Unfortunately, as the allograft becomes vascularized and incorporates into the wound bed the highly immunogenic allogenic epithelial cells trigger the host's immune response and the allograft is ultimately rejected several weeks after grafting. As a result of this complication, allografts are generally considered a temporary wound dressing to be used until permanent closure can be achieved with a split-thickness

skin graft or an alternative bioengineered skin strategy. The allogenic nature of this approach also increases the risk of infection and disease transmission and as such a rigorous screening process must become an integral part of the skin bank protocols. Glycerolization or lyophilization of allografts destroys an allograft's incorporated cells thus reducing the risk of immune response and transmitted diseases and infection. This process leaves behind the dermal matrix and gives rise to the dermal matrix derived skin substitutes such as Alloderm<sup>®</sup>, described in Section 2.3.2.2 Dermal Skin Substitutes.

Apligraf<sup>®</sup> is a composite bioengineered skin substitute that is comprised of bovine collagen and allogenic cells isolated from neonatal human foreskin tissue. The Apligraf<sup>®</sup> matrix utilizes neonatal fibroblasts grown in a type I bovine collagen gel lattice and topped with a confluent superficial layer of neonatal keratinocytes in order to mimic the structure of native human skin. The live epidermal layer in Apligraf<sup>®</sup> provides the wound site with a natural barrier to pathogens and mechanical injury, while the dermal ECM promotes cell ingrowth from the wound margins and acts as a delivery system of growth factors that stimulate the native wound healing cascade [23]. Apligraf<sup>®</sup> has been shown to improve wound healing in patients with diabetic foot ulcers as well as reduce the time to complete wound closure when compared to the state-of-the-art treatment control group [59, 60]. Apligraf<sup>®</sup> has also been successful in the treatment of other lower-extremity ulcers following revascularization procedures and has been shown to decrease the cost of wound care in patients with chronic ulcers [23]. Although there has been some investigation into the use of Apligraf<sup>®</sup> to treat burn wounds [18], there are no results of large clinical trials yet available. In fact, it may be difficult to assess the effect of Apligraf<sup>®</sup> in burn wounds because the material is not designed to persist in the wound bed, but rather to “condition” the wound and promote and heighten the native wound healing cascade, which is a much more effective strategy in chronic ulcers where this cascade is often severely compromised by diabetes or other insufficiencies [18].

Despite the use of allogenic cells, Apligraf® does not produce a host immunogenic reaction, however, as in allografts, these cells only survive one to two months *in vivo* [61, 62]. As such, Apligraf® can only be considered a temporary wound dressing and not an organotypic skin substitute as it was originally marketed and combination with other wound closure strategies may be a necessity in full-thickness wounds that are not able to reepithelialize themselves [1, 5]. Additional drawbacks of Apligraf® include its relatively short shelf life, only 5-10 days, requiring careful coordination between shipping and the patient's clinic visit [1]. Furthermore, Apligraf® is quite expensive (approximately \$30 per cm<sup>2</sup>) and also requires delicate handling and application procedures [1, 5, 18]. There is also a risk of disease transfer associated with Apligraf® because of its allogenic components. Despite these complications, Apligraf® is widely considered the most clinically successful product in its category and is one of only a handful of tissue engineered products to receive FDA approval [1].

Orcel® is a similar product to Apligraf® that combines allogenic neonatal keratinocytes and fibroblasts from the same foreskin tissue sample with a type I bovine collagen sponge dermal component coated with a non-porous collagen gel that acts as a basal lamina analog on which the keratinocytes are seeded to form a confluent layer. The collagen sponge dermal component serves as a biocompatible, absorbable matrix that is favorable for host fibroblast infiltration and has been shown to contain a variety of growth factors that stimulate wound healing processes. Orcel® is FDA approved for the treatment of acute surgical excisions such as donor sites in epidermolysis bullosa patients and burn victims undergoing excision and autografting [63]. Additionally, when compared to Biobrane®, a commercially available acellular bioactive wound dressing (described in Section 2.3.2.2 Dermal Skin Substitutes), for treating donor sites in burn patients, Orcel® showed reduced scarring and shorter healing time than Biobrane® [64]. However, as with allografts and Apligraf®, Orcel® performs as a temporary dressing. The allogenic cells incorporated in Orcel®'s collagen matrix do not persist *in vivo* and the matrix itself resorbs in 7-14 days post-application [5]. These limitations make it unclear as to

whether products based on allogenic cells like Apligraf® and Orcel® will find widespread use in the treatment of burns and other large wounds.

**Table 7: Commercially available composite skin substitutes. This table contains a subset of clinically used products with a description of the components, advantages, and disadvantages of each.**

Skin Substitute Type/Name	Components	Advantages	Disadvantages
<b>Composite</b>			
<b>allograft (cadaveric)</b>	<ul style="list-style-type: none"> <li>• <u>Scaffold</u> – allogenic, native human skin</li> <li>• <u>Cells</u> – allogenic, native dermal and epidermal cells</li> </ul>	<ul style="list-style-type: none"> <li>• Effectively provides pain relief and temporary durable cover during first few weeks post-injury [5]</li> </ul>	<ul style="list-style-type: none"> <li>• Highly immunogenic, provides only temporary wound cover</li> <li>• Risk of disease transmission</li> <li>• Limited availability of skin banks</li> </ul>
<b>Apligraf®</b>	<ul style="list-style-type: none"> <li>• <u>Scaffold</u> – Bovine type I collagen gel matrix</li> <li>• <u>Cells</u> – allogenic keratinocytes and fibroblasts</li> </ul>	<ul style="list-style-type: none"> <li>• Ready availability due to allogenic cell sourcing</li> <li>• Delivers ECM components, cytokines and growth factors to wound bed</li> <li>• Improved functional and cosmetic outcomes when combined with autologous SSG over traditional autologous SSG treatment</li> </ul>	<ul style="list-style-type: none"> <li>• Limited cell viability <i>in vivo</i> [61, 62]</li> <li>• Co-grafting with autologous epithelial source [65]</li> <li>• Short product shelf-life</li> <li>• Risk of disease transmission</li> <li>• High cost (~\$28/cm<sup>2</sup>)</li> <li>• Lack of mechanical stability at dermal-epidermal junction</li> </ul>
<b>Orcel®</b>	<ul style="list-style-type: none"> <li>• <u>Scaffold</u> – Bovine type I collagen sponge with non-porous collagen-gel coating</li> <li>• <u>Cells</u> – allogenic keratinocytes and fibroblasts</li> </ul>	<ul style="list-style-type: none"> <li>• Ready availability due to allogenic cell sourcing</li> <li>• Produces favorable cytokines and growth factors</li> <li>• Reduced scarring</li> </ul>	<ul style="list-style-type: none"> <li>• Limited cell viability <i>in vivo</i> [61, 62]</li> <li>• Co-grafting with autologous epithelial source [65]</li> <li>• Short product shelf-life</li> <li>• Risk of disease transmission</li> </ul>

#### 2.3.2.4 The Future of Bioengineered Skin Substitutes

The numerous products described in the preceding sections show that currently available bioengineered skin substitutes have achieved some clinical success in improving the treatment of a

variety of severe skin injuries. Although not perfect, these products improve survival rates and quality of life after injury of patients with full-thickness extensive burns, chronic ulcers, and other severe skin injuries and diseases. Among the most significant limitations of the current commercially available products is that they generally target limited, specific steps of the wound healing cascade. For example, cultured epithelial autografts focus on rapid restoration of the epidermal layer while acellular dermal constructs emphasize neo-dermal formation and angiogenesis. Current bioengineered skin strategies act as temporary biologically active dressings which provide short term wound care while the patient's own skin regenerates to be used for serial autografting. To date there are no products that fully replace damaged skin.

The ultimate goal in the future development of bioengineered skin products is to produce a construct that rapidly restores normal physiological skin function and homeostasis. There is agreement among scientists that ultimately complete skin restoration will depend on the manipulation of the cells involved in the wound healing cascade. Strategies involving the creation of tissue engineered products based on autologous keratinocytes and fibroblasts have shown promise in this area, but many of the expectations, both clinical and commercial have been unrealistic. These strategies are plagued by long, complicated, and expensive manufacturing, transport, and application procedures and ultimately their cost may outweigh their clinical benefit. Perhaps the real future of skin regeneration lies in the engineering of "smart" biomaterials, those that specifically and molecularly interact with cells to guide regeneration [66].

Development of smart biomaterials for skin regeneration should aim to strategically control skin regeneration mechanisms and mimic the structure and biomechanics of the physical scaffold. Biomaterials may be able to control regeneration mechanisms through the incorporation of cytokines and growth factors that directly affect specific cells in the wound healing cascade. Incorporation of

growth factors and/or cytokines allows the biomaterial scaffold to manipulate specific cell functions such as adhesion, migration, proliferation, and differentiation which direct tissue regeneration. The biomechanics of the scaffold also plays a role in these cell functions. An ideal scaffold for skin regeneration should be flexible and elastic, but also durable and should, largely, resemble the mechanical properties of native skin tissue. Additionally, the physical structure of the scaffold is important. Currently commercially available skin substitutes generally are not designed to mimic the native extracellular matrix structure or topography. Recently, particularly in dermal regeneration strategies, more attention and focus has been given to designing a scaffold that more closely resembles the fibrous structure of native human dermis. Regeneration may also be aided by controlled fiber size and porosity, allowing for cells to adhere and migrate into the scaffold and an intelligent degradation profile which balances the rate of cellular infiltration and growth and degradation allowing cells to replace the implanted material with native tissue.

## **2.4 Electrospinning**

Electrospinning has been used recently to create nanofibrous scaffolds for tissue engineering applications. Electrospinning can be used to create scaffolds made of natural and synthetic polymers with fiber diameters that range from a few nanometers to well over 5  $\mu\text{m}$ . The process provides a high level of consistency and control over fiber diameter and orientation, pore size and porosity, mechanical properties, and degradation rate and can be used to create scaffolds with specifically tailored properties [67-69].

### **2.4.1 The Electrospinning Process**

Electrospinning is a process that uses a potential electric field to spin a polymer solution or melt into small diameter fibers. This is most often accomplished using an apparatus similar to the basic setup shown in Figure 5 with modifications depending on specific desired parameters which make it possible

to spin a wide variety of fibers. The basic setup includes a syringe pump with a syringe connected to a high voltage source. As the polymer solution or melt to be spun is forced through the syringe, high voltage is applied inside the syringe using an immersed electrode which induces free charges into the polymer solution. The charged ions then move towards the electrode of opposite polarity in response to the applied electric field and transfer tensile forces to the polymer liquid. In the presence of the electric field, the polymer drop at the syringe capillary tip becomes a cone like projection and when the applied potential is able to overcome the surface tension of the liquid, the polymer is ejected as a jet from the cone tip. After ejection, the liquid polymer jet undergoes chaotic motion and is directed toward the oppositely charged collector plate. While travelling through the atmosphere, the polymer solvent evaporates from the liquid jet and results in dry fibers being collected on the collection device.

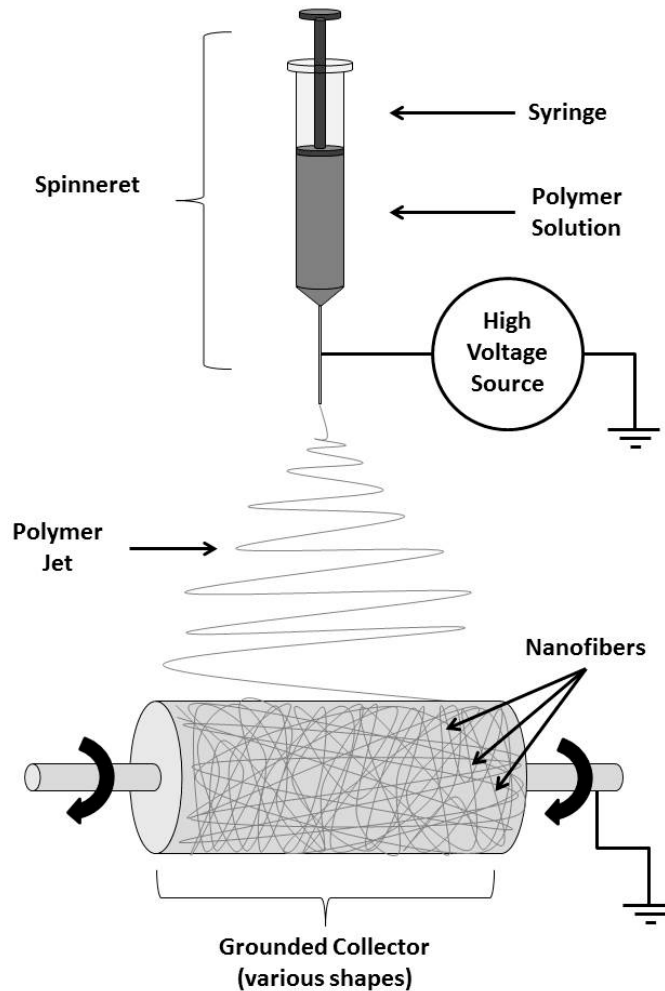


Figure 5: Schematic of the basic electrospinning setup.

The properties of the final collected fibers are influenced by both the electrostatic forces produced by the electrospinning process and by the viscoelastic behavior of the polymers chosen for the specific application. Process parameters that affect nanofiber production include solution feed rate, applied voltage, nozzle-collector distance, and spinning environment, while material properties include solution concentration, viscosity, surface tension, conductivity, and solvent vapor pressure [67]. The specific effects of these process parameters and material properties on the structure and properties of the final collected nanofibers are outlined in Table 8.



Table 8: Effect of process parameters and material properties on electrospun nanofibers [67, 69, 70].

Process parameters	Effects
<b>Polymer flow rate</b>	<ul style="list-style-type: none"> <li>• Influences jet velocity and material transfer rate</li> <li>• In polystyrene (PS) fibers:               <ul style="list-style-type: none"> <li>○ ↑ flow rate = ↑ fiber diameter and pore diameter</li> </ul> </li> </ul>
<b>Applied voltage</b>	<ul style="list-style-type: none"> <li>• ↑ applied voltage = Δ shape of jet initiating point</li> <li>• ↑ applied voltage = ↑ deposition rate, higher mass flow from needle tip</li> <li>• In a PEO/water system:               <ul style="list-style-type: none"> <li>○ ↑ applied voltage = ↑ beaded morphology</li> <li>○ Beaded morphology reduces surface area and influences filtration ability of nanofibers</li> </ul> </li> <li>• In PS fibers and silk like polymer fibers (SLPF):               <ul style="list-style-type: none"> <li>○ ↑ applied voltage = ↓ fiber diameter</li> <li>○ No significant change in pore size distribution</li> </ul> </li> </ul>
<b>Nozzle-collector distance</b>	<ul style="list-style-type: none"> <li>• Influences deposition time, evaporation rate, and instability interval</li> <li>• In SLPF and nylon fibers:               <ul style="list-style-type: none"> <li>○ ↓ nozzle-collector distance = ↑ beaded morphology</li> </ul> </li> <li>• Aqueous polymer systems require ↑ nozzle-collector distance for dry fiber formation than volatile organic solvent systems</li> </ul>
<b>Spinning environmental conditions</b>	<ul style="list-style-type: none"> <li>• Environmental conditions = relative humidity, vacuum conditions, surrounding gas</li> <li>• In acrylic fibers:               <ul style="list-style-type: none"> <li>○ ↑ RH (60%+) = ↓ drying, ↑ entanglement</li> </ul> </li> <li>• Breakdown voltage of atmospheric gases influences fiber charge retaining capacity</li> </ul>

Material properties	Effects
<b>Solution concentration</b>	<ul style="list-style-type: none"> <li>• Influences fiber formation ability: <ul style="list-style-type: none"> <li>○ ↓↓ concentration = droplet formation due to influence of ↑ surface tension</li> <li>○ ↑↑ concentration = no fiber formation due to ↑ viscosity</li> </ul> </li> <li>• In PS fibers: <ul style="list-style-type: none"> <li>○ ↑ concentration = ↑ fiber diameter, narrow pore size distribution</li> </ul> </li> <li>• In PEO/water system: <ul style="list-style-type: none"> <li>○ ↑ concentration = bimodal distribution in fiber diameter</li> </ul> </li> </ul>
<b>Viscosity</b>	<ul style="list-style-type: none"> <li>• ↑ viscosity = fiber jet formation</li> <li>• ↓ viscosity = droplet formation</li> </ul>
<b>Surface tension</b>	<ul style="list-style-type: none"> <li>• ↑ surface tension = droplet formation</li> <li>• ↓ surface tension = fibers form</li> </ul>
<b>Conductivity</b>	<ul style="list-style-type: none"> <li>• Highly influential in jet formation</li> <li>• Jet radius varies inversely as the cube root of the electrical conductivity of the solution</li> </ul>
<b>Solvent volatility</b>	<ul style="list-style-type: none"> <li>• Solvent volatility influences formation of nanostructures within electrospun fibers by influencing the phase separation process</li> <li>• Highly volatile substances = ↑ nanofeatures</li> <li>• Solvent volume ratio affects fiber diameter and morphology <ul style="list-style-type: none"> <li>○ ↑ solvent = ↓ fiber diameter</li> </ul> </li> </ul>

## 2.4.2 Electrospinning for Skin Regeneration

As discussed in section 2.3.1 Design Considerations for Tissue Engineered Skin, one approach to the design of bioengineered skin is the design and development of degradable matrices that support the ingrowth of native cells from wound margins which subsequently degrade the scaffold material and replace it with new tissue [13]. This approach requires a scaffold with specific mechanical and biological properties that are similar to those of native extracellular matrix (ECM) in order to direct the cell functions that ultimately result in new tissue formation. In skin, the native ECM is comprised of a complex network of nano-sized proteins and glycosaminoglycans which create a spatial and temporal environment which influences cell behavior by providing in-direct and direct signaling cues [1]. Consequently, the more closely the scaffold can recapitulate the *in vivo* environment (a combination of ECM composition, physical morphology, surface functional groups, etc.) the more likely it will succeed as a tissue engineered scaffold [71].

Electrospinning has an enormous potential for applications in engineering biologically functional tissue scaffolds due to its ability to create nanofibrous sheets with diverse physical morphologies from a variety of biocompatible natural and synthetic polymers [67, 69]. For skin regeneration in particular, electrospinning shows strong potential due to its ability to create fibrous scaffolds that mimic the fibrillar structure of native dermal tissue [68, 70, 72-74]. The resulting fibrous, three dimensional scaffolds have a high surface area and porosity, allowing cells to readily infiltrate and attach to the scaffold and also provide easy passage for nutrients and metabolic waste exchange [70].

Through simple manipulation of processing parameters, electrospinning provides the ability to easily create scaffolds that have finely tuned fiber and pore sizes and structures that mimic those of native tissue [67]. The mechanical properties of electrospun nanofibrous scaffolds can be specifically tailored to different tissue engineering application needs by varying not just material type, but also solution concentration and fiber orientation [67]. Additionally, electrospinning can be used to create scaffolds that have specific degradation profiles that coincide with or mimic the rate of neo-tissue formation. These degradable scaffolds can also be functionally modified to release various growth factors and cytokines to help direct tissue formation or function as drug carriers in a controlled drug delivery system [68, 74]. Current development has investigated electrospinning technology to create a host of temporary wound dressings, degradable dermal templates, and full-thickness organotypic skin substitutes as treatment options for severe skin regeneration. These are fabricated from a wide variety and combination of natural and synthetic polymers, as shown below in Table 9.

Babaeijandaghi et al. [72] and Khil et al. [75] have utilized electrospun scaffolds as non-degradable, temporary wound dressings. The nanofibrous, porous morphology of their electrospun scaffolds provides better gas permeation, preventing fluid build-up (edema) and its opposite, dehydration, in the wound bed while also providing a mechanical barrier to protect the wound from

infection and applied forces. In *in vivo* wound healing models, both groups found that their electrospun wound dressings showed improved wound healing when compared to control dressings. Babajandaghi et al. [72] found that using their electrospun polyethersulfone (PES) dressings resulted in wounds with greater collagen deposition, more fibroblastic maturation, improved edema, and quicker wound closure when compared to a standard Vaseline coated gauze dressing and a commercially available absorbent wound dressing product, TIELLE® Xtra (Systagenix, North Yorkshire, UK). Similarly, Khil, et al. [75] found that wounds dressed with their electrospun polyurethane (PU) dressing had a less pronounced inflammatory response that was faster to reduce, as well as faster reepithelialization, and evidence of well-organized dermal tissue when compared to the 3M™ Tegaderm™ dressing.

As a biodegradable dermal scaffold, electrospun nanofibers have been shown to support fibroblast growth *in vitro*, and also show increased cellular proliferation and migration over other scaffold morphologies [76]. Collagen has been investigated extensively as an electrospun material for biodegradable dermal scaffolds, both alone and combined with various synthetic polymers, due to its ability to mimic the composition of native dermal tissue. Venugopal, et al. [77, 78] showed that their electrospun polycaprolactone (PCL)-collagen blended scaffolds had better cellular proliferation than PCL alone, and that the PCL-collagen blended scaffolds had better mechanical stability than collagen alone. Liu et al. [79], found that increasing the ratio of collagen to poly(lactic-co-glycolic acid) (PLGA) in their PLGA-collagen blended scaffolds decreased the average fiber diameter. This group also performed a full-thickness *in vivo* wound healing model in rats and found faster and more complete wound healing in wounds dressed with their electrospun PLGA-collagen scaffolds compared to control dressings (DuoDerm and a standard gauze dressing). After 3 weeks the electrospun scaffolds showed complete reepithelialization with newly synthesized tissue and sparse inflammation in the dermis, while the control dressings has incomplete reepithelialization and predominant inflammation.

Schneider et al. [68], used electrospinning technology to create a biofunctionalized dermal dressing by incorporating epidermal growth factor (EGF) directly into their silk nanofibers as a part of the electrospinning process. These biofunctionalized electrospun silk scaffolds showed improved reepithelialization in an *in vitro* wound model by providing physical protection to the wound and by slowly releasing EGF directly into the wound bed. The addition of the growth factor increased the rate of wound closure by more than 3.5-fold in comparison to non-biofunctionalized electrospun silk scaffolds. The ability to incorporate growth factors into electrospun nanofibers and then release them directly into the wound bed is a promising treatment for chronic wound application. Many chronic wound pathologies are compounded by a compromised native wound healing response , especially in terms of the skin's ability to regulate growth factor production and delivery to the wound site.

The idea of creating a full-thickness skin scaffold that incorporates an electrospun scaffold to mimic the structure of native dermal ECM seeded with a cellular epidermal layer has also been investigated by several groups. Powell and Boyce [80] created a full-thickness, organotypic scaffold by seeding an electrospun gelatin scaffold with human keratinocytes and fibroblasts. They demonstrated that development of a thick, well-stratified epithelium and organized dermal component in their electrospun scaffolds was dependent on scaffold morphology. In particular an interfiber distance, which was influenced by polymer solution concentration, plays a key role in cellular function. Interfiber distances between 5 and 10 $\mu$ m appeared to promote high cell viability, optimal cell organization, and excellent barrier formation [80], but this technology requires the use of living cells and could be expected to suffer from many of the same limitations as commercially available composite, organotypic bioengineered skin substitutes (see list in 2.3.2.3 Composite Skin Substitutes).

Blackwood et al. [73] utilized a synthetic electrospun dermal substitute that ultimately when seeded with autologous keratinocytes and fibroblasts as a full-thickness, organotypic skin substitute,

aims to reduce disease transmission and lead to greater clinical uptake of tissue engineered skin. They investigated different PLGA solutions and showed that their poly(lactic-co-glycolic acid) (PLGA) were able to support the growth of human keratinocytes, fibroblasts, and endothelial cells *in vitro* using an MTT assay. They also showed that *in vitro* collagen deposition was enhanced in grafts that were seeded with a co-culture of fibroblasts and keratinocytes. An *in vivo* subcutaneous implant study showed that acellular electrospun scaffolds became fully impregnated with native skin cells 7 weeks after implantation, with the most promising scaffold PLGA blends having full impregnation by 4 weeks. The same *in vivo* study was used to investigate scaffold degradation, which showed that the most promising PLGA scaffold blends lost approximately 50% of their mass 3-4 months after implantation and were almost completely degraded by 5-6 months post-implantation.

In a separate study [74], this group showed that they could dissolve an anti-inflammatory drug (Ibuprofen) in the organic solvent used to create the PLGA polymer solution prior to electrospinning and then directly spin it into the scaffold fibers. These scaffolds showed a steady, sustained release of Ibuprofen over a period of more than a week, and found that the addition of the drug did not hinder the attachment or function of seeded cells. The incorporation of soluble drugs and growth factors directly into electrospun fibers is a promising strategy that may help to enhance and accelerate aspects of the wound healing process, such as inflammation, which may be compromised in patients with chronic skin ulcers.

There may be some significant limitations in the creation of full-thickness, organotypic, electrospun scaffolds. Studies of clinically available organotypic bioengineered skin substitutes, such as Apligraf®, have shown that the implanted cells only remain viable for one to two months *in vivo* following implantation. As a result, these organotypic skin substitutes actually perform more like temporary wound dressings, and often need to be used in combination with other wound closure

strategies in order to close full-thickness wounds that are unable to reepithelialize themselves [5]. While no studies have investigated whether long-term viability of cells poses the same issue in organotypic scaffolds that include an electrospun component, it could certainly be a limitation of this approach. Other potential limitations of this strategy may include a short shelf-life and a high manufacturing cost which are also limitations of Apligraf® [5].

One approach to engineering a full-thickness scaffold while circumventing some of these limitations may be in the creation of an acellular, bi-layered, composite electrospun scaffold for skin regeneration. A composite scaffold could incorporate a non-degradable electrospun barrier or pseudo-epidermal layer similar to the temporary electrospun wound dressings developed by Babaeijandaghi et al. [72] and Khil et al. [75], which provide mechanical protection to the wound and also maintain appropriate moisture flux, with a biodegradable electrospun dermal layer to attract and support fibroblasts and encourage dermal regeneration. Composite scaffolds have been developed as biomimetic strategies for other tissues with layered or zonal structures, such as repairing defects in tendon-bone insertion sites [81], but to date this strategy has not been utilized for skin regeneration.

Table 9: Electrospun strategies for skin regeneration

Research Group	Scaffold	Approach/Motivation/Major Findings
Babaeijandaghi et al., 2010 [72]	Polyethersulfone (PES)	<p><b>Approach</b></p> <ul style="list-style-type: none"> <li>• Non-degradable, temporary wound dressing</li> </ul> <p><b>Motivation</b></p> <ul style="list-style-type: none"> <li>• Create a wound dressing to accelerate healing and restore skin function and appearance</li> <li>• Investigate utility of electrospun scaffolds in <i>in vivo</i> wound healing</li> </ul> <p><b>Major Findings</b></p> <ul style="list-style-type: none"> <li>• Able to modify process parameters to create thicker (~3mm) dressings with nanofibers of ~500nm diameter and 76% porosity</li> <li>• Electrospun PES showed similar biocompatibility and proliferation to tissue culture polystyrene (TCPS)</li> <li>• 90% wound healing closure by electrospun PES by day 10</li> <li>• Greater collagen deposition, more fibroblastic maturation, and improved edema in PES vs. control dressings</li> </ul>
Khil et al., 2003 [75]	Polyurethane (PU)	<p><b>Approach</b></p> <ul style="list-style-type: none"> <li>• Non-degradable, temporary wound dressing</li> </ul> <p><b>Motivation</b></p> <ul style="list-style-type: none"> <li>• Create a wound dressing with better gas permeation to protect wound from infection and dehydration and edema</li> <li>• Investigate <i>in vivo</i> wound healing compared to commercially available control wound dressing (Tegaderm)</li> </ul> <p><b>Major Findings</b></p> <ul style="list-style-type: none"> <li>• By day 3, PU dressing showed reduced inflammation and scab formation compared to control dressing</li> <li>• At 15 days, PU dressing had less inflammation and evidence of well-organized dermis formation</li> <li>• PU dressings showed faster inflammatory reduction and epithelialization rate compared to control</li> </ul>



<p>Schneider et al., 2009 [68]</p>	<p>Silk functionalized with epidermal growth factor (EGF)</p>	<p><b>Approach</b></p> <ul style="list-style-type: none"> <li>• Temporary, bioactive wound dressing to promote reepithelialization</li> </ul> <p><b>Motivation</b></p> <ul style="list-style-type: none"> <li>• Create a wound dressing that promotes rapid healing by promoting reepithelialization</li> </ul> <p><b>Major Findings</b></p> <ul style="list-style-type: none"> <li>• EGF was incorporated into silk dressings during the electrospinning process</li> <li>• EGF increased the rate of wound closure by more than 3.5-fold compared to silk dressings without EGF in an <i>in vitro</i> wound healing model</li> <li>• Silk dressings improve <i>in vitro</i> reepithelialization by providing physical protection and slowly releasing EGF directly into the wound bed</li> </ul>
<p>Liu et al., 2010 [79]</p>	<p>PLGA/collagen (varied ratios)</p>	<p><b>Approach</b></p> <ul style="list-style-type: none"> <li>• Biodegradable dermal matrix</li> </ul> <p><b>Motivation</b></p> <ul style="list-style-type: none"> <li>• Develop biodegradable, biomimetic scaffolds to attract and support fibroblasts for dermal regeneration</li> <li>• Investigate <i>in vivo</i> wound healing compared to commercially available control dermal scaffold (DuoDerm)</li> </ul> <p><b>Major Findings</b></p> <ul style="list-style-type: none"> <li>• No signs of <i>in vitro</i> cytotoxicity</li> <li>• 50/50 PLGA/collagen showed significance in proliferation level over other ratios</li> <li>• PLGA/collagen demonstrated superior <i>in vivo</i> wound healing compared to gauze and DuoDerm</li> <li>• At 3 weeks, PLGA/collagen showed newly synthesized dermal tissue with sparse inflammatory cells and complete reepithelialization</li> </ul>

Cantón et. al., 2010 [74]	Ibuprofen-releasing biodegradable PLA/PGA	<p><b>Motivation</b></p> <ul style="list-style-type: none"> <li>• Temporary guide for promoting tissue formation in chronic wounds (biodegradable scaffold)</li> <li>• Reduce pain and excessive inflammation (Ibuprofen)</li> </ul> <p><b>Major Findings</b></p> <ul style="list-style-type: none"> <li>• Ibuprofen is effectively loaded into and released from scaffolds <ul style="list-style-type: none"> <li>○ Reduces response of cells to major inflammatory cytokines</li> <li>○ Does not compromise fibroblast attachment and migration in scaffold</li> </ul> </li> <li>• Acid soluble Ibuprofen is dissolved in the same solvent as the polymer and can be spun directly into the scaffold fibers</li> <li>• Spinning environment affects scaffold variability</li> <li>• Scaffold degrades completely in 6 days <ul style="list-style-type: none"> <li>○ Avoids need to remove the dressing</li> </ul> </li> </ul>
Blackwood et al., 2008 [73]	PLA/PGA different ratios	<p><b>Approach</b></p> <ul style="list-style-type: none"> <li>• Full thickness organotypic skin substitute comprised of a synthetic, electrospun dermal matrix seeded with autologous cells</li> </ul> <p><b>Motivation</b></p> <ul style="list-style-type: none"> <li>• Using autologous keratinocytes and fibroblasts seeded into a synthetic dermal scaffold may reduce disease transmission and lead to greater clinical uptake compared to current organotypic approaches</li> </ul> <p><b>Major Findings</b></p> <ul style="list-style-type: none"> <li>• Scaffolds support the growth of human keratinocytes, fibroblasts, and endothelial cells <i>in vitro</i></li> <li>• Strong collagen synthesis/deposition <i>in vitro</i></li> <li>• Scaffolds implanted sub-cutaneously in rats showed full impregnation by native cells within 7 weeks of implantation</li> <li>• The most promising scaffold blends were the PLGA 85:15 and 75:25 blends which both showed full cellular impregnation within 4 weeks and complete scaffold degradation in 3-4 months <i>in vivo</i></li> </ul>

## 2.5 Summary

To summarize, chronic skin ulcers pose a significant problem due to their inability to properly heal following the native wound healing cascade. The current gold standard treatment is autografting which has the ability to quickly close severe skin wounds with a graft of intact matrix, cells, and growth factors, but is limited by high incidences of infection, severe scarring, lack of suitable donor sites, and donor site morbidity. A variety of bioengineered skin substitutes have been developed in an effort to address these limitations and have achieved some level of clinical success, but are themselves limited by infection, scarring, sub-optimal wound healing, slow rates of tissue ingrowth, and a lack of mechanical stability. There is a need to develop bioengineered skin substitutes which mimic the structural and mechanical properties of native skin tissue while encouraging rapid cellular ingrowth and vascularization and protecting the wound from bacterial insult.

We propose novel bi-layered electrospun polymer composite matrices as a potential scaffold for dermal regeneration. Electrospinning has been used to create nanofibrous dermal scaffolds, which mimic the fibrillar collagen extracellular matrix of native dermal tissue, as well as temporary wound dressings whose porous structure allows for better gas exchange to minimize dehydration and edema and prevent infection. Our proposed matrices utilize a biodegradable electrospun dermal component, which potentially contains a mitogenic growth factor, to encourage dermal tissue ingrowth. This will be combined with a non-degradable electrospun barrier component which potentially contains an antimicrobial and acts as a porous, temporary mechanical wound barrier to protect the wound from bacterial insult and applied stresses and strains while allowing for gas exchange.

## Chapter 3: Hypothesis and Specific Aims

The goal of this project is to engineer a novel scaffold for dermal regeneration that mimics the structure and functions of native tissue, promotes rapid neodermal tissue formation, and provides a robust wound barrier. Towards this goal, we hypothesize that an electrospun polymer composite scaffold will support human dermal fibroblast attachment and outgrowth and provide an appropriate structural and mechanical matrix for dermal tissue regeneration. Characterization of the structural and mechanical properties of the scaffold will verify that the scaffolds are suitable for integration into native dermal tissue. Additionally, qualitative analysis of cell attachment and migration will show that scaffolds are capable of supporting the migration and growth of native cells from the native tissue surrounding severe skin wounds.

This project specifically investigated two different electrospun composite matrices each with a unique polymer blend. Each blend incorporates a non-degradable barrier layer which functions as a pseudo-epidermis, the intent being to provide some temporary wound coverage while dermal regeneration occurs. Blend A has a barrier layer made up of electrospun polyethylene terephthalate/polybutylene terephthalate (PET/PBT), two polyesters which are non-degradable, biocompatible, rigid polymers designed to provide a physical barrier and mechanical integrity for the scaffold. Knitted and woven polyester scaffolds have been used extensively in medical applications where a non-degradable and mechanically robust polymer blend is desired such as in large diameter vascular grafts, arterial patches, and valve sewing rings [82]. The particular polymer blend used in the barrier layer of our Blend A scaffold (PET/PBT) was selected for the mechanical strength (tensile strength and suture retention) these polyesters provide to the scaffold. Additionally, the PET gives the scaffold with excellent material handling properties (soft flexibility). The Blend B barrier layer is comprised of polyurethane/polyethylene terephthalate (PU/PET), combining one rigid polyester (PET) with a more flexible polymer (PU) to provide mechanical integrity while mimicking some of the elasticity of native

tissue. Previously, Khil et al. [75] investigated a PU electrospun scaffold as a non-degradable, temporary wound dressing. This group sought to utilize electrospinning technology to create a scaffold with better gas permeation which reduces infection and the occurrence of dehydration and edema in the wound bed. They found that compared to control dressings, the electrospun dressing had less inflammation, faster epithelialization rate, and a well-organized underlying dermis.

Blend A and Blend B have the same dermal layer, which is electrospun directly onto each barrier layer to form composite scaffolds. The dermal layer is composed of electrospun polycaprolactone/polyglycolic acid (PCL/PGA) combining the two biodegradable, biocompatible polymers to form a nanofibrous matrix to support tissue ingrowth and neodermis formation. The combination of PGA and PCL was chosen to take advantage of two different degradation profiles. PGA undergoes rapid degradation *in vivo* (complete degradation occurs in 2-4 weeks) while PCL persists longer (complete degradation may not occur for several months to a year) allowing us to create a scaffold that degrades in phases [82]. The first phase is intended to coincide with the infiltration and proliferation of fibroblasts into the scaffold with the PGA degrading to make room while the PCL maintains the scaffold structure. In future iterations of our scaffold design, the rapid degradation of PGA could be harnessed as a vessel for incorporating growth factors to stimulate rapid wound healing directly into the dermal layer of our scaffold. A schematic of the two investigated blends is shown in Figure 6.

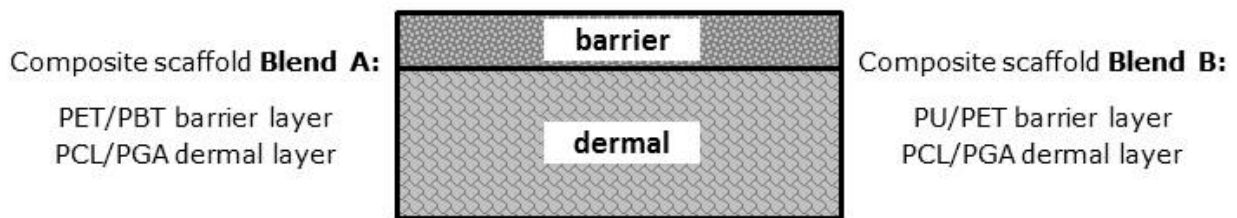


Figure 6: Schematic showing two different blends of electrospun polymer composite matrix

In order to characterize these electrospun matrices two specific aims were identified for this project:

**Specific Aim 1: Evaluate the physical and mechanical properties of the proposed scaffolds and compare them to native tissue.**

This aim hypothesizes that the electrospun polymer composite scaffolds have physical and mechanical properties that are similar to native tissue to support dermal regeneration. To test this, we used scanning electron microscopy (SEM) images and measured fiber diameter and fiber orientation in the various layers of the scaffolds. The resulting distributions of measurements were analyzed by plotting the measurements as histograms and comparing the data to published observations of native dermal tissue. Fiber diameter measurements were also used to calculate the specific surface area of individual blends and layers of our electrospun scaffolds. Mechanical properties of the proposed scaffolds were measured by loading dog bone shaped scaffolds under uniaxial tension and various properties including ultimate tensile strength (UTS), strain at failure, and tangent elastic modulus were extrapolated.

Each of the experiments in specific aim one was conducted on composite scaffolds (for SEM imaging composite scaffolds were mounted with either the barrier or dermal side upward) and all results were compared to published values of native skin and/or dermal tissue. All physical and mechanical properties were measured with respect to scaffold orientation dictated by a cylindrical mandrel collection plate utilized during electrospun scaffold fabrication.

**Specific Aim 2: Evaluate the biologic activity of the proposed scaffold**

The hypothesis of this aim is that the electrospun polymer composite scaffolds will support the outgrowth of normal human fibroblast cells. To test this hypothesis we conducted two experiments. The first study utilized a colorimetric MTT assay to quantify initial fibroblast attachment on the various layers

of the proposed scaffolds four hours after seeding. Results were compared to fibroblast attachment on tissue culture polystyrene (TCPS) and collagen-glycosaminoglycan sponges which served as control substrates. In the second experiment dermal fibroblast outgrowth was investigated using a custom outgrowth culture platform. This culture platform allowed us to measure the outgrowth of cells from a fibroblast populated collagen gel onto proposed scaffolds over the course of 14 days. The rate of outgrowth was compared to published data from studies that investigated fibroblast migration in collagen-GAG sponges and native tissue.

Each of the experiments in specific aim two was conducted on composite scaffolds. Scaffolds in the attachment study were seeded such that either the barrier or dermal side was oriented upward in a 24-well plate. Fibroblasts were then seeded only on the surface of the substrate. Cell outgrowth studies were performed on thin strips of electrospun scaffold and measurements were made only of cells on the dermal layer.

## Chapter 4: Materials and Methods

This section contains a description of the procedures and materials used to test the hypothesis and accomplish the specific aims of this project. It provides a detailed description of scaffold characterization including morphology characterization using scanning electron microscopy, uniaxial tensile testing, the use of an MTT assay to determine cell attachment, a cellular outgrowth assay, and statistical analysis.

### 4.1 Electrospun Polymer Composite Matrices

Custom blended electrospun polymer composite matrices were obtained from BioSurfaces, Inc. (Ashland, MA). Two different polymer blends were investigated: Blend A is comprised of a polycaprolactone/polyglycolic acid (PCL/PGA) dermal layer electrospun directly onto a polyethylene terephthalate/polybutylene terephthalate (PET/PBT) barrier layer. Blend B utilizes the same dermal layer component electrospun directly onto a polyurethane/ polyethylene terephthalate (PU/PET) barrier. A schematic of the two investigated blends is shown in Figure 7.

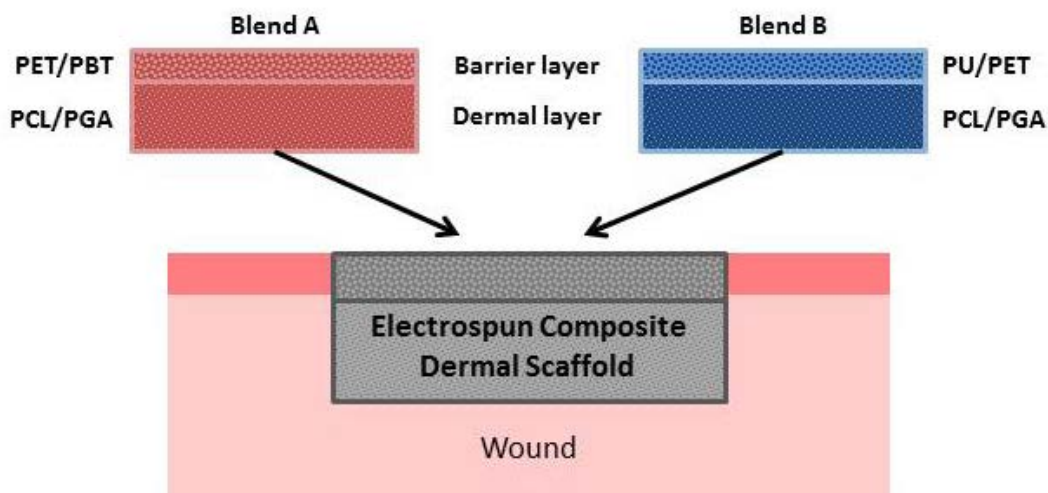


Figure 7: Schematic showing two different blends of electrospun polymer composite matrix.



## 4.2 Physical and Mechanical Properties of Electrospun Scaffolds

In order to evaluate the physical and mechanical properties of our electrospun scaffolds, we used scanning electron microscopy and uniaxial tensile testing. Scanning electron microscopy allowed us to visualize scaffold morphology and make quantitative measurements of fiber diameter and fiber angle for each electrospun scaffold blend and layer. We compared these measurements to published fiber diameter and orientation profiles for native tissue. Pulling composite electrospun scaffolds to failure under uniaxial tension to generate force and extension data, allowed us to quantify ultimate tensile strength, strain at failure, and tangent elastic modulus for each blend. These mechanical properties were also compared to published values for native skin.

### 4.2.1 Scaffold Morphology

Scaffold morphology was analyzed using scanning electron microscopy (SEM). Representative images of each layer (barrier or dermal) of each material blend (Blend A or B) were taken using a JEOL JSM-7000F field emission scanning electron microscope and the associated software. Pieces of composite electrospun scaffolds were mounted on stainless steel stubs (12.2 mm diameter x 10 mm; Ted Pella, Inc.; Redding, CA) using carbon tape (Electron Microscopy Sciences; Hatfield, PA) with either the barrier or dermal side oriented upward, as shown in Figure 8. Samples were prepared from a single batch of Blend A electrospun scaffolds and two different batches of Blend B scaffolds. The stubs were sputter coated with gold palladium for 1 minute at 25 mA using an EMS 550 sputter coater (Electron Microscopy Sciences) immediately before imaging. Samples were mounted and imaged in such a way that the orientation of the sample and its relationship to the orientation of the cylindrical mandrel collecting plate used during the electrospinning were known (images were taken such that the bottom of the image was aligned parallel to the long (longitudinal) axis of the mandrel and perpendicular to the circumferential axis as shown in Figure 8). Images were taken at four random locations on each sample at both 500x and 1500x magnification. Additional images were taken of the failure plane of samples that

had been previously loaded to failure as a part of the uniaxial tensile testing experiments (described in 4.2.3 Mechanical Properties).

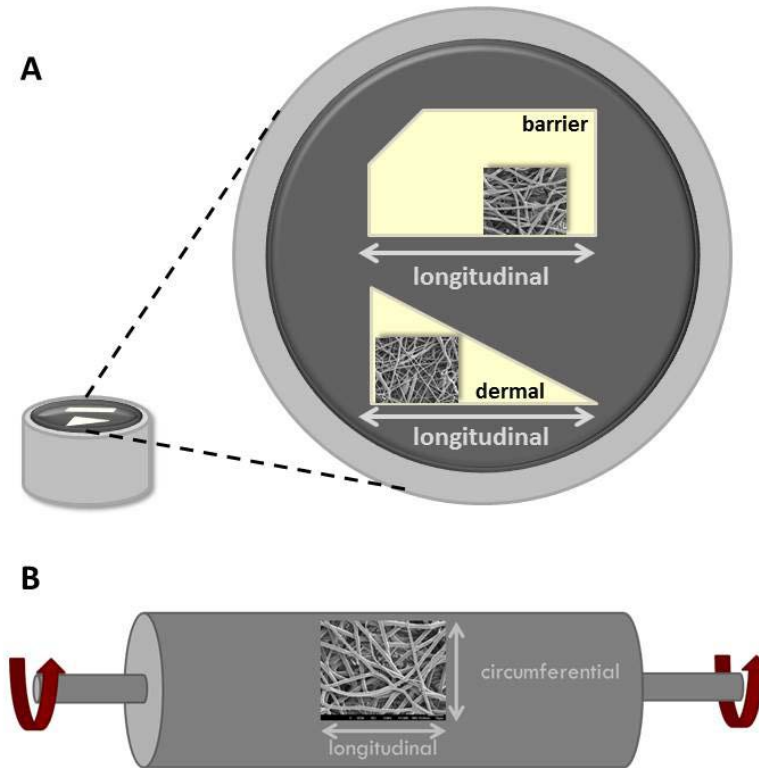


**Figure 8:** Samples were prepared for SEM by mounting on stainless steel stubs with carbon tape [A]. Particular attention was paid when cutting, adhering, and imaging samples such that the longitudinal axis of the samples (as dictated by the cylindrical mandrel collecting plate used during scaffold production [B]) was oriented along the long axis of the images.

In order to measure fiber diameter, each SEM image was overlaid with a grid of four equally spaced vertical and four equally spaced horizontal lines using Microsoft PowerPoint (Figure 9A) creating a grid of 25 rectangles each measuring 90 x 72 pixels . Image J (NIH) analysis software was then used to measure the diameter of fibers in the uppermost plane of each image. Each fiber was marked (Figure 9B) with a small dot and then measured (Figure 9C) once per grid square. At least 400 measurements were made per image. Diameter measurements were exported from ImageJ to Microsoft Excel and

binned in 100nm increments. The number of measurements per bin was counted and histograms of percent frequency (Equation 1) vs. bin were plotted for each blend and layer (Figure 9D).

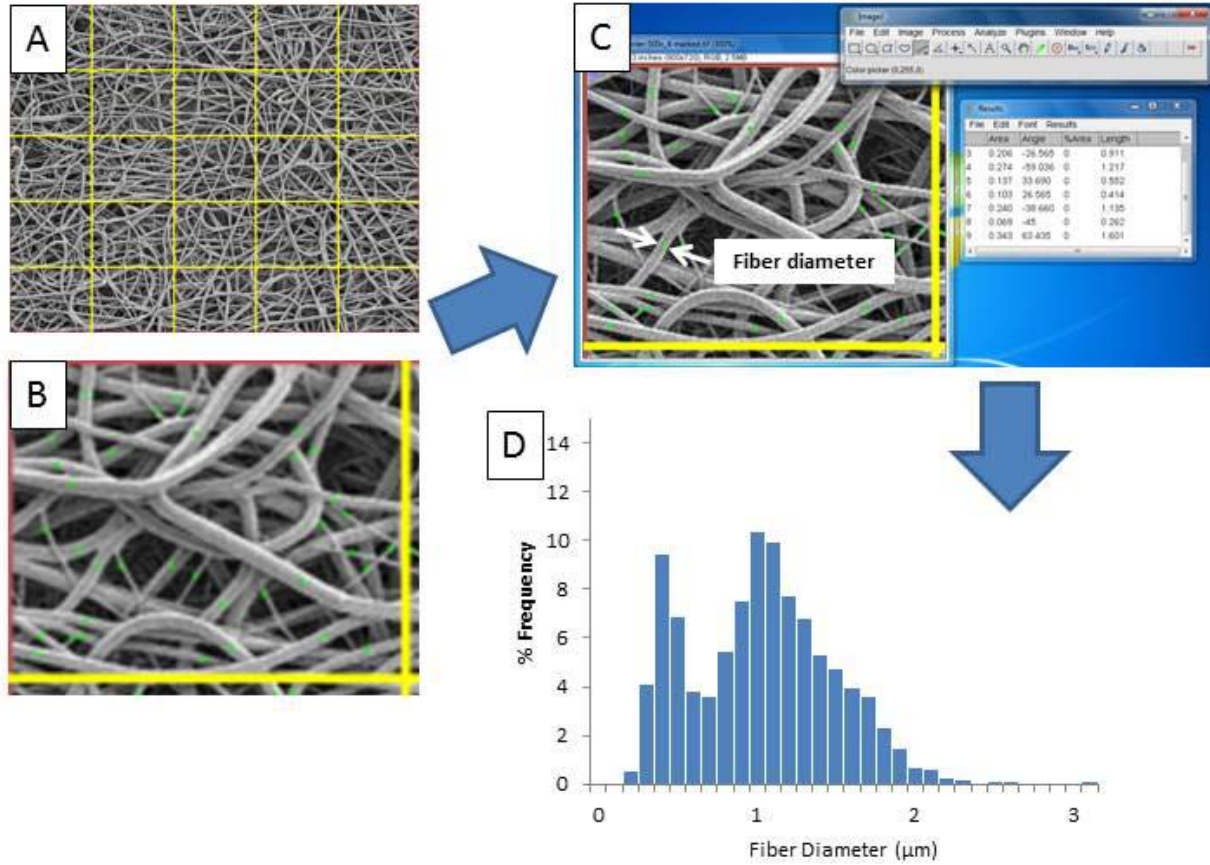


Figure 9: Method for quantifying the distribution of fiber diameter in electrospun scaffolds. ImageJ was used to measure fibers (A-C) and Microsoft excel was used to create histograms showing frequency of various fiber diameters in each blend/layer (D).

Equation 1: Calculating percent frequency (%Frequency) of scaffold morphology measurements.

$$\% \text{ Frequency} = \frac{\text{number of measurements in particular bin}}{\text{total number of measurements}} \times 100\% \quad (1)$$

Fiber angle was also measured using the SEM images with an overlaid grid (Figure 10A). Image J was used to measure the angle of fibers where they crossed the grid. Only the fibers the focus plane of the image were measured and a measurement was made at each point at which a fiber crossed the

horizontal or vertical gridlines (Figure 10B). Between 180-500 measurements were made per image. Angle measurements were exported from ImageJ to Microsoft Excel and binned in 5° increments. The number of measurements per bin was counted and histograms of percent frequency (Equation 1) vs. bin were plotted for each blend and layer (Figure 10C). Additional analysis was also made to determine the percentage of fibers aligned locally ( $\pm 15^\circ$ ) to the horizontal and vertical image axis, which correspond to the longitudinal and circumferential axes respectively of the spinning mandrel used during the electrospinning process as shown in Figure 8. A separate percentage was calculated for each image and then averaged.

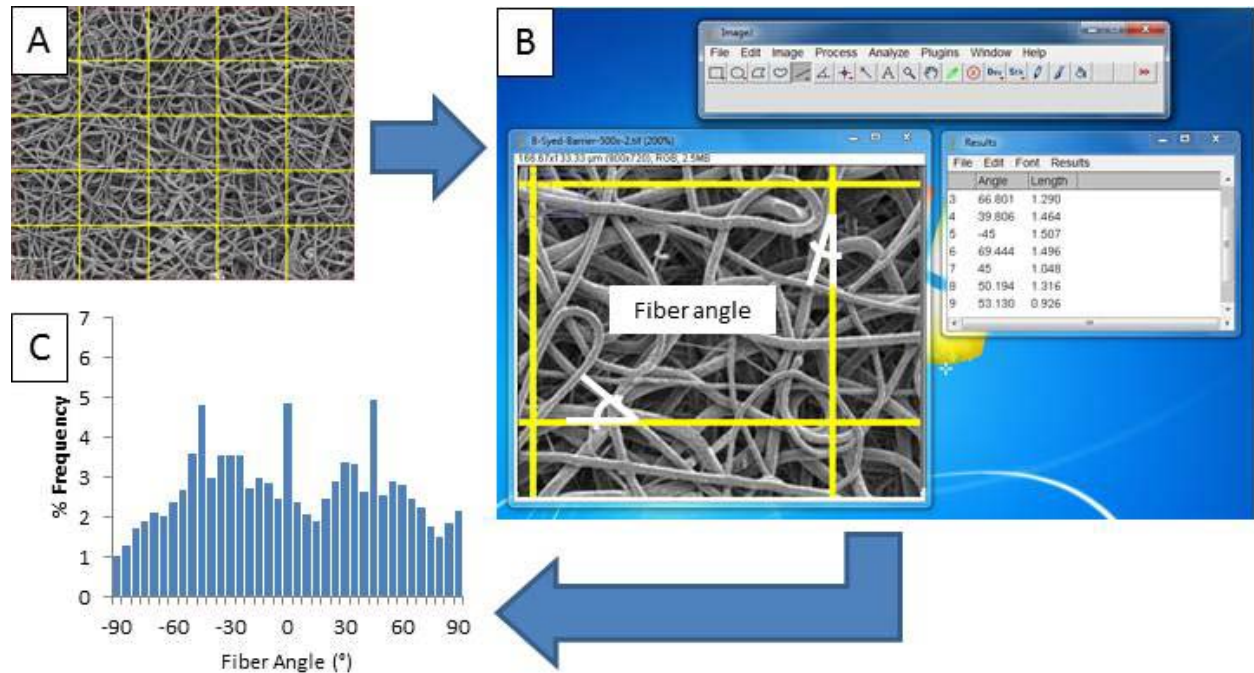


Figure 10: Method for quantifying the distribution of fiber angle in electrospun scaffolds. ImageJ was used to measure fiber angles with respect to the horizontal axis (A-B) and Microsoft excel was used to create histograms showing frequency of various fiber angles in each blend/layer (C).

#### 4.2.2 Specific Surface Area

The specific surface area (SSA; surface area/volume) of each scaffold blend and layer was calculated using the following equation [83]:

Equation 2: Equation for calculating specific surface area (SSA) of nanofibrous electrospun scaffolds

$$SSA = \frac{\text{total surface area}}{\text{total volume}} = \frac{2\pi r l}{\pi r^2 l} = \frac{4 \sum_{i=1}^n D_i f_i}{\sum_{i=1}^n D_i^2 f_i} \quad (2)$$

Where D is fiber diameter measured from SEM images using ImageJ as described in 4.2.1 Scaffold Morphology and f is fiber frequency.

#### 4.2.3 Mechanical Properties

Uniaxial tensile testing was performed in order to determine ultimate tensile strength (UTS), strain at failure, and tangent elastic modulus (TEM) as well as to investigate the relationship between the nanofibrous directionality of the electrospun polymer composite matrices and their mechanical properties. Matrices of each polymer blend were cut into dog-bone shaped samples using a custom die punch with dimensions defined in Figure 11.

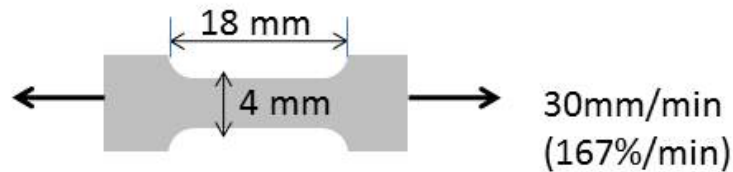


Figure 11: Dimensions of dog bone shaped scaffolds for uniaxial tensile testing

Samples were cut along either the “x” or “y” orientation of the material as defined relative to the orientation of the rotating cylindrical mandrel collecting plate utilized during the electrospinning process. For all samples the x-direction was defined as being cut along the length of the mandrel

(longitudinal axis) and the y-direction was cut circumferential to the mandrel as illustrated in Figure 12. The thickness of each sample was measured using a digital micrometer and was used to calculate the cross-sectional area, assuming rectangular cross-sectional geometry.

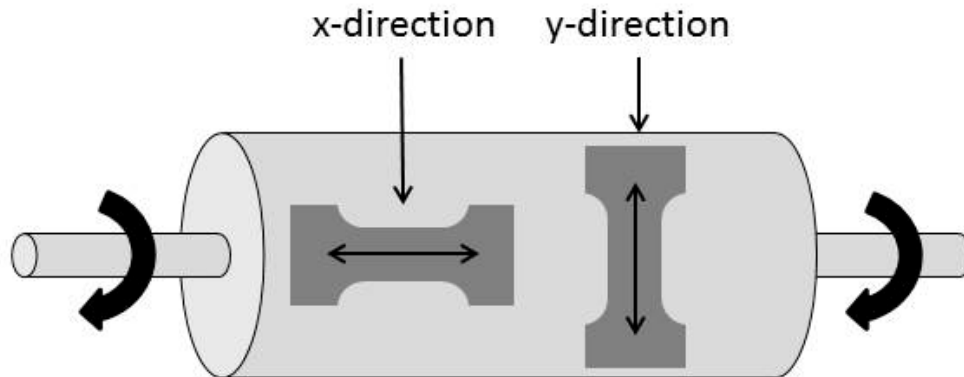


Figure 12: Sample cutting orientation for uniaxial tensile testing

Samples were loaded onto the Instron ElectroPuls E1000 uniaxial testing machine (Instron Inc., Norwood, MA) with a 50N load cell and screw action grips. Matrices were then pulled to failure at a constant strain rate of 30mm/min. Stress vs. strain curves were generated from force and extension data generated by the machine. As shown in Figure 13, ultimate tensile strength (UTS) was defined as the peak stress value on the stress-strain curve for each sample and the corresponding strain value was recorded as the strain at failure. Tangent elastic modulus (TEM) was calculated using Microsoft Excel as the slope of a best fit line ( $R^2 > 0.95$ ) for the initial linear (elastic) portion of each stress-strain curve.

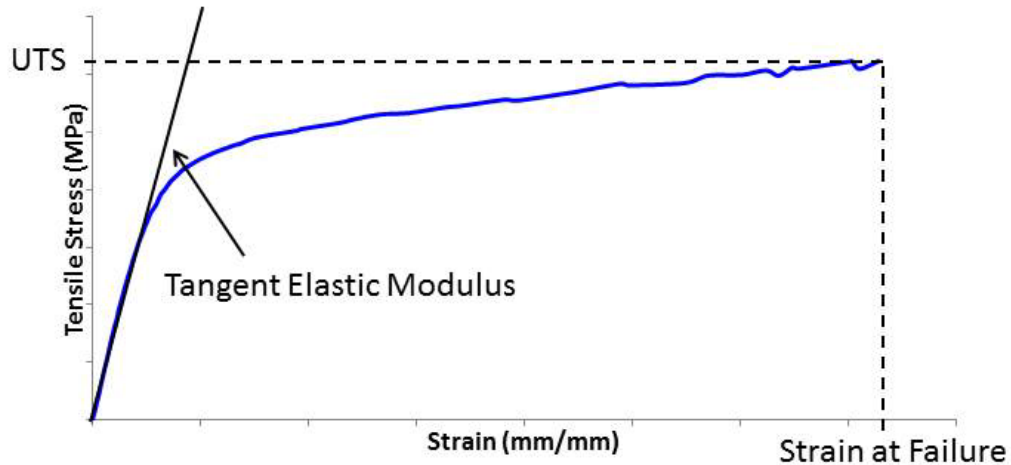


Figure 13: Using the stress-strain curve to define mechanical properties of electrospun polymer composite matrices.

### 4.3 Biologic Activity of Electrospun Scaffolds

We performed two experiments to evaluate the biologic activity of our electrospun scaffolds by quantifying the behavior of primary dermal fibroblasts on the scaffolds *in vitro*. An MTT (3-(4,5-dimethylthiazol-2-yl)-2,5-diphenyltetrazolium bromide) assay allowed us to quantify initial attachment and viability of cells seeded on our scaffolds compared to control substrates. A custom outgrowth platform allowed us to model outgrowth of dermal fibroblasts from an *in vitro* wound model (fibroblast populated collagen gel) onto our electrospun scaffolds over a period of 14 days.

#### 4.3.1 Cell Culture

Human dermal fibroblasts isolated from neonatal foreskin tissue as previously described [84] were used for all experiments. Fibroblasts (were cultured in a medium composed of Dulbecco's modified Eagles medium (DMEM; Gibco, Gaithersburg, MD) supplemented with 10% fetal bovine serum (FBS; Hyclone, Logan, UT), 100 U penicillin and 100 $\mu$ g streptomycin per mL (Gibco). Cells were incubated at 37°C in 10% CO<sub>2</sub> and atmospheric oxygen. For the cellular outgrowth assay, the fibroblasts used were modified to overexpress green fluorescent protein (GFP) as previously described [85, 86]. GFP-

fibroblasts were used at passages 8-12 for these experiments. Unmodified fibroblasts (passage 6-10) were used for all other assays.

#### 4.3.2 Quantifying Cell Attachment by MTT Assay

To measure cellular attachment on our electrospun polymer composite scaffolds, matrices of each blend were cut into 9/16 inch diameter discs and sterilized by exposure to ethylene oxide gas for 12 hours using an Anprolene AN74i gas sterilizer (Anderson Products, Inc., Haw River, NC). Prior to cell seeding, scaffolds were placed in non-tissue culture treated 24-well plates with either the barrier or dermal side oriented upward. Samples were rinsed in phosphate buffered saline (PBS; EMD Chemicals Inc., Gibbstown, NJ) for 30 minutes and gently compressed with a sterile scoopula to encourage complete wetting of the scaffolds before the PBS was aspirated (Figure 14A). Fibroblasts were trypsinized and counted using a hemocytometer and spot seeded on the surface of the prepared scaffolds in a 50 $\mu$ L drop at a concentration of  $5.0 \times 10^5$  cells/mL (Figure 14B). Tissue culture treated polystyrene (TCPS) and collagen-GAG sponge controls (fabricated as described previously [84]) were prepared as positive controls and seeded using the same methods. A standard curve of known concentrations of fibroblasts on a 96-well TCPS plate was also prepared. All samples were incubated at 37°C for 4 hours and then rinsed with PBS to remove non-adherent cells. Thiazoyl blue tetrazolium bromide (MTT; Sigma, St. Louis, MO) was prepared at a final concentration of 1 mg/mL and 0.5mL was added to each well and incubated for 2 hours at 37°C (Figure 14C). After incubation, each sample was rinsed with PBS and a 3/4 inch punch was used to remove the excess material around the cell spot (Figure 14D). To lyse the cells, dimethyl sulfoxide (DMSO; Sigma) was added to each well and plates were placed on an orbital shaker plate for 10 minutes (Figure 14E).



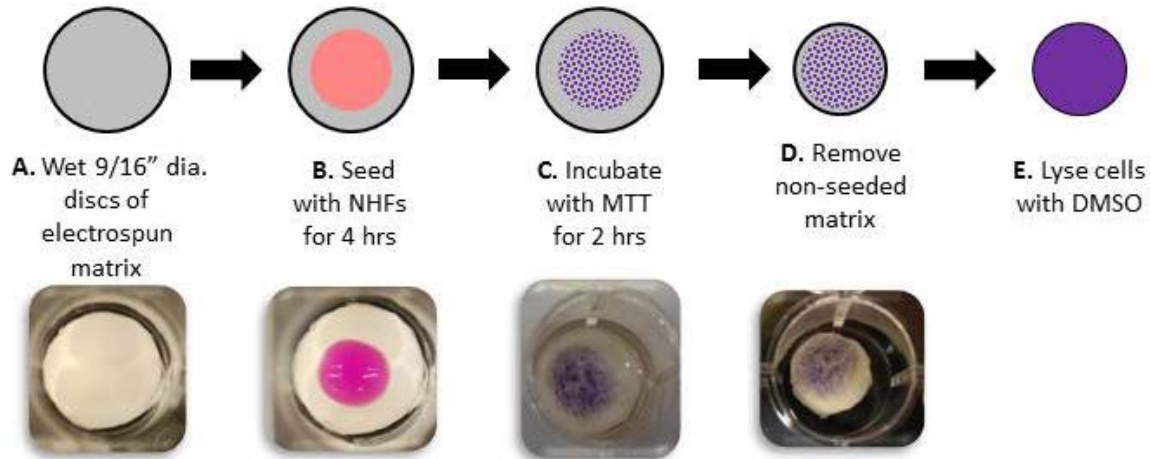


**Figure 14: Scaffold seeding method for quantification of cell viability with MTT assay.**

A 100 $\mu$ L sample of the DMSO cell lysate from each electrospun polymer scaffold and control sample well was read in a SpectraMax250 spectrophotometer (Molecular Devices, Sunnyvale, CA) to measure the amount of dye absorbed by the cells in each well. Absorbance values from the experimental groups were compared with absorbance values from the standard curve of known concentrations of fibroblasts and a linear regression ( $R^2 > 0.99$ ) was used to quantify the number of cells attached to each scaffold, as shown in Figure 15.

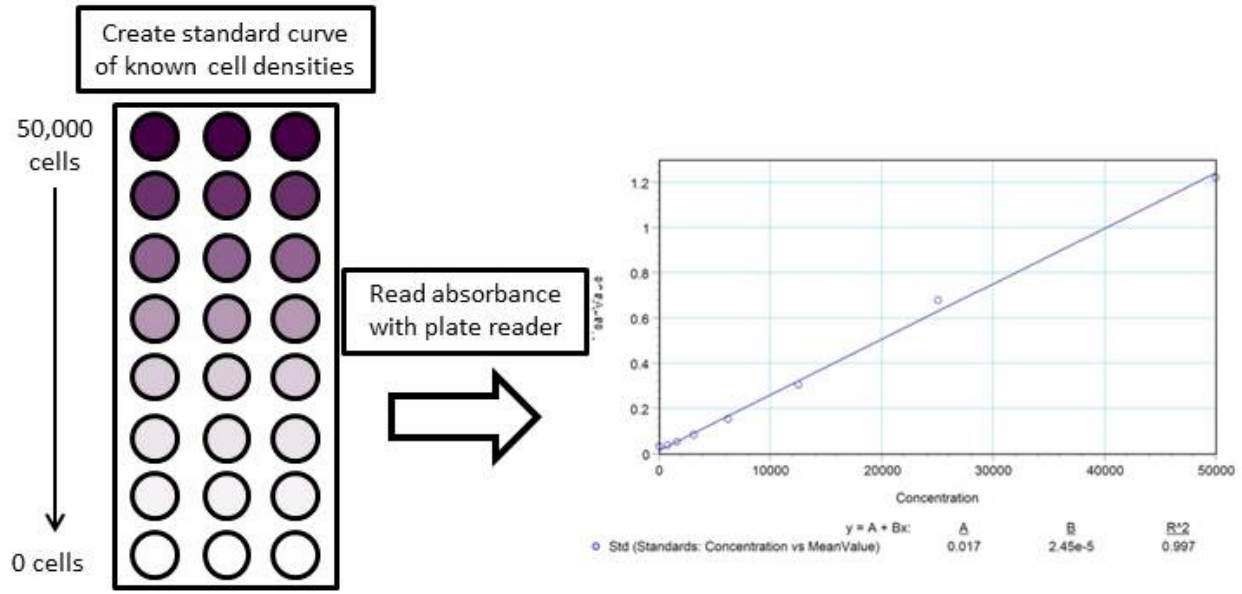


Figure 15: Use of standard curve to create linear regression relating absorbance to number of cells.

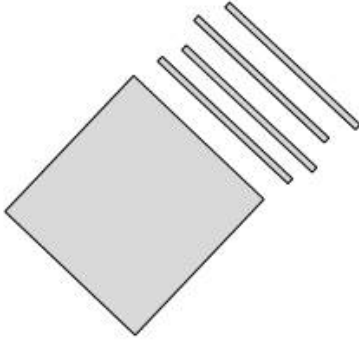
### 4.3.3 Cell Outgrowth

Tissue culture systems for measuring cellular outgrowth of GFP-modified fibroblasts onto electrospun polymer matrices were constructed using methods similar to those previously described by our lab[87]. Electrospun polymer scaffolds of each blend were cut into thin strips (approximately 1mm wide by 30mm long) using a razor blade (Figure 16A). A custom cell culture platform comprised of a Thermanox™ coverslip (Nalge Nunc International, Rochester, NY) raised above a stainless steel washer (Seastrom Manufacturing, Twin Falls, ID; inner diameter, 0.750 in.; outer diameter, 1.188 in.; thickness, 0.005 in.) with polydimethylsiloxane (PDMS; Sylgard 184, Dow Corning, Midland, IN) posts using medical grade silicone adhesive (Factor II, Lakeside, AZ) was assembled with electrospun polymer scaffold strips laid across the raised platforms dermal side up. The ends of the scaffolds were attached to the stainless steel washers using silicone adhesive as shown in Figure 16B. Outgrowth tissue culture systems including all electrospun polymer scaffolds were sterilized by exposure to ethylene oxide gas for 12 hours. Sterile culture systems were moved to 6-well tissue culture plates prior to cell seeding.

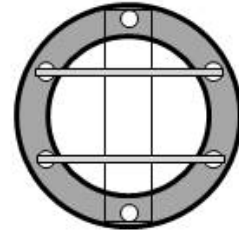
To seed cellular outgrowth culture systems, 0.5mL aliquots of GFP-modified fibroblast populated collagen lattices were cast onto each culture platforms (Figure 16C). In order to make these lattices, a 2.5 mg/mL solution of type I collagen was made from lyophilized collagen extracted from rat tail tendon as previously described [84], dissolved in 5mM HCl and 0.03% chloroform (for sterilization) and stirred for 2 days at 4°C. GFP-modified fibroblasts were trypsinized and counted, and  $1 \times 10^6$  cells were mixed with 2.0mL DMEM supplemented with 20% FBS, 0.4mL of 5x DMEM, and 1.6mL of 2.5mg/mL type I collagen solution, which was stored on ice. Lattices were allowed to gel for 2 hours at room temperature before wells were filled with fibroblast culture medium to a height just above the platforms and matrices. Culture medium was replaced daily.

Cellular outgrowth culture systems were cultured at 37°C and 10% CO<sub>2</sub> for 14 days. Plates were imaged daily on a Nikon Eclipse E600 upright epifluorescent microscope coupled with a SpotRT CCD camera (Diagnostic Instruments, Sterling Heights, MI). For each time point, measurements of cell outgrowth were made from the edge of the coverslip platform to the furthest fluorescently labeled cell (Figure 16D) using ImageJ (NIH).

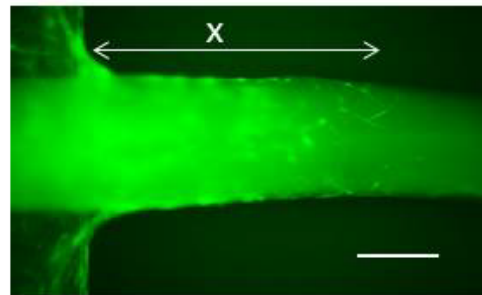
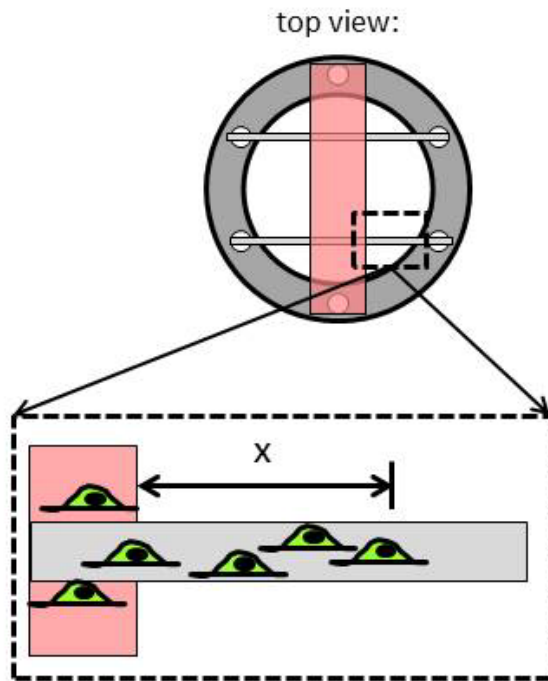
A. Cut electrospun matrices into thin strips



B. Glue onto steel washer over raised thermanox coverslip



C. Cast GFP-fibroblast populated collagen gel onto coverslip



D. Measure cell outgrowth from collagen gel over time

Figure 16: Experimental method for measuring cellular outgrowth of GFP-modified fibroblasts onto electrospun polymer composite matrices

## 4.4 Statistics

In experiments with two or more sample groups, including quantification of cell viability, statistical comparisons between sample groups were performed using a one-way analysis of variance (ANOVA) with  $p < 0.05$  indicating significance between samples. Post-hoc comparisons between sample groups were made with a Holm-Sidak pairwise multiple comparison test using an overall significance level of  $p < 0.05$ .

For characterization of mechanical properties, two types of comparisons were made. Directional comparisons within a blend type (eg. Blend A x-direction vs. Blend A y-direction) or comparisons between blends within a particular direction (eg. Blend A x-direction vs. Blend B x-direction). Individual Student's t-tests were performed for each of these comparisons with  $p < 0.05$  indicating significance. A Student's t-test was also performed in instances where only two conditions were being compared including comparison of fiber alignment local to axis orientation and comparison of cellular outgrowth on each electrospun scaffold blend.

The data are reported as means  $\pm$  standard deviations for the mechanical characterization and means  $\pm$  standard errors for quantification of cell viability. SigmaPlot 11.0 software (SyStat Software Inc., San Jose, CA) was used to perform ANOVA tests and Microsoft Excel was used to perform Student's t-tests.

## Chapter 5: Results

### 5.1 Physical and Mechanical Properties of Electrospun Scaffolds

This section details the results of the studies pertaining to Specific Aim 1 which aimed to characterize the physical and mechanical properties of the proposed electrospun dermal scaffolds. Three studies were completed in order to make these characterizations. The first and second utilized scanning electron microscopy to measure electrospun fiber diameters and angles and the third was a uniaxial tensile test to determine mechanical properties.

#### 5.1.1. Characterization of scaffold morphology by measurement of fiber diameter and angle

To characterize the morphology of the electrospun scaffolds scanning electron microscopy (SEM) was used to take high magnification images of each layer of the proposed scaffolds. Particular attention was paid to the orientation of each image such that the horizontal axis of each image corresponds to the horizontal (longitudinal) axis of the cylindrical mandrel collecting plate used during fabrication. Representative scanning electron microscopy images for each blend and layer are shown in Figure 17. Qualitative observation of the SEM images in Figure 17 shows that the scaffolds are indeed fibrous and that the fiber diameter appears to vary between the different polymer blends and layers. Qualitatively, there is no obvious observed alignment of the fibers. Additionally, the scaffolds appear to have interconnected pores that vary in size depending on the polymer blends used.

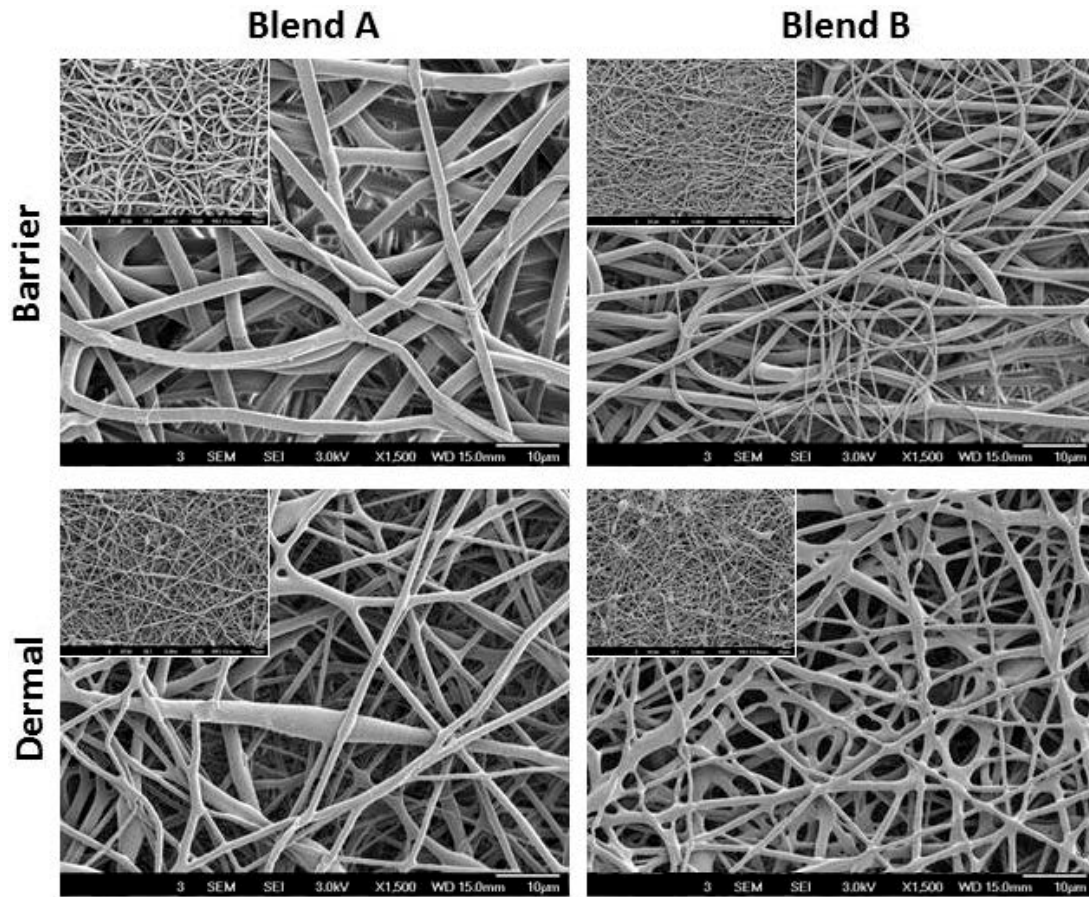


Figure 17: Representative SEM images of different layers of electrospun polymer dermal scaffolds taken at 1500x and 500x (inset). Scale bars = 10µm.

ImageJ was used to measure the diameter of fibers in SEM images of each electrospun scaffold blend and layer. Table 10 summarizes the distribution of fiber diameter values measured. The full diameter range represents the minimum and maximum fiber diameters for each blend/layer. The mean and median diameter values are also shown along with peak bin. The peak bin is the particular 100nm range in which the highest percentage of measured values lies. The distributions of fiber diameters were also plotted as histograms of percent frequency (the percentage of values falling within a particular 100nm range) versus fiber diameter for each blend/layer as shown in Figure 18.

Table 10: Summary of fiber diameter measurements made on each electrospun polymer scaffold blend and layer.

Blend/Layer	n	Full Diameter Range ( $\mu\text{m}$ )	Mean Diameter ( $\mu\text{m}$ )	Median Diameter ( $\mu\text{m}$ )	Peak Bin ( $\mu\text{m}$ )
Blend A - Barrier	1074	0.393 – 6.528	1.809	1.807	1.8 – 1.9
Blend A - Dermal	1667	0.309 – 6.44	1.068	0.942	0.8 – 0.9
Blend B - Barrier	4670	0.138 – 3.070	0.981	0.984	0.9 – 1.0 <i>(secondary: 0.3 – 0.4)</i>
Blend B - Dermal	4756	0.191 – 12.312	1.217	1.040	0.8 – 0.9

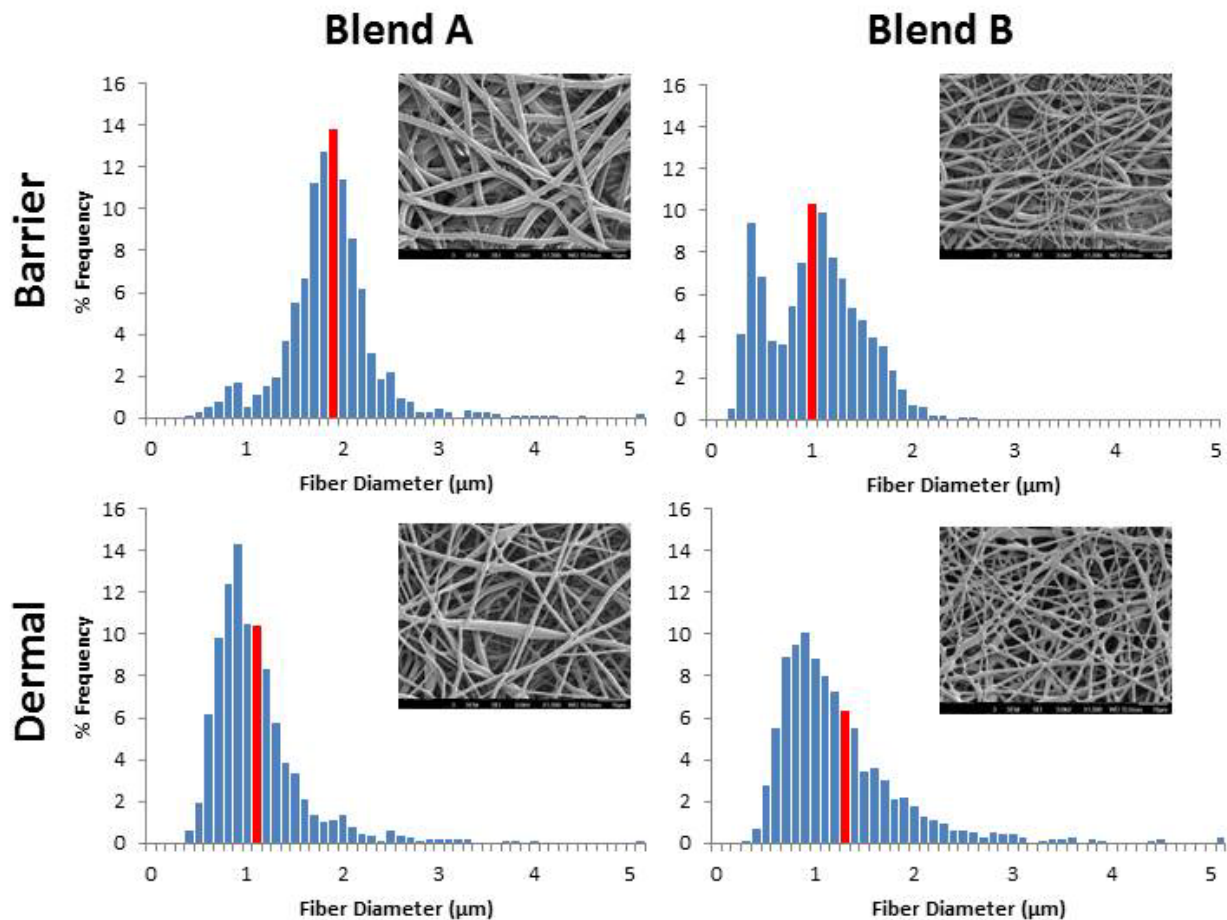


Figure 18: Histograms showing the distribution of fiber diameter (between 0 and 5.0 $\mu\text{m}$ ) as percent frequency versus fiber diameter for each electrospun polymer blend/layer with corresponding representative SEM images (500x, inset). In all groups over 99.7% of measurements were less than 5.0 $\mu\text{m}$ . Red bars indicate bins that contain the mean fiber diameter value. Histograms have a bin size of 100nm.



Additional measurements were made using the SEM images to investigate the angle of the fibers in the proposed electrospun polymer scaffolds with respect to the longitudinal axis of the cylindrical mandrel collecting plate. Each image was overlaid with a grid of four equally spaced horizontal and four equally spaced vertical lines and ImageJ was used to measure the angle of fibers where they crossed this grid. The distributions of fiber angles were also plotted as histograms of percent frequency (the percentage of values falling within a particular 5° bin) versus fiber angle for each blend/layer as shown in Figure 19. Table 11 shows a summary of the fiber angle measurements including average fiber angle for each blend and layer and a comparison of the percentage of fibers oriented local to each axis of the image.

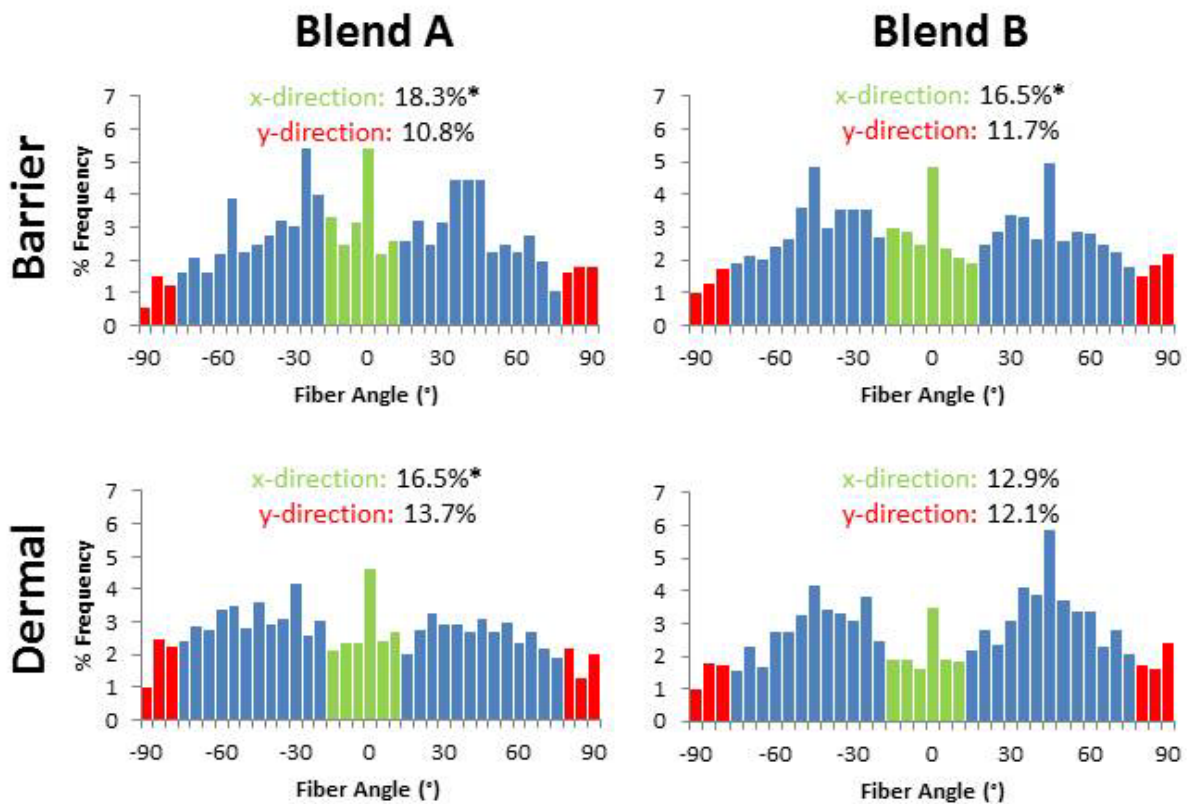


Figure 19: Histograms showing the distribution of fiber angle with respect to the horizontal axis (parallel to the longitudinal axis of the cylindrical collecting plate used in scaffold fabrication) as percent frequency versus fiber angle for each electrospun polymer blend/layer. Green and red bars represent fibers oriented within  $\pm 15^\circ$  of the x and y image axes respectively. \* represents a significant difference between the percentage of fibers oriented  $\pm 15^\circ$  of the x vs. y axis. Histograms have a bin size of  $5^\circ$ .

In the barrier layer of Blend A, fibers range from 0.393 – 6.528 $\mu\text{m}$ , with the highest percentage of fibers lying between 1.8 – 1.9 $\mu\text{m}$ . In Blend A, the dermal layer fibers range between 0.309 – 6.440 $\mu\text{m}$  (highest percentage between 0.8 – 0.9 $\mu\text{m}$ ) and in the dermal layer of Blend B, fibers were measured between 0.191 – 12.312 $\mu\text{m}$  (highest percentage also between 0.8 – 0.9 $\mu\text{m}$ ). In the distribution of the fiber diameters in the barrier layer of Blend B two peaks were found with high percentages of measurements one at 0.3 – 0.4 $\mu\text{m}$  and one between 0.9 – 1.0 $\mu\text{m}$ . This is confirmed visually in the representative images where distinct areas of smaller and larger fibers can be observed. Overall, the fibers in the Blend B barrier layer range from 0.138 – 3.070 $\mu\text{m}$ . In all of the electrospun scaffold blends and layers we studied over 99.7% of fibers measured were less than 5.0 $\mu\text{m}$  in diameter.

Measuring the percentage of fibers oriented locally (within  $\pm 15^\circ$ ) to the horizontal and vertical image axis allowed us to answer a fundamental question about how the electrospinning process and setup affect fiber alignment. In all of our electrospun scaffold blends and layers we found that there was a higher percentage of fibers oriented in along the x-axis of the images, which correspond to the longitudinal axis of the spinning mandrel used during the electrospinning process. Statistical analysis showed significant differences between local orientation for all but blend B's dermal layer.

**Table 11: Summary of fiber angle measurements including the total number of measured fibers (n-number), the average fiber angle with respect to horizontal axis measured on each electrospun scaffold blend and layer, and the percentage of fibers oriented longitudinally and circumferentially with respect to the electrospinning mandrel for each blend and layer. Statistical significance between local fiber orientation in the longitudinal and circumferential direction for each blend/layer was determined using a one-tailed, unpaired, homoscedastic Student's t-test. \* denotes a statistically higher percentage of fiber oriented in the longitudinal vs. circumferential direction for the indicated blend/layer combination.**

Blend/Layer	Total number of measured fibers (n-number)	Average fiber angle	% fibers oriented longitudinally	% fibers oriented circumferentially
Blend A - Barrier	1051	-0.129°	18.3%*	10.8%
Blend A - Dermal	1595	-5.012°	16.5%*	13.7%
Blend B - Barrier	4108	1.849°	16.5%*	11.7%
Blend B - Dermal	3677	-1.514°	12.9%	12.1%

### 5.1.2 Mechanical properties measured using uniaxial tensile testing

To characterize the mechanical properties of electrospun scaffolds with respect to orientation (as dictated by cylindrical mandrel collecting plate used in fabrication), dog bone shaped cutouts of the proposed scaffolds were loaded under uniaxial tension until failure. Samples in the x-direction were cut longitudinally from the cylindrical mandrel while samples in the y-direction were cut circumferentially as shown in Figure 12. This testing provided measurements of load and deformation from which ultimate tensile strength, strain at failure, and tangent elastic modulus of each composite matrix polymer blend with respect to orientation could be determined. A summary of these results and published values for native skin are shown in Table 12. Figure 20 shows representative stress vs. strain curves for each sample type while Figure 21, Figure 22, and Figure 23 show bar graphs of average ultimate tensile strength (UTS), strain at failure, and tangent elastic modulus respectively for each sample type.

**Table 12: Summary of measured tensile properties and published values for native skin tissue. Measured values presented as average  $\pm$  SEM.**

Blend/Direction	Sample Size	UTS (MPa)	Strain at Failure (mm/mm)	Tangent Elastic Modulus (MPa)	Thickness (mm)
Blend Ax	9	3.74 $\pm$ 0.18	0.35 $\pm$ 0.11	62.94 $\pm$ 8.81	0.363 $\pm$ 0.05
Blend Ay	9	2.90 $\pm$ 0.20	0.49 $\pm$ 0.16	33.44 $\pm$ 4.77	0.356 $\pm$ 0.06
Blend Bx	8	3.15 $\pm$ 0.21	0.44 $\pm$ 0.18	49.48 $\pm$ 5.51	0.352 $\pm$ 0.04
Blend By	8	2.39 $\pm$ 0.41	0.53 $\pm$ 0.12	23.15 $\pm$ 6.75	0.385 $\pm$ 0.07
Native Skin (full range) [12]		21	0.75	70	
Native Skin (average for elderly) [12]		17	0.60	60	
Native Skin (average for children) [12]		5-30	0.35 – 1.15	15-150	

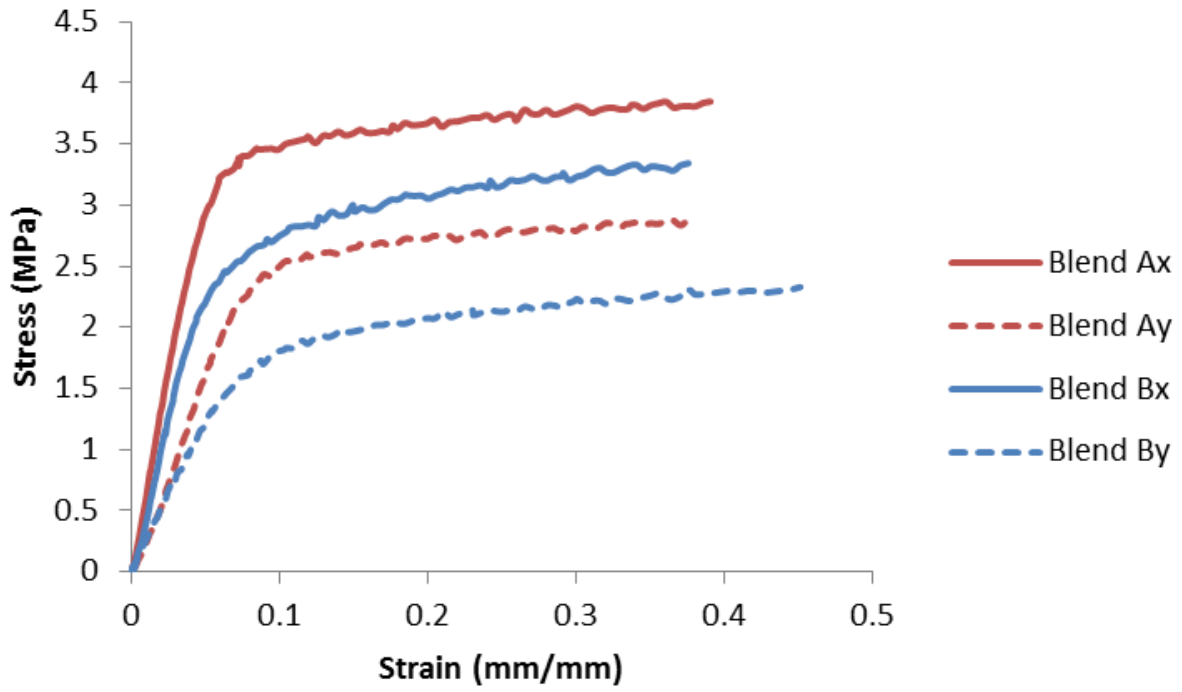


Figure 20: Characteristic plots of tensile stress vs. strain with respect to polymer blend and orientation. All curves show a distinct linear (elastic) region followed by a region of plastic deformation.

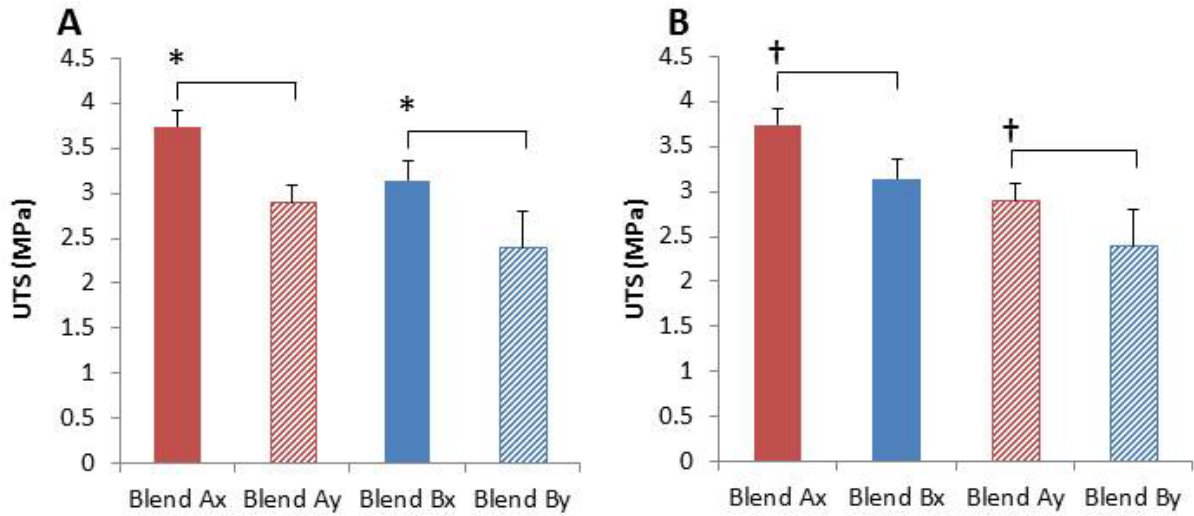


Figure 21: Comparison of ultimate tensile strength (UTS) with respect to polymer blend and orientation. For both blends samples cut in the x-direction showed a greater UTS than samples cut in the y-direction [A]. Samples from Blend A have a greater UTS than samples from Blend B when comparing samples cut in both the x-direction and y-direction [B]. Data are presented as averages  $\pm$  standard error. Statistical significance determined using Student's t-test with \* and † denoting a significant difference as indicated ( $p < 0.05$ ).

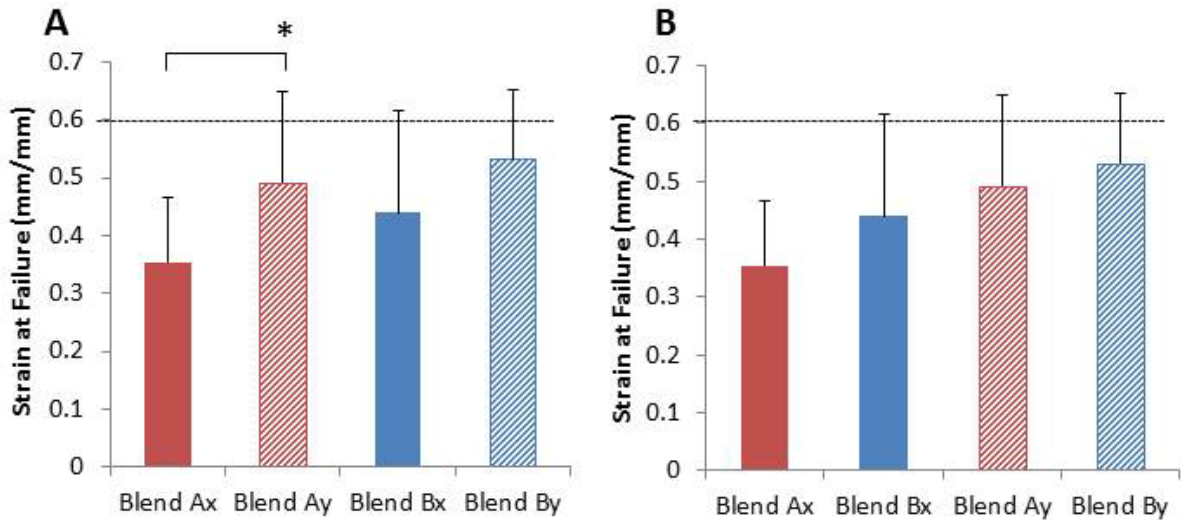
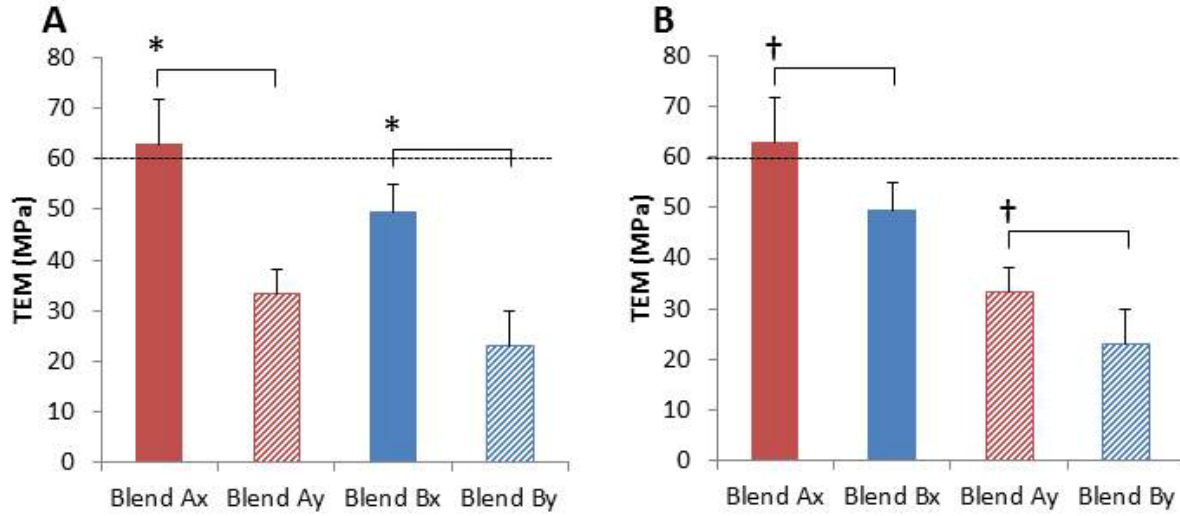


Figure 22 Comparison of strain at failure with respect to polymer blend and orientation. For Blend A samples cut in the y-direction showed a greater strain at failure than samples cut in the x-direction, but no significant directional difference was observed in Blend B [A]. There was no significant difference when comparing samples from Blend A to Blend B in either the x-direction or the y-direction [B]. Data are presented as averages  $\pm$  standard error. Dashed line represents native tissue benchmark [12]. Statistical significance determined using Student's t-test with \* denoting a significant difference as indicated ( $p < 0.05$ ).



**Figure 23: Comparison of tangent elastic modulus (TEM) with respect to polymer blend and orientation. For both blends samples cut in the x-direction showed a greater TEM than samples cut in the y-direction [A]. Samples from Blend A have a greater TEM than samples from Blend B when comparing samples cut in both the x-direction and y-direction [B]. These findings show a consistent trend with the UTS data. Data are presented as averages  $\pm$  standard error. Dashed line represents native tissue benchmark [12]. Statistical significance determined using Student's t-test with \* and † denoting a significant difference as indicated ( $p < 0.05$ ).**

The characteristic tensile stress vs. strain curves for the proposed electrospun polymer matrices all showed an initial linear region indicating recoverable elastic deformation followed by a non-linear region indicating non-recoverable plastic deformation before failure. In terms of UTS, the samples cut along the longitudinal axis of the cylindrical mandrel used during scaffold fabrication (x-direction) were significantly stronger than those cut along the circumferential axis (y-direction) for both electrospun polymer blends (Figure 21A). Additionally, when comparing the UTS of two blends (Blend A vs. Blend B) within a particular direction (either the x-direction or the y-direction) as shown in Figure 21B, Blend A had a significantly higher UTS in both directions. A similar trend was observed in the measured tangent elastic modulus (TEM) of the scaffolds, which was calculated from the slope of the linear (elastic) portion of the stress vs. strain curve for each sample. Longitudinal (x-direction) samples had significantly higher values for tangent elastic modulus than circumferential (y-direction) samples for both blends (Figure 23A).. Additionally, the measured tangent elastic modulus values for all samples lie within the range

reported for native skin and the tangent elastic modulus of Blend A-x samples exceed the average native skin values published by Edwards and Marks [12]. Although there only statistical confirmation in Blend A, the observed trend in the measured strain at failure is that samples cut circumferentially (y-direction) strain more than those cut longitudinally (x-direction) (Figure 22A). There is no statistical significance in strain at failure when comparing the two blends (Blend A vs. Blend B) within a particular direction (x-direction or y-direction) as shown in Figure 22B. The circumferentially oriented (y-direction) samples from polymer blend B (PU/PET-PCL/PGA) have the highest observed average strain at failure at  $0.53 \pm 0.12$  mm/mm.

SEM images of the failure point of scaffolds after undergoing uniaxial tensile testing were also taken and are shown in Figure 24. These images show distinct areas of material necking as well as a qualitative increase in fiber alignment in the direction parallel to the applied strain when compared to images of the unfailed scaffolds. The observed necking (white arrows) is consistent with the region of plastic deformation in the stress-strain curves which is followed by material failure as indicated by the failed fiber ends indicated by the yellow arrows.

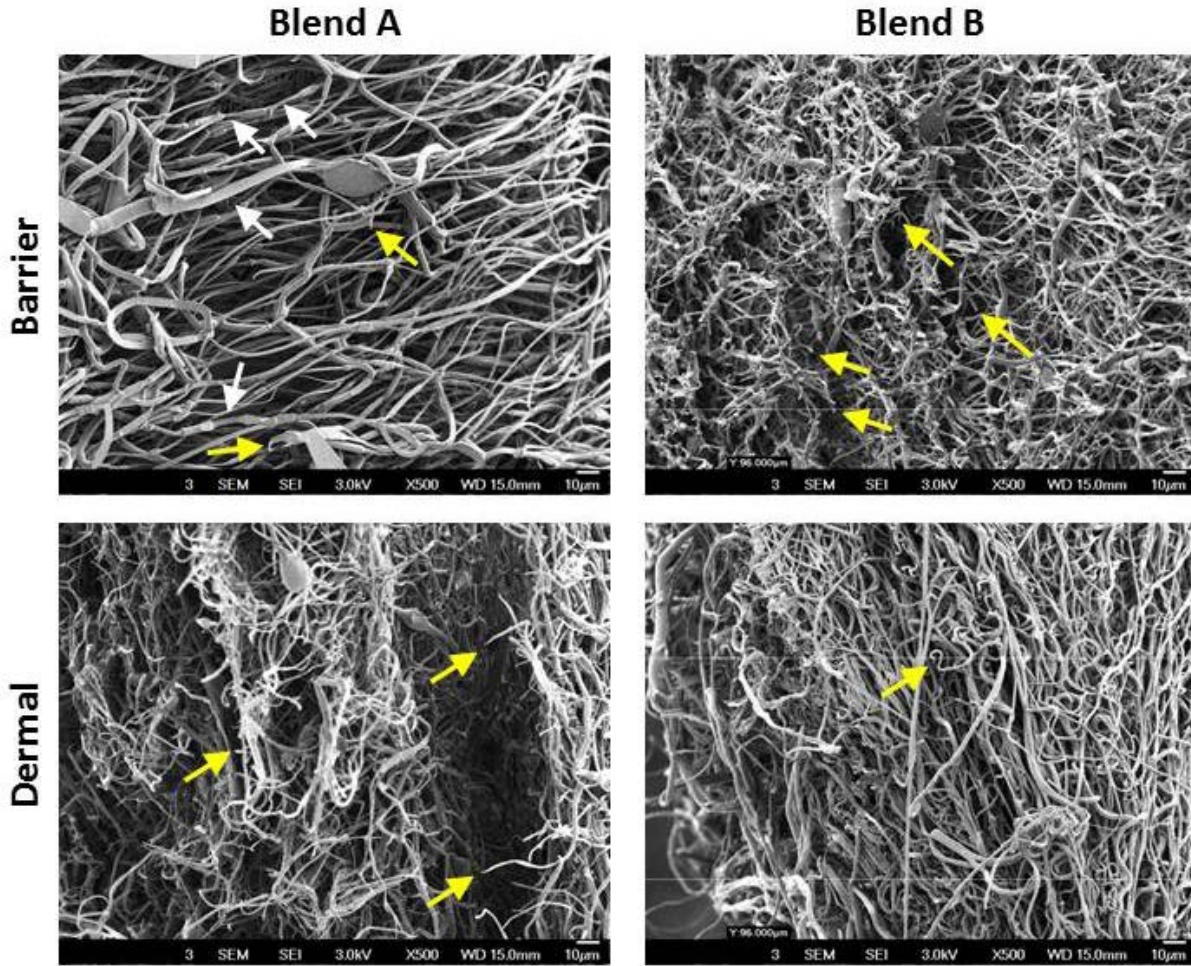


Figure 24: SEM images of failed ends of electrospun scaffolds after undergoing mechanical testing via uniaxial tensile testing. White arrows indicate necking in the polymer fibers, yellow arrows indicate failure points.

## 5.2 Biologic Activity of Electrospun Scaffolds

This section details the results of the studies pertaining to Specific Aim 2 which aimed to evaluate the biologic activity of the proposed electrospun dermal scaffolds. Two studies were completed in order to make these evaluations. The first was an MTT assay which measured cell attachment to the proposed scaffolds and the second a cellular outgrowth assay which utilized a custom culture device in order to measure growth of cells onto samples of the electrospun dermal scaffolds.



### 5.2.1 In Vitro Analysis of Cell Attachment

An MTT assay was used as an initial characterization of the *in vitro* viability of dermal fibroblasts on the electrospun dermal scaffolds. This colorimetric assay, measures cellular metabolism and compares cell attachment between the various layers of the proposed electrospun scaffolds, as well as two control substrates, tissue culture polystyrene (TCPS) and collagen-GAG sponges. The number of cells attached to each scaffold 4 hrs. after seeding was quantified using a standard curve of known cell concentrations. The number of cells attached to each scaffold type is shown in Figure 25 and summarized in Table 13.

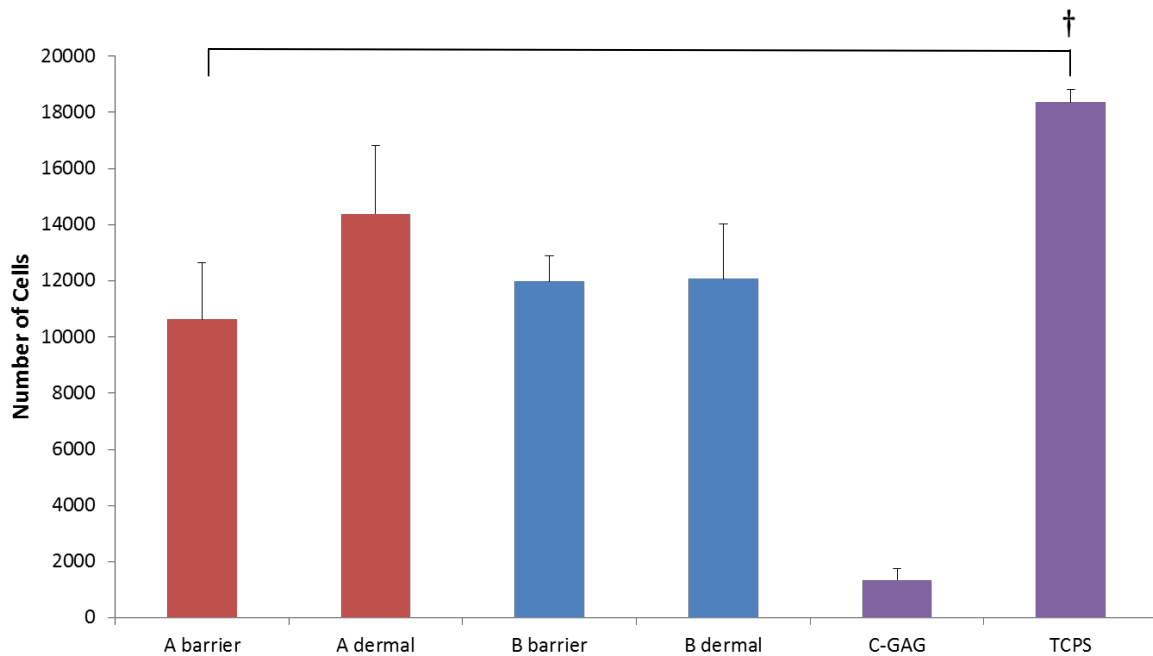


Figure 25: Average number of viable cells detected on different layers of electrospun dermal regeneration composite matrices using MTT assay (n=3). † indicates statistical significance between indicated groups. \* indicates statistically significant difference between condition and all other groups as determined using ANOVA with Tukey post-hoc (p<0.05).

**Table 13: Summary of cell attachment (4 hours post seeding) to electrospun composite polymer dermal matrices. Cells attached are reported as averages  $\pm$  SEM.**

<b>Scaffold Type</b>	<b>Sample Size</b>	<b>Cells Attached <math>\pm</math> SEM</b>
<b>Blend A Barrier</b>	6	10620 $\pm$ 2020 cells
<b>Blend A Dermal</b>	6	14380 $\pm$ 2440 cells
<b>Blend B Barrier</b>	6	11970 $\pm$ 910 cells
<b>Blend B Dermal</b>	6	12070 $\pm$ 1960 cells
<b>Collagen-GAG Sponge Control</b>	6	1340 $\pm$ 400 cells
<b>TCPS Control</b>	6	18360 $\pm$ 440 cells

This initial attachment data shows that while tissue culture polystyrene has more cells attached than the barrier layer of Blend A (PET/PBT-PCL/PGA) four hours after seeding, there is no significant difference between the number of cells attached to TCPS and the remaining electrospun scaffold layers. Additionally, all electrospun scaffolds and TCPS have significantly more cells attached than the collagen-GAG sponge control.

### 5.2.2 In Vitro Analysis of Cellular Outgrowth

Cell outgrowth from the surrounding wound margin into the scaffold is essential for its clinical success as cells must migrate into the scaffold to be degraded and replaced with native tissue. To measure cellular outgrowth a custom designed culture platform device was developed. This device allowed for measurement of the outgrowth of GFP labeled human dermal fibroblasts from a collagen gel onto strips of electrospun scaffold material. Figure 26 shows representative images of outgrowth measurements taken at various time points on the dermal layer of both blends of our electrospun scaffolds. Figure 27 shows representative curves of cellular outgrowth over time for both electrospun polymer scaffold blends and Figure 28 shows a plot of their average daily measured outgrowth.

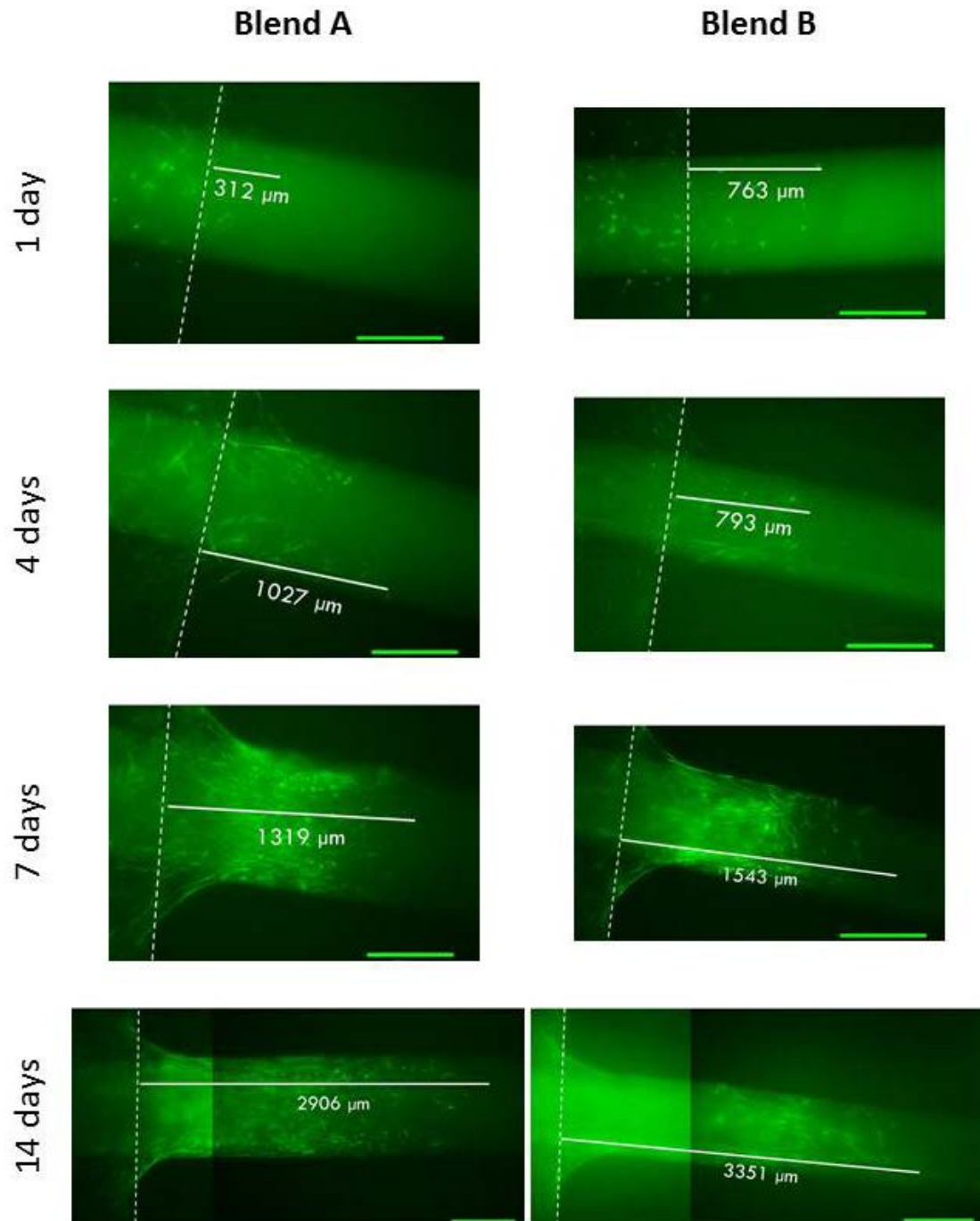


Figure 26: Representative images of the outgrowth of GFP-labeled fibroblasts onto the dermal layer of electrospun scaffolds at 1, 4, 7, and 14 days post seeding. Scale bars, 500 $\mu$ m. Dashed lines indicate edge of fibroblast populated collagen gel. Measurements indicate the measured distance to the furthest cell observed on the scaffold strips.

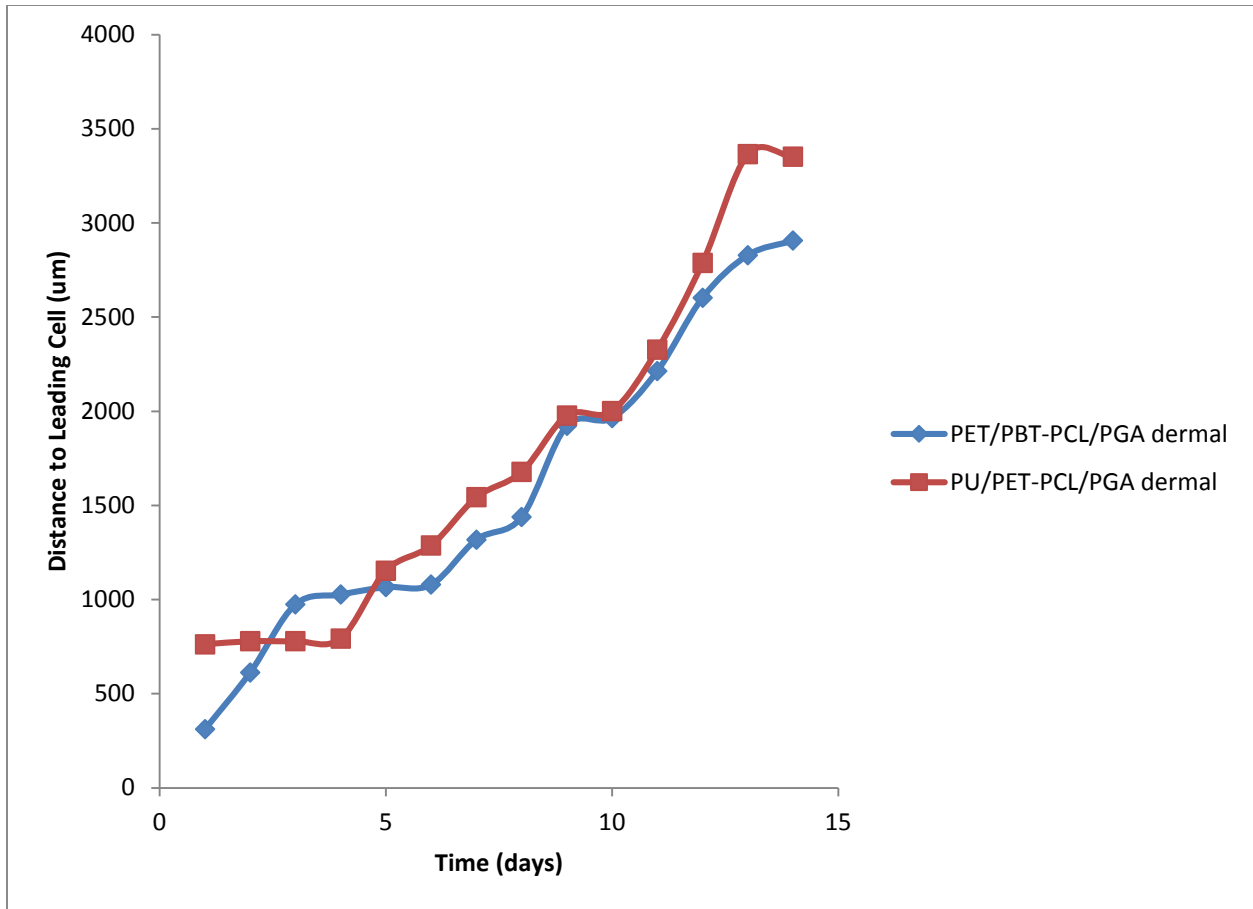


Figure 27: Representative plots of measured distance to leading cell over time on dermal layer of electrospun dermal regeneration composite matrices.

## Average Cell Outgrowth

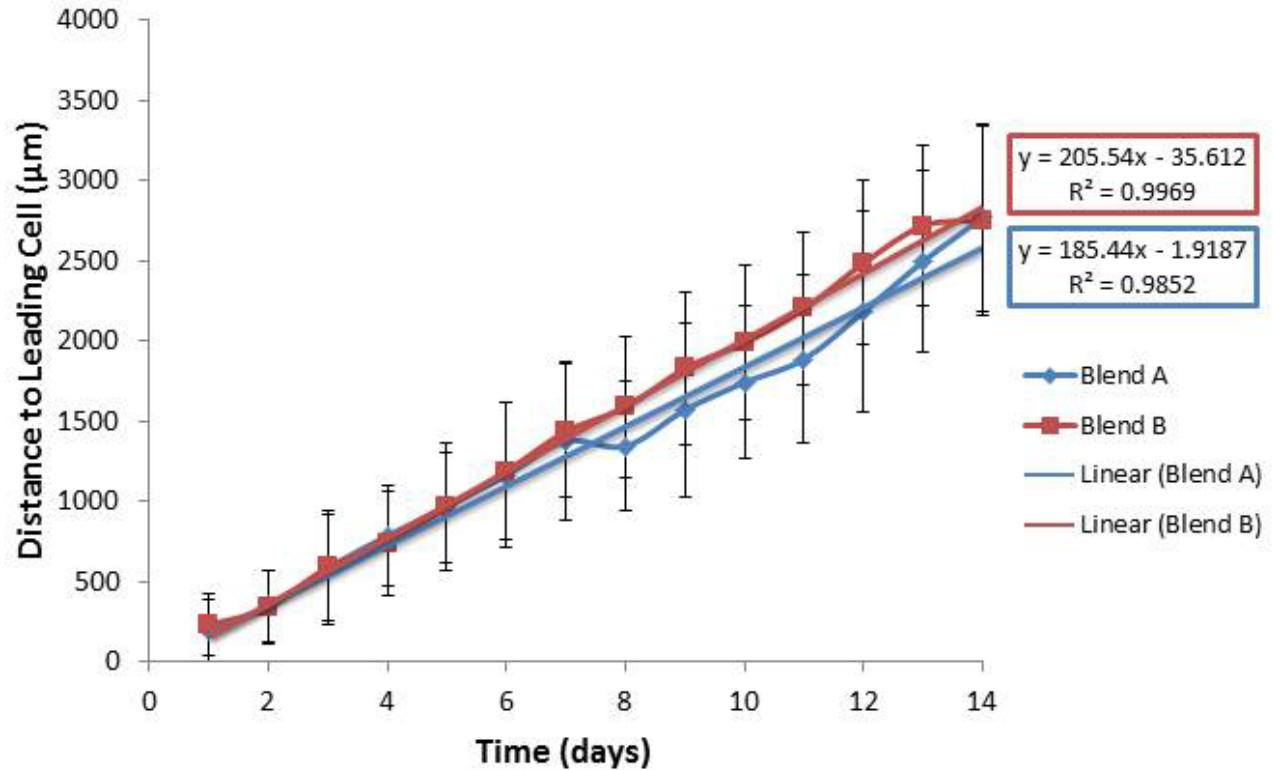


Figure 28: Average measured distance to leading cell over time on dermal layer of electrospun dermal matrices. Points represent daily averages for each blend  $\pm$  SEM. Linear regressions were also performed to investigate linearity. Trendlines with equations and  $R^2$  values are also shown. For Blend A,  $n=24$ . For Blend B,  $n=20$ .

Cells grow outward onto strips of the electrospun dermal scaffolds as a function of time. As shown in Figure 26, Figure 27, and Figure 28, the distance to the leading cell on each blend shows a steady increase over the 14 days of measurement. Additionally the high  $R^2$  values (0.9852 and 0.9969 for blends A and B respectively) calculated for the linear regression shown in Figure 28 indicate that the cellular outgrowth over time is linear and the outgrowth rate for each blend can be approximated by the slope of its linear trend line. These trend lines indicate an approximate outgrowth rate of 185  $\mu\text{m}/\text{day}$  for Blend A and 206  $\mu\text{m}/\text{day}$  for Blend B.

## Chapter 6: Discussion

The long-term goal of this project is to design an anti-microbial, pro-angiogenic scaffold for dermal regeneration in chronic skin wounds. Currently, clinicians use a variety of synthetic wound dressings to treat chronic wounds and in severe cases that require surgical intervention, split-thickness autografts and bioengineered skin substitutes, are used [88]. Current treatments have achieved some success, but are plagued by limitations in their mechanical stability, sub-optimal wound healing rates, infection, and scarring [3-5, 7-9]. Towards that goal we have evaluated two novel, bi-layered electrospun polymer composite scaffold blends for their physical and mechanical properties and biologic activity. In this study, we investigate the design and development of scaffolds which combine an electrospun degradable dermal component with a non-degradable barrier layer. The dermal component is designed to address the limitations of current chronic wound treatments by improving the rate of wound healing and minimizing scarring by acting as a provisional matrix for the wound. The matrix is designed to support and encourage the ingrowth of cells from the wound margins which subsequently degrade the scaffold in the wound bed and replace it with native dermal tissue. The non-degradable barrier layer provide acts as a protective physical barrier for the developing dermal tissue and as a porous, breathable wound dressing that allows for gas exchange, while also protecting the wound from pathogens and preventing microbial infection. To characterize the structural morphology of our novel electrospun scaffolds we used scanning electron microscopy. High magnification images of each blend and layer revealed that the diameters and orientation of the fibers in our electrospun scaffolds are similar to properties of fibers in native papillary dermis. Measurement of mechanical properties under uniaxial tension showed that our scaffolds exhibit mechanical behavior that is similar to native tissue. Additionally, we determined that our electrospun scaffolds promote *in vitro* fibroblast attachment and outgrowth.

## 6.1 Physical and Mechanical Properties of Electrospun Scaffolds

### 6.1.1. Characterization of scaffold morphology by measurement of fiber diameter and orientation

To investigate scaffold morphology and quantify fiber diameter and orientation we use scanning electron microscopy. In this study, we provide evidence that our electrospun scaffolds provide a structural matrix that is similar to native tissue. Brown [11] previously used scanning electron microscopy to examine the structure of native dermal tissue and found that the dermis has several structurally distinctive layers. The connective tissue of the dermis is composed predominantly of fibrous collagen in addition to other fibrous proteins like elastin and reticulin [89]. The dermis' upper, papillary layer is composed of an open network of fine fibers, mostly collagen, ranging from 0.3 – 3 $\mu$ m in diameter while the underlying reticular layers have densely intertwined coarse collagen fibers ranging from 10 – 40 $\mu$ m. Brown [11] observed no preferential fiber orientation in the samples he studied, however, other studies have reported regular lattice patterns in the reticular dermis [90]. Qualitatively, the fiber size and arrangement of our electrospun scaffolds closely resemble the open network structure of the papillary dermis. Our measurement of scaffold morphology from SEM images shows that greater than 99.7% of the fibers measured in each blend and layer of our electrospun scaffolds is between 0.2 – 5 $\mu$ m in diameter and there is no obvious observed orientation. These quantitative measurements are similar to those made by Brown [11] in his studies of papillary dermis confirming qualitative observations of similarity between this native tissue layer and our electrospun scaffolds.

One limitation of using SEM to characterize scaffold morphology is that the images produced are two-dimensional and thus three-dimensional morphological properties such as pore size are difficult to characterize. Characterization of scaffold pores is important for implanted biomaterial scaffolds because previous research suggests that there is a minimum pore size is required for cellular infiltration. It has

been suggested that the minimum pore size required is approximately the size of a cell, on the order of 10 $\mu$ m diameter, or even slightly smaller in flexible tissues. Yannas, et al. [27] found that the critical pore diameter for maintenance of balance between scaffold degradation and wound healing in their collagen-GAG scaffolds was between 20 – 125 $\mu$ m. Previous studies have measured inter-fiber diameter from SEM images as an estimation of pore size [73, 78, 80] or used more advanced pore measurement techniques, such as capillary flow porometry [91] or mercury porosimetry [92]. Qualitatively, it appears from estimating the inter-fiber distance in the SEM photos of our electrospun scaffolds that there are at least some pores on the order of 10 $\mu$ m or larger, but it will certainly be important to quantify pore size in the future.

### **6.1.2. Mechanical properties measured by uniaxial tensile testing**

The results of our uniaxial tensile testing indicate that our electrospun scaffolds have mechanical properties that are similar to native skin tissue. Edwards and Marks [12] have previously reported mechanical properties for native human skin tested under uniaxial tension which are summarized in Table 4. We tested dog bone shaped cut outs of our composite electrospun scaffolds under uniaxial tension in two directions as dictated by the spinning cylindrical mandrel collecting plate used during the electrospinning process (see Figure 12). By testing in two directions we sought to answer a fundamental question about how the mandrel shape and spinneret movements during the electrospinning process affect material properties of the scaffolds, namely a directionally induced difference in mechanical properties. We found that our composite scaffolds had similar mechanical properties to the published properties of human tissue in terms of tangent elastic modulus (TEM) and strain at failure. We also found that in ultimate tensile strength (UTS) and TEM there was a statistically significant difference between properties measured in scaffolds cut in the longitudinal direction (x-direction) and the circumferential direction (y-direction).



Previous studies have shown that local fiber orientation directly modulates material properties, specifically, scaffold mechanics in electrospun scaffolds [93-96]. Nerurkar, et al. [96] compared the mechanical properties of aligned electrospun scaffold tested parallel to fiber alignment, perpendicular to alignment, and non-aligned (random) electrospun scaffolds. They found scaffolds tested parallel to alignment had an elastic modulus that was three times greater than non-aligned scaffolds and ten times greater than scaffolds tested perpendicular to alignment. Li, et al. [93] showed that even slight fiber alignment, due to slow collecting plate rotation, lead to an increase in elastic modulus between scaffolds tested parallel to the presumed principal fiber direction over scaffolds tested perpendicular to fiber direction with greater differences observed between parallel and perpendicularly tested scaffolds as collecting plate rotation speed was increased. At slow mandrel rotation speeds (0.3 m/s), they observed a greater than three-fold increase in elastic modulus in scaffolds tested parallel to fiber alignment compared to those tested perpendicular to fiber alignment.

In our electrospun composite scaffolds we observed a 1.88 and 2.13-fold increase in tangent elastic modulus (TEM) in the x-direction (longitudinal) with respect to the y-direction for scaffold blends A and B respectively. Comparing these results with those from the previous study [93], suggest that there is some level of slight fiber alignment in our electrospun scaffolds. Our initial qualitative observations and fiber alignment measurements do not show any obvious orientation, but previous studies have shown that mechanical properties are directly modulated by local fiber orientation [93-95]. If we consider only the fibers locally aligned around the test directions or, within 15% of the x-direction ( $0^\circ$ ) and within 15% of the y-direction ( $-90^\circ/+90^\circ$ ), there are statistically more fibers locally aligned to the x-direction than to the y-direction in all scaffold blends and layer, except the dermal layer of Blend B. A limitation of the mechanical testing is that all tensile tests wer performed on composite scaffolds (barrier and dermal layers present in sample) and it is therefore difficult to isolate the effects that each layer has on the mechanics of the total scaffold. Performing mechanical testing on the individual layers

may provide further insight into the relationship between sample cutting orientation and mechanical properties in our electrospun scaffolds.

## 6.2. Biologic Activity of Electrospun Scaffolds

### 6.2.1. *In Vitro* Analysis of Cell Attachment

We used an MTT assay to quantify cellular attachment on our electrospun scaffolds. The positive results of this study show that our electrospun scaffolds support the attachment of normal human fibroblast cells *in vitro*. Cellular attachment is important to our scaffold design because it relies on the infiltration and attachment of native inflammatory cells and fibroblasts from the wound margins to degrade the preliminary matrix and to regenerate the dermal tissue by synthesizing their own matrix. Previous studies have shown that electrospun polymer scaffolds are capable of supporting a variety of cell types including human keratinocytes, fibroblasts, and endothelial cells [68, 72-74, 77-80, 91]. In this study we used an MTT assay to quantify human fibroblast attachment to our electrospun scaffolds and compared the results directly to fibroblast attachment on tissue culture polystyrene and collagen-GAG sponges, a well characterized biomaterial scaffold for dermal regeneration. Our direct comparisons revealed that with the exception of Blend A's barrier layer, there is no statistically significant difference in fibroblast attachment between our electrospun scaffolds and tissue culture polystyrene. Additionally, we observed significantly higher cell attachment on our electrospun scaffolds compared to collagen-GAG sponges. O'Brien [97, 98], et al. previously characterized fibroblast attachment on collagen-GAG sponges and found that depending on the pore size of the sponges the seeding efficiency (percent of cells attached vs. cells seeded) was 20-40%, this is compared to only about 5% seeding efficiency on collagen-GAG sponges observed in our studies. We did however find greater than 42% seeding efficiency on all of our electrospun scaffold blends and layers with up to 58% seeding efficiency on the dermal layer of Blend A.

The drastic differences in cell attachment between our electrospun scaffolds and collagen-GAG sponges may be influenced by the differences we observed in specific surface area between these types of scaffolds. It has been hypothesized previously that cellular attachment and migration are dependent on pore size and specific surface area [27, 98, 99]. Efficient binding of a critical number of cells to the scaffold requires a scaffold that has pores large enough to allow for cellular infiltration, but small enough to provide a sufficiently high specific surface area to support a minimum cellular ligand binding density [98, 99]. Published values of specific surface area (surface area/volume) for similar collagen-GAG sponges range from  $4.77 \times 10^{-3} - 7.49 \times 10^{-3} \mu\text{m}^{-1}$  [98] depending on pore size as a result of scaffold freezing temperature, while the specific surface areas we calculated for our electrospun scaffolds range from  $2.05 - 3.35 \mu\text{m}^{-1}$ . Previous studies have also shown that the percent cell attachment increases with increasing specific surface area in collagen-GAG sponges [98], which supports the increase in cellular attachment in scaffolds with higher surface area observed in our experiments. Additionally, a previous study showed that attachment time significantly effects fibroblast attachment in collagen-GAG spongesan maximum attachment is not achieved until about 22 hours post seeding, suggesting that perhaps investigating longer attachment time points would be beneficial in future studies.

The results of this short-time course experiment are encouraging, but longer time points should be investigated to confirm long-term cell attachment and also to probe for cell viability and proliferation. Previous studies have used MTT or similar assays to quantify the number of cells present on electrospun scaffolds at various time points up to 14 days post seeding [72, 77-79, 91]. Comparisons between samples are then used to evaluate cell viability and comparisons between time points can be used as an indication of cell proliferation [72, 91].

### 6.2.2. *In Vitro* Analysis of Cellular Outgrowth

To measure cellular outgrowth on our electrospun scaffolds, we utilized a custom outgrowth assay. In this study, we provide evidence that our electrospun scaffolds support the outgrowth of normal human fibroblasts *in vitro*. The success of our scaffold as a dermal regeneration matrix is dependent on its ability to promote ingrowth of cells from the wound margins. To quantify the rate at which cells move into the scaffold we designed a custom outgrowth assay which allowed us to measure the outgrowth of GFP-labeled human fibroblasts from a collagen gel onto thin strips of the dermal layer of our electrospun scaffolds. By measuring the distance to the leading cell every 24 hours for 14 days we were able to generate plots of outgrowth over time and calculate an average outgrowth rate from a linear regression. Through these experiments we found outgrowth rates of 185 $\mu\text{m}/\text{day}$  on the dermal layer of Blend A and 206 $\mu\text{m}/\text{day}$  on the dermal layer of Blend B. Outgrowth experiments were performed only on the degradable dermal layer of full-thickness scaffolds because our scaffold design relies on cellular infiltration only in that layer (the non-degradable barrier is removed after dermal regeneration has begun).

Previous studies by Harley et al. [14] have investigated real-time migration of mouse fibroblasts in collagen-GAG sponges which have been used as control scaffolds in several of our other experiments. This study showed that the migration rate in collagen-GAG sponges was dependent on pore size and ranged from 6.38 $\mu\text{m}/\text{hour}$  which translates to approximately 153 $\mu\text{m}/\text{day}$  in sponges with larger pores (151 $\pm$ 32 $\mu\text{m}$ ) and 11.98 $\mu\text{m}/\text{hour}$  which translates to approximately 288 $\mu\text{m}/\text{day}$  in scaffolds with smaller pores (96 $\pm$ 12 $\mu\text{m}$ ). Additionally, in their seminal paper on the design of an artificial skin substitute, Yannas and Burke [13] estimate that the migration rate of fibroblasts in their scaffolds is about 200 $\mu\text{m}/\text{day}$  through the thickness direction and perhaps slightly slower in the transverse plane of the membrane. These results align very well with the results of our experiments on electrospun scaffolds

indicating that our scaffolds have similar cellular outgrowth behavior to collagen-GAG sponges and commercially available dermal regeneration matrices.

While our custom outgrowth assay was very successful at measuring overall outgrowth of the bulk cell population on our electrospun scaffolds, the assay is limited in its ability to measure the migration rate of specific cells. Additionally, this assay allows for measurements to be made only on the surface of the electrospun scaffolds, which being porous, may also have cells that travel through the pores to infiltrate the thickness of the scaffolds. To date, we have not performed any studies that investigate the infiltration and migration rate of cells through the thickness of our scaffolds, which as Harley et al. [14] showed in collagen-GAG sponges is likely related to the size of the pores in our scaffolds.

A previous study [87] performed by our lab group used a similar outgrowth assay to measure fibroblast outgrowth on various types of discrete collagen microthreads with native rat tail tendon threads (NTT) and polypropylene suture (PPT) serving as controls. This study found outgrowth rates of approximately  $490\mu\text{m}/\text{day}$  for the negative control (PPT) and approximately  $1060\mu\text{m}/\text{day}$  for the positive control (NTT) [87], much higher than the outgrowth rates we observed on our electrospun scaffolds. Although the outgrowth rates we observed in our electrospun scaffolds were similar to those measured in other dermal scaffolds, the rate of tissue ingrowth and wound healing continues to be a limitation of the current clinically available technologies *in vivo* [3-5, 7-9]. Future development of our scaffold could potentially improve fibroblast outgrowth through the inclusion of a mitogenic growth factor. Previous studies have shown that electrospinning can be used to incorporate growth factors and drugs directly into scaffold fibers and subsequently release them into the wound bed [68, 74]. We propose using this method to incorporate a mitogenic growth factor, such as fibroblast growth factor-2 (FGF-2) directly into the dermal layer of our electrospun scaffolds. FGF-2 has been shown to enhance

the rate of fibroblast infiltration and proliferation and also affects angiogenesis in wound healing all of which may help to enhance neodermal formation [16]. We will also investigate the addition of an antimicrobial, such a Moxifloxacin, into the barrier layer in order to prevent microbial infection, which is a common mode of failure in split-thickness skin grafts and current bioengineered skin substitutes [3-5, 7-9].

## Chapter 7: Future Work and Recommendations

At the outset of this project we investigated the potential development of two different electrospun composite matrices for dermal regeneration. The results of our studies of physical morphology (fiber diameter and orientation), mechanical properties, cellular attachment, and cellular outgrowth, along with their respective comparisons to benchmarks including properties of native tissue and/or other commercially available skin substitutes, revealed strengths and weaknesses for each of the two blends. While both blends were equally successful in terms of physical morphology and cellular outgrowth, we observed some important differences between the blends in our studies of mechanical properties and cellular attachment. When considering the TEM of our scaffolds, we observed a statistically significant directional difference (x-direction > y-direction) in both scaffold blends, with Blend Ax reaching the stiffness levels of native skin and Blend Bx only marginally below the native value. However, when we investigated the strain at failure for each blend we saw a slight increase in both directions of Blend B, which was accompanied by less directional variation compared to Blend A. In addition to these observations of the mechanical properties, the results of our cellular attachment study showed a statistically significant decrease in cellular attachment on the barrier layer of Blend A when compared to tissue culture polystyrene.

The nominally more directionally consistent mechanical properties, coupled with superior cellular attachment incline us to suggest that future development of an electrospun composite matrix for dermal regeneration focus on polymer Blend B. Additionally, further studies are recommended before our scaffolds can be implemented as an alternative to autografting in the future treatment of chronic wounds. This chapter details additional *in vitro* characterizations recommended for the short term advancement of this project as well as scaffold modifications and an *in vivo* animal study to characterize wound healing response which should be performed in the future.

## 7.1 Additional *In Vitro* Characterizations

There are several additional characterizations recommended for the short term advancement of this research. These recommendations focus on further quantification of the physical properties of the scaffold and on further understanding of the *in vitro* cellular response.

### 7.1.1 Pore size and porosity

We recommend that experiments be performed to quantify the pore size and porosity of our electrospun scaffolds. The pores in our dermal regeneration matrix will make up the space in which cells will move and reside. Pore properties, such as porosity and pore diameter are important for directing cell migration and accommodation as well as for regulating the exchange of nutrients and metabolic waste between the scaffold and the environment. Previous studies have identified that there is an optimal pore size for scaffolds for skin regeneration and that it is dependent on maintaining a balance between having pores that are large enough to accommodate and encourage cell migration, but not so large that the scaffold loses mechanical integrity and induce rapid degradation. For collagen-GAG sponges, Yannas, et al. identified this range as scaffolds with pore diameters of 20 - 125 $\mu$ m [27]. Individual optimizations should be made on our scaffolds, but this study provides a good starting point.

Pore size and porosity measurements can be made using a variety of methods. Li, et al. [92] used mercury porosimetry to measure various pore properties in their electrospun PLGA scaffolds such as: porosity (as % porosity), total pore volume (in mL/g), and total pore area (in m<sup>2</sup>/g). The mercury porosimetry study also produced a plot of the pore diameter distribution observed in the samples. This study will help us gain a better understanding of the physical properties of our electrospun scaffolds, how they compare to native tissue, and whether they have suitable properties for use as a dermal regeneration matrix.



### 7.1.2 *In vitro* scaffold degradation

The success of our dermal regeneration matrix hinges not just on the scaffold's ability to recruit and support cells which will produce new dermal tissue, but also on the concurrent degradation of the dermal layer. It is, therefore, important to understand and tune the degradation profile of our electrospun scaffolds. Blackwood, et al. [73] and Canton, et al. [74] evaluated *in vitro* degradation of their electrospun scaffolds by immersing their scaffolds in Ringer's solution at 37°C. Physical changes in the scaffolds were then analyzed using phase contrast micrographs and scanning electron microscopy [73]. Chemical analysis (ex. pH) was also performed on the solution as the scaffolds degraded [74]. Performing these *in vitro* degradation studies would allow us to quantify the *in vitro* degradation rate of our electrospun scaffolds as well as investigate any chemical by products or changes induced by the degrading scaffold.

As described in section 2.3.1 Design Considerations for Tissue Engineered Skin, the rate of degradation of bioengineered skin substitutes must be in delicate balance with the rate of wound healing. One of the benefits of using electrospinning to create our dermal regeneration scaffolds is that if we find that the dermal layer of our electrospun scaffolds does not have an optimal degradation profile, simple changes can be to the polymer concentrations and polymer ratios in order to manipulate the degradation of the scaffold. Additionally, PCL has a long degradation time, which we intended to harness as a means of providing an extended structural scaffold for dermal regeneration. If we find that the degradation of PCL is too slow, we could investigate the use of alternative degradable polymers, such as PLA, which has a shorter degradation time than PCL, but maintains its structure longer than PGA, allowing us to maintain the material degradation strategy described in Chapter 3: Hypothesis and Specific Aims.

### 7.1.3 *In vitro* scaffold permeability

In native tissue, the mass transport needs of cells, such as nutrient flow and metabolic waste removal, are performed by blood vessels throughout the tissue. Because our electrospun scaffold design relies on cellular ingrowth to regenerate dermal tissue including blood vessels, it is important that the scaffold accommodate the mass transport needs of the infiltrating cells by allowing for nutrient and waste flow. This flow is most certainly influenced and enhanced by the porosity of the electrospun scaffolds, but measuring permeability *in vitro* will confirm proper mass transfer. Powell and Boyce [80] used a simple set-up to quantify permeability of hydrated electrospun gelatin scaffolds *in vitro* using Darcy's Law. The Darcy's Law equation relates permeability to flow rate, sample thickness, flow area, and change in hydraulic head. We recommend performing this experiment to quantify the permeability of our electrospun scaffolds and confirm that it is suitable for nutrient and waste diffusion.

### 7.1.4 Long term *in vitro* cell viability and proliferation

As a part of this study, we quantified short term fibroblast attachment to our scaffolds by using an MTT assay to measure the number of cells attached four hours after seeding. While these results showed promising levels of attachment compared to controls, further experiments are necessary to confirm long term cell viability *in vitro*. Several groups have used an MTT assay to confirm long term viability of fibroblasts cultured on electrospun scaffolds in experiments with time points from 2 to 21 days [73, 76, 80]. Using multiple longer time points will allow us to evaluate not only cell viability, but also cellular proliferation by comparison of changes in number of cells measured using the MTT assay between time points.

Additionally, studies of *in vitro* keratinocyte viability and ingrowth should be performed. Keratinocyte viability can be measured using the MTT assay similar to our analyses of fibroblast viability. Schneider et al. [68] utilized a *in vitro* skin-equivalent wound healing model to study *in vitro*

reepithelialization (keratinocyte ingrowth) on a collagen matrix seeded with fibroblasts and keratinocytes. Incisions were made to wound the skin-equivalents and electrospun scaffolds incorporating EGF were applied to the *in vitro* wound. Wound closure over time was evaluated using histology. We propose a similar method to measure keratinocyte ingrowth in our scaffolds. In our composite scaffolds we would hope to see keratinocyte ingrowth between the barrier and dermal layers, encouraged by the rapid degradation of PGA in the dermal layer. We have also considered adding a third, thin, rapidly degrading sacrificial layer between the dermal and barrier layers (perhaps incorporating a growth factor that stimulates keratinocyte proliferation and migration, such as EGF [16, 68]) to encourage reepithelialization between the scaffold layers.

#### **7.1.5 Three-dimensional *in vitro* cell distribution and movement**

While this study includes an experiment that quantifies cell outgrowth, one of the limitations of this experiment is that it only allows us to measure outgrowth on the two-dimensional surface of our electrospun scaffolds. Because our scaffolds are porous, we expect that cells will actually move in three-dimensions and would in the future like to be able to investigate the movement and distribution of cells throughout the three-dimensional structure of the scaffold. Confocal microscopy will allow us to focus on cells in different planes of the sample without physically sectioning the sample. Liu et al. [100] used confocal microscopy to visualize three-dimensional distribution and morphology of fluorescently labeled cells in their electrospun PMMA scaffolds. By seeding cells only on one side of the scaffold and using confocal microscopy to visualize their progressive three-dimensional distribution over time we could also measure 3-D cell movement including the time it takes for cells to fully populate the scaffold.

One of the limitations of the outgrowth assay utilized in our studies was that it did not allow us to distinguish between cellular migration and cellular movement as a result of population proliferation. Utilizing a proliferation marker such as Ki67 to mark proliferating cells and measure the overall

proliferation level of cells on our scaffolds would be an interesting addition to 2-D and 3-D cell distribution and movement experiments.

### **7.1.6 *In vitro* barrier function**

In native skin, the epidermis serves as a protective barrier against the loss of fluids from within the tissue and exogenous microbial invasion and among the most fundamental requirements for the closure and healing of skin injuries with autografts or bioengineered skin substitutes is the restoration of this barrier. Several current commercially available dermal regeneration products also include a pseudo-epidermal component to act as a barrier whilst dermal regeneration occurs, but are often criticized for their lack of effective gas exchange through this layer [5]. In our electrospun dermal regeneration matrices, we have utilized a porous electrospun barrier layer, which we hope will provide the healing wound with a robust mechanical and microbial barrier, while still allowing for appropriate gas exchange between the healing tissue and the exogenous environment.

Several methods have that been established for testing the barrier function of skin tissue *in vivo* have also been utilized in *in vitro* testing of barrier function in bioengineered skin substitutes. Transepidermal water loss (TEWL) can be measured using a variety of commercially available instruments and has been used to assess the permeability of the epidermal or barrier layer of bioengineered skin substitutes [101]. Powell and Boyce [50] used a NOVA dermal phase meter to quantify surface electrical capacitance (SEC) which is a direct measurement of skin surface hydration and is inversely related to barrier function. We propose the *in vitro* measurement of barrier function in our electrospun scaffolds using one of these methods.

## 7.2 *In Vivo* Animal Model

For the long term advancement of this research we recommend the use of an animal model to study scaffold performance *in vivo*. These recommendations in this section focus on investigation of *in vivo* scaffold biocompatibility and degradation as well as a full-thickness wound healing model.

### 7.2.1 *In vivo* biocompatibility and degradation

In order to be successful as a dermal regeneration matrix, it is important that we characterize the *in vivo* biocompatibility and degradation of our electrospun scaffolds. Blackwood, et al. [73] investigated *in vivo* biocompatibility and degradation by implanting their electrospun PLGA scaffolds subcutaneously in Wistar rats. In addition to providing a way to measure the *in vivo* degradation profile, this implantation study allowed for visualization and measurement of cellular penetration and vascularization (histology) as well as immune response and the types of cells present in the scaffold over time (immunostaining). This study would allow us to determine whether the degradation rate of our scaffold is appropriate for dermal regeneration and confirm the *in vitro* biocompatibility results.

### 7.2.2 *In vivo* wound healing model

Before beginning clinical trials on human subjects we will test the ability of our electrospun scaffolds to act as a dermal regeneration matrix in an animal model. Implantation of biological dressings into full-thickness wounds in athymic mice is a well-established method for characterizing *in vivo* tissue responses and wound healing [10, 102]. This model allows for macroscopic evaluation of wound healing and contraction of the electrospun dressings by photographing the wound and quantifying the wound area with image analysis software. Scaffolds can also be explanted from animals to assess cellular and tissue infiltration, collagen deposition and angiogenesis using histology and immunostaining.

The *in vivo* wound healing model can also be used to measure the barrier function and permeability of our electrospun scaffolds over time. As described in the section about *in vitro*

characterizations, maintenance of barrier function during wound healing is one of the most important functions of a successful bioengineered skin substitute. We suggest using a non-disruptive method such as TEWL or SEC (described in section 7.1.6 *In vitro* barrier function) to measure *in vivo* barrier function throughout the duration of the *in vivo* wound model. Results should be compared to the *in vitro* barrier function measurements and *in vivo* measurements of intact skin.

## 7.3 Scaffold Modifications

### 7.3.1 Polymer composition

As described throughout this chapter, the results of future studies, especially the *in vitro* and *in vivo* degradation studies, may call for changes to be made to the polymer composition of our electrospun dermal regeneration matrices. In particular, the dermal layer, which is the same in both blends and is comprised of PGA (a rapidly degrading polymer incorporated to degrade as initial cellular infiltration occurs in the scaffold) and PCL (a slow degrading polymer incorporated to maintain scaffold integrity as native ECM is deposited in the wound bed), could potentially degrade too slowly due to the presence of PCL. However, one of the advantages of utilizing electrospinning technology to manufacture our scaffolds is the ease with which we can make changes to the types of polymers used in our scaffolds as well as the polymer concentrations and polymer ratios which directly modulate scaffold properties like scaffold degradation.

### 7.3.2 Scaffold thickness

We suggest that future studies consider increasing the thickness of the electrospun dermal regeneration matrices we studied. The current scaffolds are manufactured with a thickness of 350-390 $\mu$ m, while the thickness of human skin ranges from 0.5-5mm depending on location[103]. Increasing the thickness of our scaffolds will also serve to improve the mechanical integrity of our scaffolds by increasing their load to failure[12].

### 7.3.3 Development of a pro-angiogenic, antimicrobial composite scaffold

The goal of this project was to provide a preliminary assessment of an acellular biomaterial scaffold for dermal regeneration. In order to better accomplish the needs of the current market, we also propose the future addition of a pro-angiogenic growth factor, such as FGF2, in the dermal layer to increase the rate of wound healing and dermal regeneration *in vivo*. We would also like to investigate the addition of an antimicrobial, such as Moxifloxacin, into the barrier layer to provide microbial resistance to the healing wound. The experiments and results outlined in this project show strong evidence for further development and investigation of our composite scaffold designs and also provide a tool box of assays to be used in order to investigate how the addition of a growth factor and antimicrobial affect scaffold properties.

## Chapter 8: Conclusions

We hypothesized that electrospun polymer composite scaffolds would support human dermal fibroblast attachment and outgrowth and provide an appropriate structural matrix for dermal tissue regeneration. We investigated two different electrospun scaffolds each with a biodegradable dermal component designed to support cellular ingrowth and dermal regeneration and a unique, non-degradable epidermal component designed to provide temporary barrier function during regeneration. We evaluated the morphology of each scaffold blend and layer by quantifying fiber diameter and orientation and evaluated mechanical properties, such as ultimate tensile strength, strain at failure, and tangent elastic modulus of the composite scaffolds. We found that our scaffolds are similar to native papillary dermal tissue and their strain at failure and tangent elastic modulus fall largely within published ranges for native skin. We also quantified *in vitro* fibroblast attachment and outgrowth and found that more cells attach to our scaffolds than to collagen-glycosaminoglycan (collagen-GAG) sponges which are currently used as the dermal component in the commercially available Integra-DRT product. We also found that outgrowth rate in our scaffolds is comparable to published outgrowth rates of dermal fibroblasts in collagen-GAG sponges. The promising findings from these *in vitro* studies warrant further investigation and development of our novel electrospun dermal regeneration matrix. Future studies could measure scaffold pore size and porosity, scaffold degradation, long term fibroblast attachment and proliferation, three-dimensional migration, and *in vivo* biocompatibility and wound healing. Future development could also lead to the incorporation of a mitogenic growth factor and antimicrobial which may enhance the cellular response and reduce bacterial infection in order to create a successful bioengineered skin substitute.



## References

1. Macri, L. and R.A. Clark, *Tissue engineering for cutaneous wounds: selecting the proper time and space for growth factors, cells and the extracellular matrix*. *Skin Pharmacol Physiol*, 2009. 22(2): p. 83-93.
2. Kuehn, B.M., *Chronic wound care guidelines issued*. *JAMA*, 2007. 297(9): p. 938-9.
3. Sheridan, R.L. and R.G. Tompkins, *Skin substitutes in burns*. *Burns*, 1999. 25(2): p. 97-103.
4. Boyce, S.T., *Design principles for composition and performance of cultured skin substitutes*. *Burns*, 2001. 27(5): p. 523-33.
5. Shevchenko, R.V., S.L. James, and S.E. James, *A review of tissue-engineered skin bioconstructs available for skin reconstruction*. *J R Soc Interface*, 2010. 7(43): p. 229-58.
6. Morgan, J.R., et al., *Burn Dressings and Skin Substitutes*, in *Biomaterials Science: An Introduction to Materials in Medicine*, B.D. Ratner, et al., Editors. 2004, Elsevier, Inc.: San Diego, CA.
7. MacNeil, S., *Progress and opportunities for tissue-engineered skin*. *Nature*, 2007. 445(7130): p. 874-80.
8. Metcalfe, A.D. and M.W. Ferguson, *Tissue engineering of replacement skin: the crossroads of biomaterials, wound healing, embryonic development, stem cells and regeneration*. *J R Soc Interface*, 2007. 4(14): p. 413-37.
9. Shepherd, J., et al., *Development of three-dimensional tissue-engineered models of bacterial infected human skin wounds*. *Tissue Eng Part C Methods*, 2009. 15(3): p. 475-84.
10. Supp, A.P., et al., *Evaluation of cytotoxicity and antimicrobial activity of Acticoat Burn Dressing for management of microbial contamination in cultured skin substitutes grafted to athymic mice*. *J Burn Care Rehabil*, 2005. 26(3): p. 238-46.
11. Brown, I.A., *Scanning electron microscopy of human dermal fibrous tissue*. *J Anat*, 1972. 113(Pt 2): p. 159-68.
12. Edwards, C. and R. Marks, *Evaluation of biomechanical properties of human skin*. *Clin Dermatol*, 1995. 13(4): p. 375-80.
13. Yannas, I.V. and J.F. Burke, *Design of an artificial skin. I. Basic design principles*. *J Biomed Mater Res*, 1980. 14(1): p. 65-81.
14. Harley, B.A., et al., *Microarchitecture of three-dimensional scaffolds influences cell migration behavior via junction interactions*. *Biophys J*, 2008. 95(8): p. 4013-24.
15. SEER Training Modules. *Skin Cancer: Melanoma*. February 22, 2013; Available from: <http://training.seer.cancer.gov/melanoma/anatomy/>.
16. Singer, A.J. and R.A. Clark, *Cutaneous wound healing*. *N Engl J Med*, 1999. 341(10): p. 738-46.
17. Falanga, V., *Wound healing and its impairment in the diabetic foot*. *The Lancet*, 2005. 366(9498): p. 1736-1743.
18. Shakespeare, P.G., *The role of skin substitutes in the treatment of burn injuries*. *Clin Dermatol*, 2005. 23(4): p. 413-8.
19. Anderson, J.M., *Inflammation, Wound Healing, and the Foreign-Body Response*, in *Biomaterials Science: An Introduction to Materials in Medicine*, B.D. Ratner, et al., Editors. 2004, Elsevier Academic Press: San Diego, CA. p. 296-304.
20. Clark, R.A.F., *The Molecular and Cellular Biology of Wound Repair*. 1996: Springer.
21. Kiritsy, C.P., A.B. Lynch, and S.E. Lynch, *Role of growth factors in cutaneous wound healing: a review*. *Crit Rev Oral Biol Med*, 1993. 4(5): p. 729-60.
22. Martin, P., *Wound healing--aiming for perfect skin regeneration*. *Science*, 1997. 276(5309): p. 75-81.
23. Woo, K., E.A. Ayello, and R.G. Sibbald, *The edge effect: current therapeutic options to advance the wound edge*. *Adv Skin Wound Care*, 2007. 20(2): p. 99-117; quiz 118-9.

24. Muschler, G.F., C. Nakamoto, and L.G. Griffith, *Engineering principles of clinical cell-based tissue engineering*. J Bone Joint Surg Am, 2004. 86-A(7): p. 1541-58.
25. Spruit, D. and K.E. Malten, *The regeneration of the water vapour loss of heavily damaged skin*. Dermatologica, 1966. 132(2): p. 115-23.
26. Levenson, S.M., et al., *THE HEALING OF RAT SKIN WOUNDS*. Ann Surg, 1965. 161: p. 293-308.
27. Yannas, I.V., et al., *Synthesis and characterization of a model extracellular matrix that induces partial regeneration of adult mammalian skin*. Proc Natl Acad Sci U S A, 1989. 86(3): p. 933-7.
28. Jayarama Reddy, V., et al., *Nanofibrous structured biomimetic strategies for skin tissue regeneration*. Wound Repair Regen, 2013. 21(1): p. 1-16.
29. Rheinwald, J.G. and H. Green, *Serial cultivation of strains of human epidermal keratinocytes: the formation keratinizing colonies from single cell is*. Cell, 1975. 6(3): p. 331-343.
30. Green, H., O. Kehinde, and J. Thomas, *Growth of cultured human epidermal cells into multiple epithelia suitable for grafting*. Proc Natl Acad Sci U S A, 1979. 76(11): p. 5665-8.
31. O'Connor, N.E., et al., *Grafting of burns with cultured epithelium prepared from autologous epidermal cells*. Lancet, 1981. 1(8211): p. 75-8.
32. Gallico, G.G., 3rd and N.E. O'Connor, *Cultured epithelium as a skin substitute*. Clin Plast Surg, 1985. 12(2): p. 149-57.
33. Gallico, G.G., 3rd, et al., *Permanent coverage of large burn wounds with autologous cultured human epithelium*. N Engl J Med, 1984. 311(7): p. 448-51.
34. Hefton, J.M., et al., *Grafting of skin ulcers with cultured autologous epidermal cells*. J Am Acad Dermatol, 1986. 14(3): p. 399-405.
35. Bush, K.A. and G.D. Pins, *Nano- and Microtechnologies for the Development of Engineered Skin Substitutes*, in *Micro and Nanoengineering of the Cell Microenvironment: Technologies and Applications*, A. Khademhosseini, Editor. 2008, Artech House Publishers. p. 579-600.
36. Barrandon, Y. and H. Green, *Three clonal types of keratinocyte with different capacities for multiplication*. Proc Natl Acad Sci U S A, 1987. 84(8): p. 2302-6.
37. Navarro, F.A., et al., *Sprayed keratinocyte suspensions accelerate epidermal coverage in a porcine microwound model*. J Burn Care Rehabil, 2000. 21(6): p. 513-8.
38. Hernon, C.A., et al., *Clinical experience using cultured epithelial autografts leads to an alternative methodology for transferring skin cells from the laboratory to the patient*. Regen Med, 2006. 1(6): p. 809-21.
39. Andree, C., et al., *Basement membrane formation during wound healing is dependent on epidermal transplants*. Plast Reconstr Surg, 2001. 107(1): p. 97-104.
40. Atiyeh, B.S. and M. Costagliola, *Cultured epithelial autograft (CEA) in burn treatment: three decades later*. Burns, 2007. 33(4): p. 405-13.
41. Williamson, J.S., et al., *Cultured epithelial autograft: five years of clinical experience with twenty-eight patients*. J Trauma, 1995. 39(2): p. 309-19.
42. Wood, F.M., M.L. Kolybaba, and P. Allen, *The use of cultured epithelial autograft in the treatment of major burn injuries: a critical review of the literature*. Burns, 2006. 32(4): p. 395-401.
43. Wainwright, D., et al., *Clinical evaluation of an acellular allograft dermal matrix in full-thickness burns*. J Burn Care Rehabil, 1996. 17(2): p. 124-36.
44. Wainwright, D.J., *Use of an acellular allograft dermal matrix (AlloDerm) in the management of full-thickness burns*. Burns, 1995. 21(4): p. 243-8.
45. Yannas, I.V., et al., *Design of an artificial skin. II. Control of chemical composition*. J Biomed Mater Res, 1980. 14(2): p. 107-32.
46. Burke, J.F., et al., *Successful use of a physiologically acceptable artificial skin in the treatment of extensive burn injury*. Ann Surg, 1981. 194(4): p. 413-28.

47. Kahn, S.A., R.J. Beers, and C.W. Lentz, *Use of acellular dermal replacement in reconstruction of nonhealing lower extremity wounds*. J Burn Care Res, 2011. 32(1): p. 124-8.
48. Silverstein, G., *Dermal regeneration template in the surgical management of diabetic foot ulcers: a series of five cases*. J Foot Ankle Surg, 2006. 45(1): p. 28-33.
49. Dantzer, E. and F.M. Braye, *Reconstructive surgery using an artificial dermis (Integra): results with 39 grafts*. Br J Plast Surg, 2001. 54(8): p. 659-64.
50. Powell, H.M. and S.T. Boyce, *Engineered human skin fabricated using electrospun collagen-PCL blends: morphogenesis and mechanical properties*. Tissue Eng Part A, 2009. 15(8): p. 2177-87.
51. Whitaker, I.S., S. Prowse, and T.S. Potokar, *A critical evaluation of the use of Biobrane as a biologic skin substitute: a versatile tool for the plastic and reconstructive surgeon*. Ann Plast Surg, 2008. 60(3): p. 333-7.
52. Gerding, R.L., A.L. Imbembo, and R.B. Fratianne, *Biosynthetic skin substitute vs. 1% silver sulfadiazine for treatment of inpatient partial-thickness thermal burns*. J Trauma, 1988. 28(8): p. 1265-9.
53. Lal, S., et al., *Biobrane improves wound healing in burned children without increased risk of infection*. Shock, 2000. 14(3): p. 314-8; discussion 318-9.
54. Gentzkow, G.D., et al., *Use of dermagraft, a cultured human dermis, to treat diabetic foot ulcers*. Diabetes Care, 1996. 19(4): p. 350-4.
55. Marston, W.A., et al., *The efficacy and safety of Dermagraft in improving the healing of chronic diabetic foot ulcers: results of a prospective randomized trial*. Diabetes Care, 2003. 26(6): p. 1701-5.
56. Kim, P.J., K.S. Dybowski, and J.S. Steinburg, *Feature: A Closer Look At Bioengineered Alternative Tissues*. Podiatry Today, 2006. 19(7): p. 38-55.
57. Clark, R.A., K. Ghosh, and M.G. Tonnesen, *Tissue engineering for cutaneous wounds*. J Invest Dermatol, 2007. 127(5): p. 1018-29.
58. Boyce, S.T., et al., *THE 1999 CLINICAL RESEARCH AWARD Cultured Skin Substitutes Combined With Integra Artificial Skin\* to Replace Native Skin Autograft and Allograft for the Closure of Excised Full-Thickness Burns*. Journal of Burn Care & Research, 1999. 20(6): p. 453-461.
59. Veves, A., et al., *Graftskin, a human skin equivalent, is effective in the management of noninfected neuropathic diabetic foot ulcers: a prospective randomized multicenter clinical trial*. Diabetes Care, 2001. 24(2): p. 290-5.
60. Sams, H.H., J. Chen, and L.E. King, *Graftskin treatment of difficult to heal diabetic foot ulcers: one center's experience*. Dermatol Surg, 2002. 28(8): p. 698-703.
61. Eaglstein, W.H., et al., *Acute excisional wounds treated with a tissue-engineered skin (Apligraf)*. Dermatol Surg, 1999. 25(3): p. 195-201.
62. Griffiths, M., et al., *Survival of Apligraf in acute human wounds*. Tissue Eng, 2004. 10(7-8): p. 1180-95.
63. Silberklang, M. *Forticell Bioscience, Inc. - Advanced Wound Care: OrCel Technology*. 2008 [cited 2013 March 29]; Available from: <http://www.forticellbioscience.com/technology.html>.
64. Still, J., et al., *The use of a collagen sponge/living cell composite material to treat donor sites in burn patients*. Burns, 2003. 29(8): p. 837-41.
65. Waymack, P., R.G. Duff, and M. Sabolinski, *The effect of a tissue engineered bilayered living skin analog, over meshed split-thickness autografts on the healing of excised burn wounds*. The Apligraf Burn Study Group. Burns, 2000. 26(7): p. 609-19.
66. Rosso, F., et al., *Smart materials as scaffolds for tissue engineering*. J Cell Physiol, 2005. 203(3): p. 465-70.
67. Pham, Q.P., U. Sharma, and A.G. Mikos, *Electrospinning of polymeric nanofibers for tissue engineering applications: a review*. Tissue Eng, 2006. 12(5): p. 1197-211.

68. Schneider, A., et al., *Biofunctionalized electrospun silk mats as a topical bioactive dressing for accelerated wound healing*. Acta Biomater, 2009. 5(7): p. 2570-8.
69. Subbiah, T., et al., *Electrospinning of nanofibers*. Journal of Applied Polymer Science, 2005. 96(2): p. 557-569.
70. Bosworth, L.A. and B. Downes, *Electrospinning for tissue regeneration*, ed. L.A. Bosworth and B. Downes. 2011: Woodhead Publishing. 432.
71. Yannas, I.V., *Emerging rules for inducing organ regeneration*. Biomaterials, 2013. 34(2): p. 321-30.
72. Babaeijandaghi, F., et al., *Accelerated epidermal regeneration and improved dermal reconstruction achieved by polyethersulfone nanofibers*. Tissue Eng Part A, 2010. 16(11): p. 3527-36.
73. Blackwood, K.A., et al., *Development of biodegradable electrospun scaffolds for dermal replacement*. Biomaterials, 2008. 29(21): p. 3091-104.
74. Canton, I., et al., *Development of an Ibuprofen-releasing biodegradable PLA/PGA electrospun scaffold for tissue regeneration*. Biotechnol Bioeng, 2010. 105(2): p. 396-408.
75. Khil, M.S., et al., *Electrospun nanofibrous polyurethane membrane as wound dressing*. J Biomed Mater Res B Appl Biomater, 2003. 67(2): p. 675-9.
76. Zhang, Y.Z., et al., *Characterization of the surface biocompatibility of the electrospun PCL-collagen nanofibers using fibroblasts*. Biomacromolecules, 2005. 6(5): p. 2583-9.
77. Venugopal, J. and S. Ramakrishna, *Biocompatible nanofiber matrices for the engineering of a dermal substitute for skin regeneration*. Tissue Eng, 2005. 11(5-6): p. 847-54.
78. Venugopal, J.R., Y. Zhang, and S. Ramakrishna, *In vitro culture of human dermal fibroblasts on electrospun polycaprolactone collagen nanofibrous membrane*. Artif Organs, 2006. 30(6): p. 440-6.
79. Liu, S.-J., et al., *Electrospun PLGA/collagen nanofibrous membrane as early-stage wound dressing*. Journal of Membrane Science, 2010. 355(1-2): p. 53-59.
80. Powell, H.M. and S.T. Boyce, *Fiber density of electrospun gelatin scaffolds regulates morphogenesis of dermal-epidermal skin substitutes*. J Biomed Mater Res A, 2008. 84(4): p. 1078-86.
81. Zhang, X., et al., *Biomimetic scaffold design for functional and integrative tendon repair*. J Shoulder Elbow Surg, 2012. 21(2): p. 266-77.
82. Ratner, B.D., et al., eds. *Biomaterials Science: An Introduction to Materials in Medicine*. 2004, Elsevier Academic Press: San Diego, CA.
83. Regis, S., et al., *Fibronectin adsorption on functionalized electrospun polycaprolactone scaffolds: Experimental and molecular dynamics studies*. J Biomed Mater Res A, 2013: p. [e-pub ahead of print].
84. Bush, K.A. and G.D. Pins, *Development of microfabricated dermal epidermal regenerative matrices to evaluate the role of cellular microenvironments on epidermal morphogenesis*. Tissue Eng Part A, 2012. 18(21-22): p. 2343-53.
85. Cornwell, K.G., et al., *Crosslinking of discrete self-assembled collagen threads: Effects on mechanical strength and cell-matrix interactions*. J Biomed Mater Res A, 2007. 80(2): p. 362-71.
86. Cornwell, K.G. and G.D. Pins, *Discrete crosslinked fibrin microthread scaffolds for tissue regeneration*. J Biomed Mater Res A, 2007. 82(1): p. 104-12.
87. Cornwell, K.G., B.R. Downing, and G.D. Pins, *Characterizing fibroblast migration on discrete collagen threads for applications in tissue regeneration*. J Biomed Mater Res A, 2004. 71(1): p. 55-62.

88. Fonder, M.A., et al., *Treating the chronic wound: A practical approach to the care of nonhealing wounds and wound care dressings*. Journal of the American Academy of Dermatology, 2008. 58(2): p. 185-206.
89. Montagna, W., *The Structure and Function of Skin 3E*. 1974: Elsevier Science.
90. Ridge, M.D. and V. Wright, *The Directional Effects of Skin*. The Journal of Investigative Dermatology, 1966. 46(4): p. 341-346.
91. Chandrasekaran, A.R., et al., *Fabrication of a nanofibrous scaffold with improved bioactivity for culture of human dermal fibroblasts for skin regeneration*. Biomed Mater, 2011. 6(1): p. 015001.
92. Li, W.J., et al., *Electrospun nanofibrous structure: a novel scaffold for tissue engineering*. J Biomed Mater Res, 2002. 60(4): p. 613-21.
93. Li, W.J., et al., *Engineering controllable anisotropy in electrospun biodegradable nanofibrous scaffolds for musculoskeletal tissue engineering*. J Biomech, 2007. 40(8): p. 1686-93.
94. Matthews, J.A., et al., *Electrospinning of collagen nanofibers*. Biomacromolecules, 2002. 3(2): p. 232-8.
95. Mauck, R.L., et al., *Engineering on the straight and narrow: the mechanics of nanofibrous assemblies for fiber-reinforced tissue regeneration*. Tissue Eng Part B Rev, 2009. 15(2): p. 171-93.
96. Nerurkar, N.L., et al., *Engineering of fiber-reinforced tissues with anisotropic biodegradable nanofibrous scaffolds*. Conf Proc IEEE Eng Med Biol Soc, 2006. 1: p. 787-90.
97. O'Brien, F.J., et al., *The effect of pore size on permeability and cell attachment in collagen scaffolds for tissue engineering*. Technol Health Care, 2007. 15(1): p. 3-17.
98. O'Brien, F.J., et al., *The effect of pore size on cell adhesion in collagen-GAG scaffolds*. Biomaterials, 2005. 26(4): p. 433-41.
99. Yannas, I.V., *Tissue and Organ Regeneration in Adults*. 2001: Springer.
100. Liu, Y., et al., *Effects of fiber orientation and diameter on the behavior of human dermal fibroblasts on electrospun PMMA scaffolds*. J Biomed Mater Res A, 2009. 90(4): p. 1092-106.
101. Parenteau, N., et al., *Biological and physical factors influencing the successful engraftment of a cultured human skin substitute*. Biotechnol Bioeng, 1996. 52(1): p. 3-14.
102. Medalie, D.A., et al., *Differences in dermal analogs influence subsequent pigmentation, epidermal differentiation, basement membrane, and rete ridge formation of transplanted composite skin grafts*. Transplantation, 1997. 64(3): p. 454-65.
103. Rook, A. and T. Burns, *Rook's Textbook of Dermatology*. 2004: Blackwell Science.

## Appendix A: Mechanical Testing Data Analysis

### Appendix A.1 Mechanical Testing Raw Data

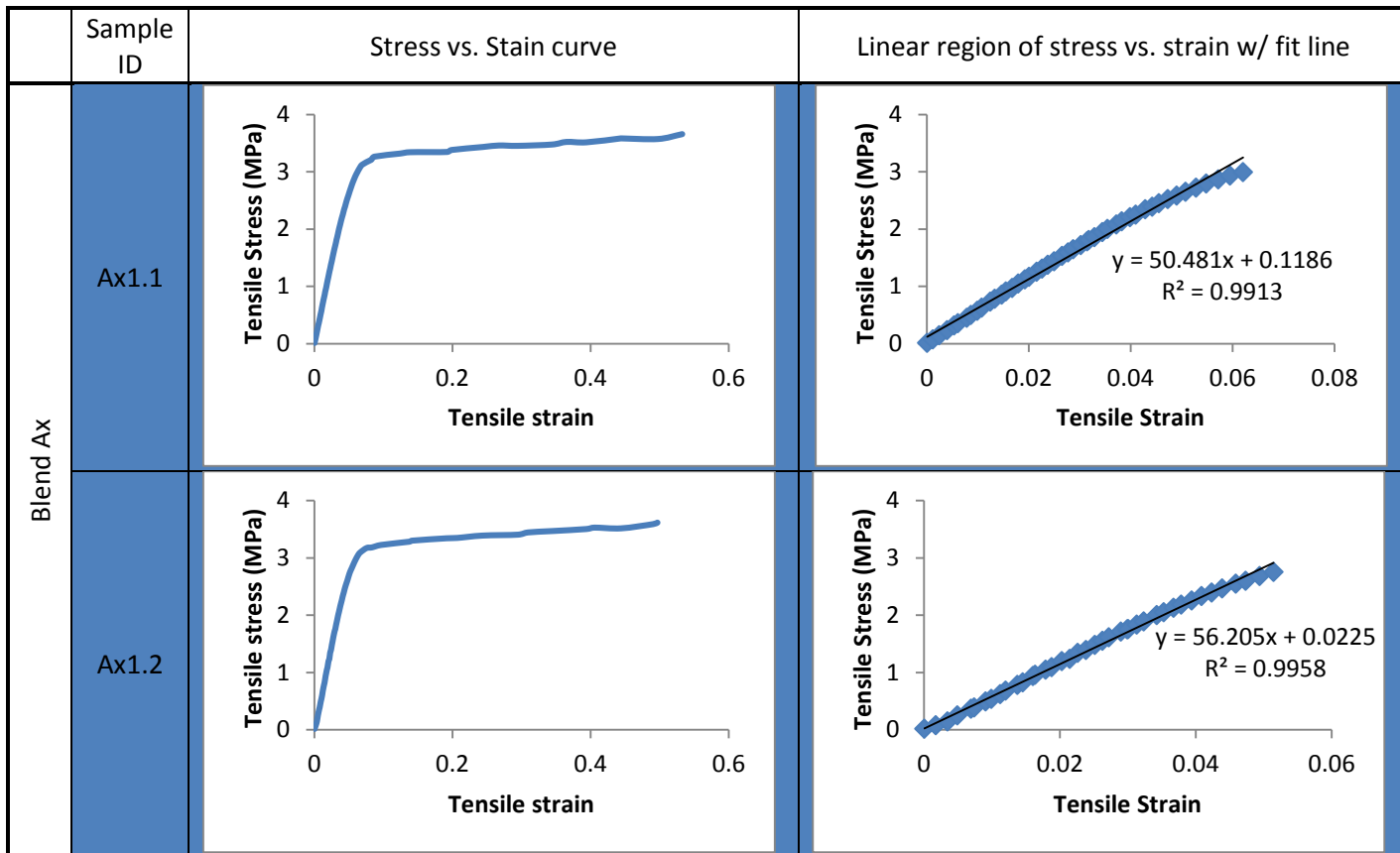
Table 14: Mechanical properties of electrospun scaffolds. Properties of each individual scaffold tested, giving the mean, standard deviation, and SEM for each scaffold blend and direction. Samples highlighted in blue were tested on 2/14/2011, those in red on 9/5/12 (Blend A) and 10/1/12 (Blend B).

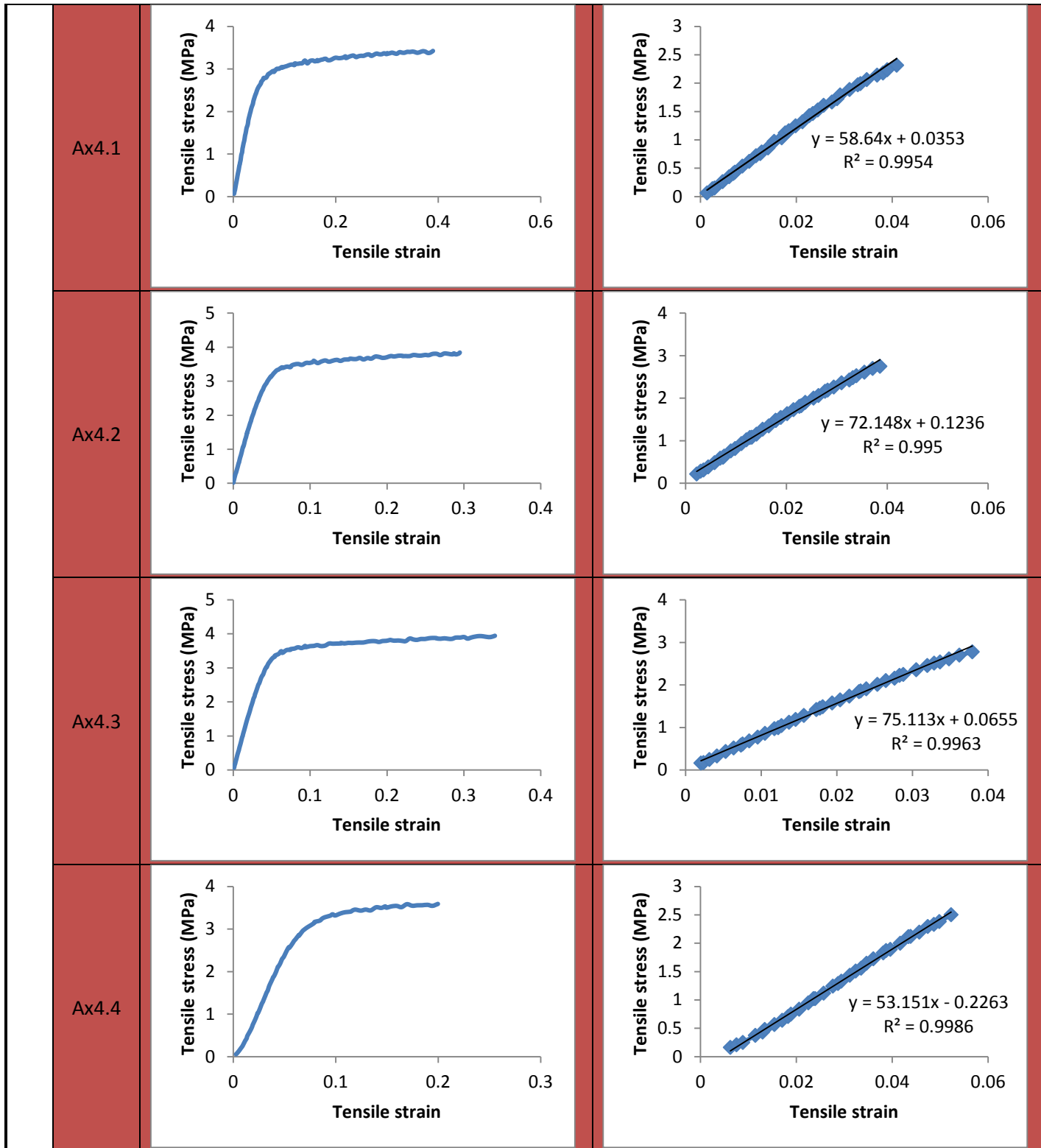
	Sample ID	UTS	S@F	Modulus (calculated)	Extension at failure (mm)	Load at failure (N)	Thickness
Blend Ax	Ax1.1	3.655	0.53256	50.481	5.3256	6.7548	0.462
	Ax1.2	3.615	0.49645	56.205	4.9645	6.3049	0.436
	Ax4.1	3.423	0.38963	58.64	3.8963	4.765	0.348
	Ax4.2	3.842	0.29455	72.148	2.9455	5.4092	0.352
	Ax4.3	3.941	0.34038	75.113	3.4038	5.644	0.358
	Ax4.4	3.593	0.1995	53.151	1.995	4.6704	0.325
	Ax4.5	3.847	0.39044	62.985	3.9044	5.2475	0.341
	Ax4.6	3.876	0.31521	67.874	3.1521	4.8529	0.313
	Ax4.7	3.88	0.22485	69.896	2.2485	5.1992	0.335
	AVG	3.741333	0.35373	62.94367	3.5373	5.427544	0.363333
	STD DEV	0.175101	0.112109	8.807687	1.121086716	0.707598	0.050882
	SEM	0.058367	0.03737	2.935896	0.373695572	0.235866	0.016961
Blend Bx	Bx1.1	3.361	0.77445	49.329	7.7445	4.7597	0.354
	Bx1.2	3.317	0.65306	48.695	6.5306	5.6782	0.428
	Bx4.1	3.342	0.37558	51.939	3.7558	4.5318	0.339
	Bx4.2	3.316	0.30755	52.509	3.0755	4.4574	0.336
	Bx4.3	3.1	0.35314	47.761	3.8585	4.6242	0.373
	Bx4.4	2.938	0.31048	37.905	3.1048	3.6778	0.313
	Bx4.5	2.917	0.33563	57.118	3.3563	3.792	0.325
	Bx4.6	2.893	0.40101	50.588	4.0101	4.0393	0.349
	AVG	3.148	0.438863	49.4805	4.4295125	4.44505	0.352125
	STD DEV	0.208594	0.175527	5.507953	1.736151721	0.636869	0.035667
SEM	0.073749	0.062058	1.947356	0.613822328	0.225167	0.01261	
Blend Ay	Ay1.1	2.708	0.75215	27.064	7.5215	4.5283	0.418
	Ay1.2	2.532	0.7843	25.264	7.843	4.2126	0.416
	Ay4.1	2.999	0.42039	35.141	4.2039	4.7386	0.395
	Ay4.2	3.172	0.45129	36.383	4.5129	4.9237	0.388
	Ay4.3	2.885	0.41545	38.13	4.1545	3.0239	0.262
	Ay4.4	2.876	0.38028	32.724	3.8028	3.7383	0.325
	Ay4.5	2.863	0.37577	35.596	3.7577	4.1576	0.363
	Ay4.6	3.142	0.42545	39.138	4.2545	3.4937	0.278
	Ay4.7	2.905	0.41592	31.545	4.1592	4.2653	0.367
	AVG	2.898	0.491222	33.44278	4.912222222	4.120222	0.356889

	STD DEV	0.198996	0.158889	4.773236	1.588886823	0.608871	0.057045
	SEM	0.066332	0.052963	1.591079	0.529628941	0.202957	0.019015
Blend By	By1.1	3.116	0.72827	33.695	7.2827	5.8836	0.472
	By1.2	2.981	0.70262	32.463	7.0262	5.5321	0.464
	By4.1	2.288	0.40545	22.272	4.0545	3.5504	0.388
	By4.2	2.33	0.45103	23.485	4.5103	3.5046	0.376
	By4.3	2.087	0.4456	18.15	4.456	2.0452	0.245
	By4.4	2.122	0.46592	22.518	4.6592	3.089	0.364
	By4.5	2.102	0.54587	16.89	5.4587	3.2872	0.391
	By4.6	2.139	0.50982	15.695	5.0982	3.2599	0.381
	AVG	2.395625	0.531823	23.146	5.318225	3.769	0.385125
	STD DEV	0.413985	0.121137	6.750408	1.211373154	1.288573	0.069686
	SEM	0.146366	0.042829	2.38663	0.428285086	0.455579	0.024638

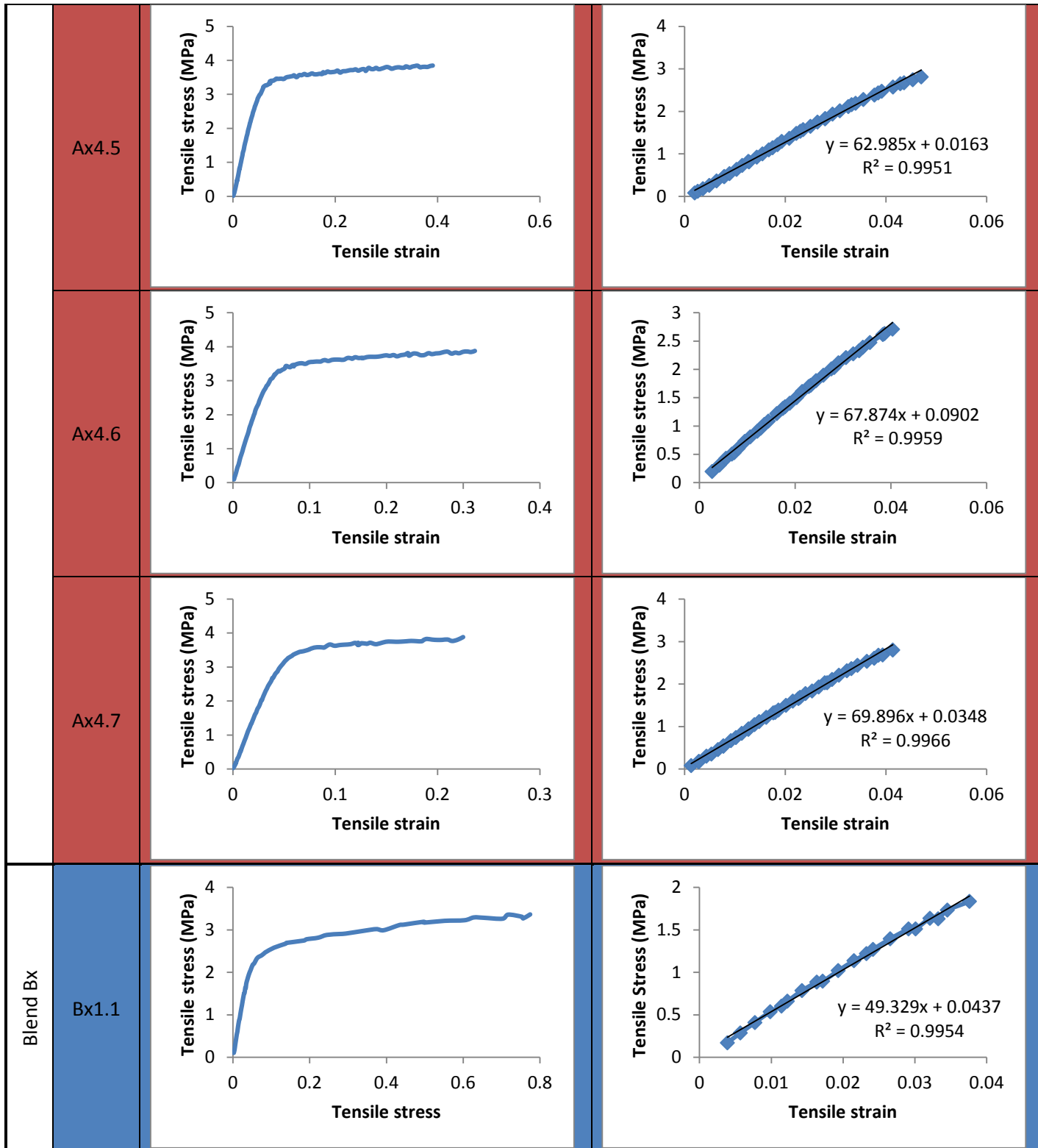
## Appendix A.2: Modulus Calculations

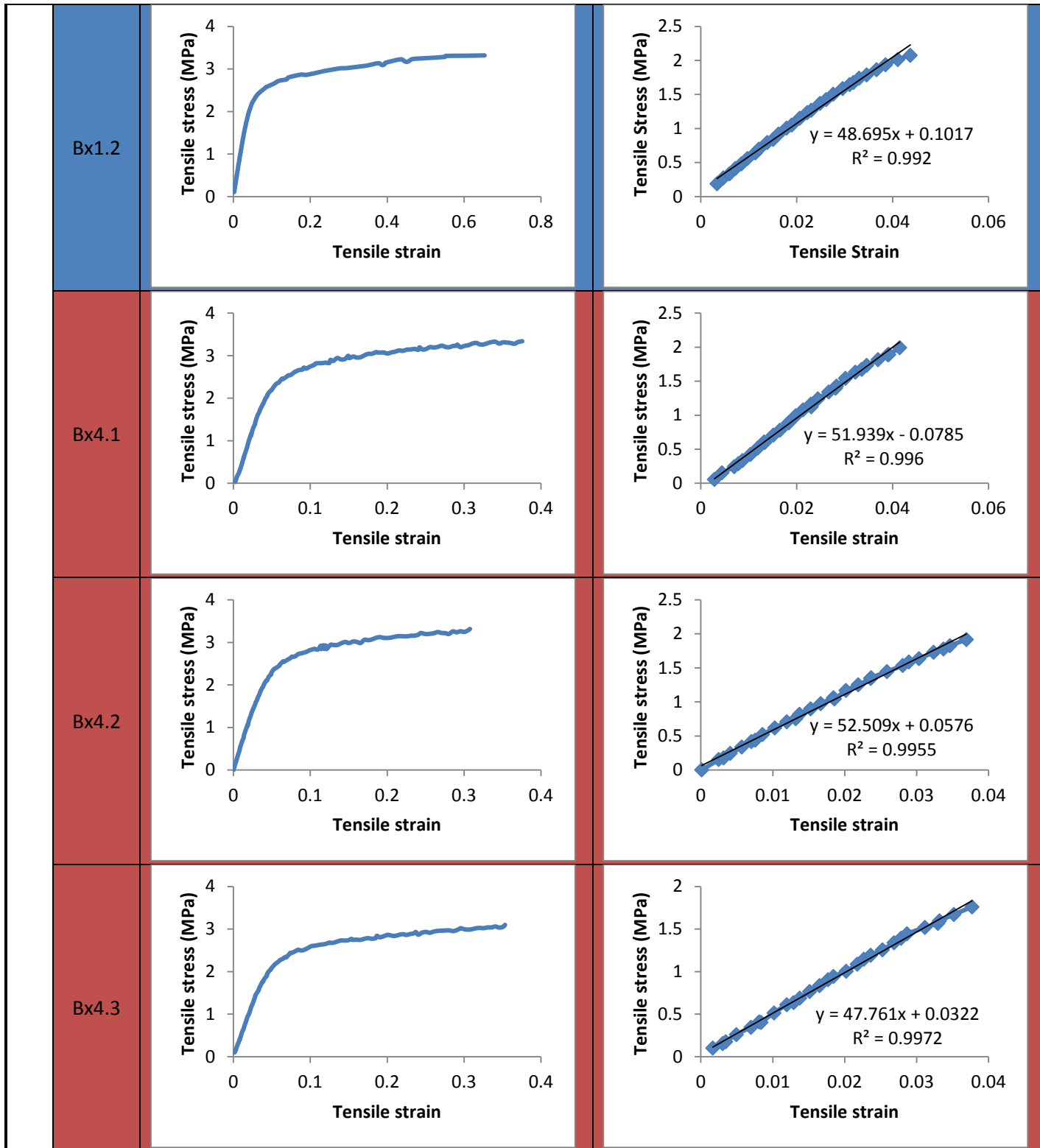
Table 15: Tensile stress vs. strain data for each sample blend and direction. Full tensile stress vs. strain curves to failure are shown in addition to a separate plot of the linear region of each curve from which the tangent elastic modulus was calculated using a linear regression ( $R^2 > 0.99$ ), also shown. Samples highlighted in blue were tested on 2/14/2011, those in red on 9/5/12 (Blend A) and 10/1/12 (Blend B).

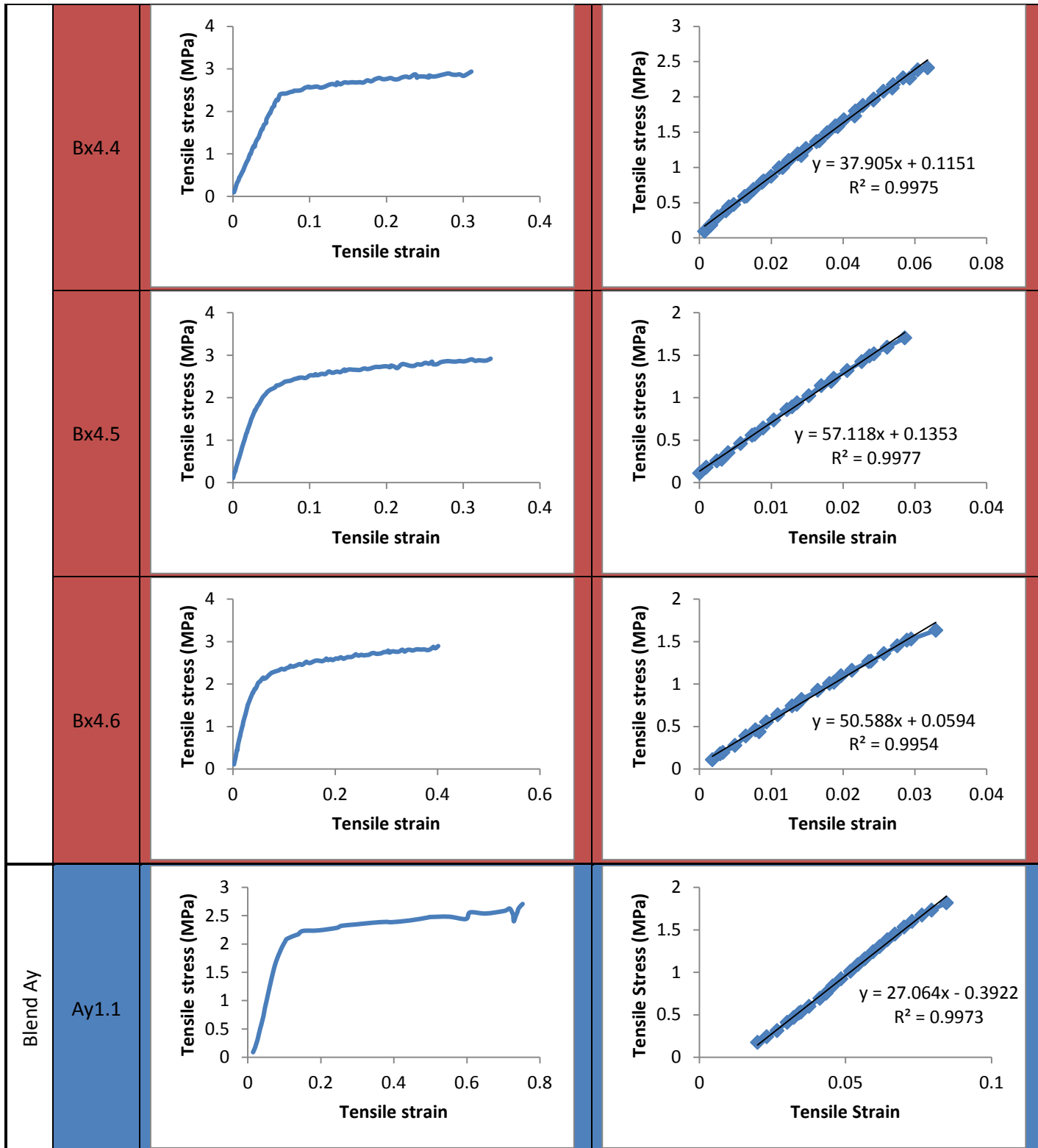


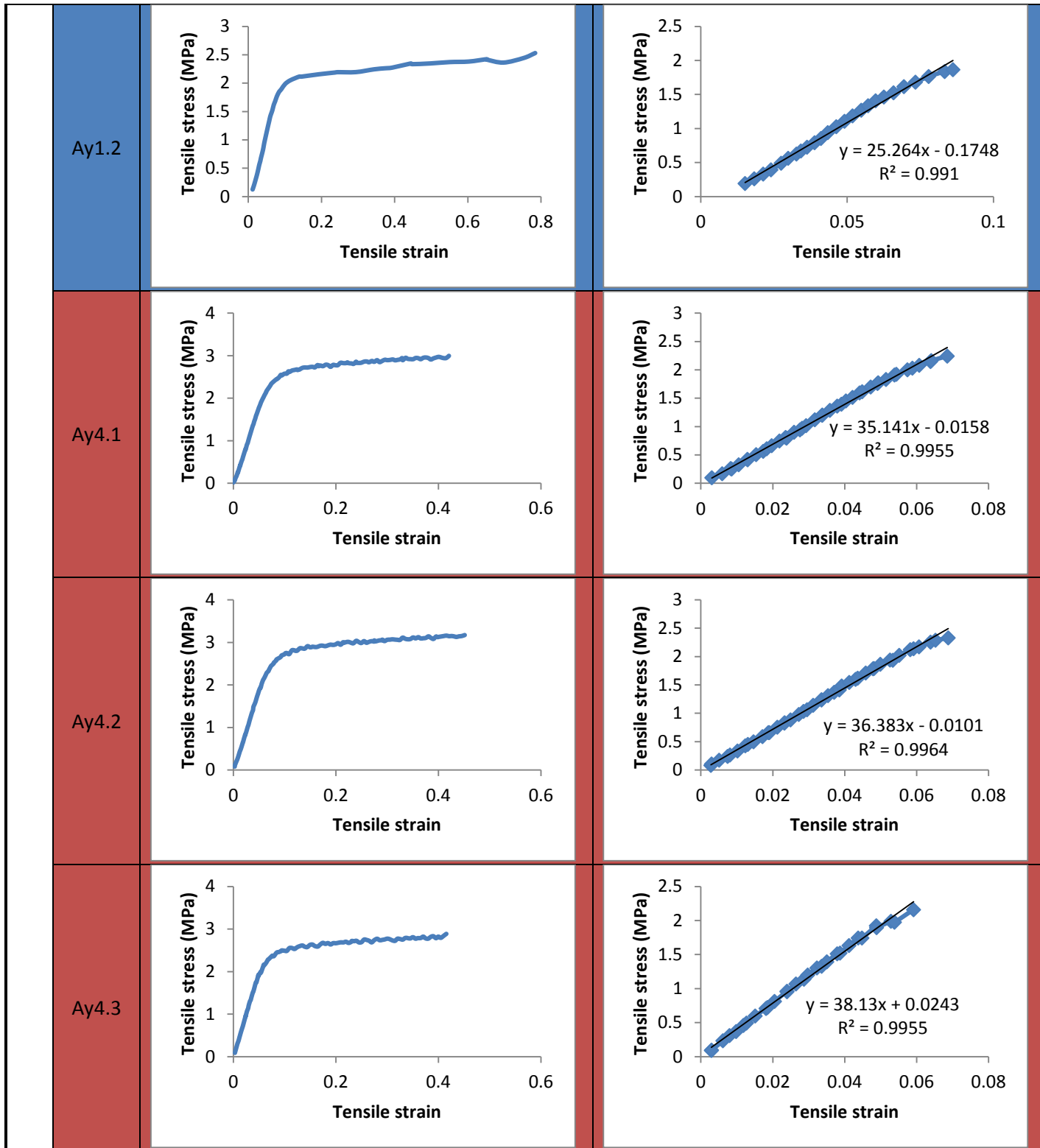


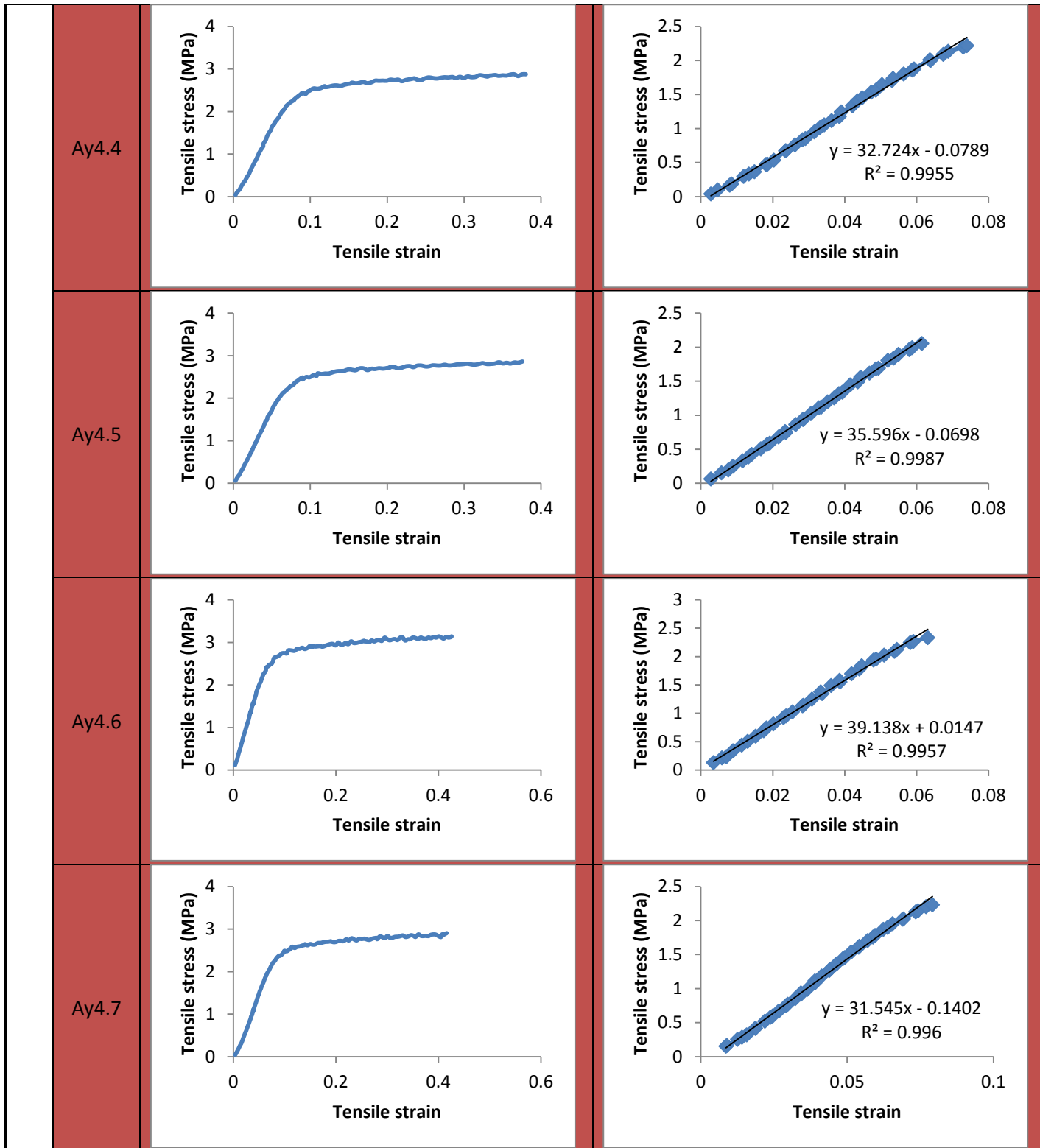


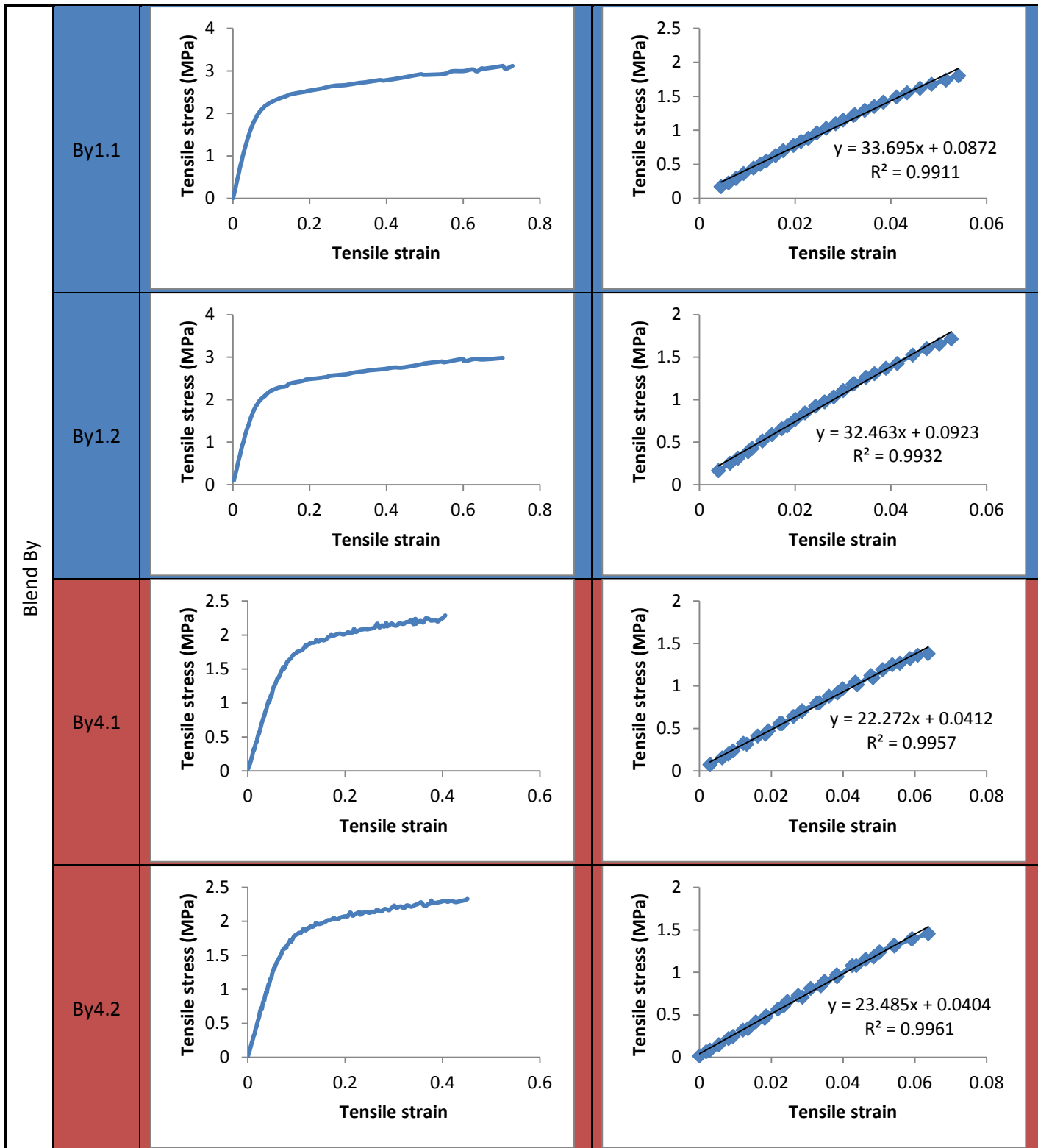


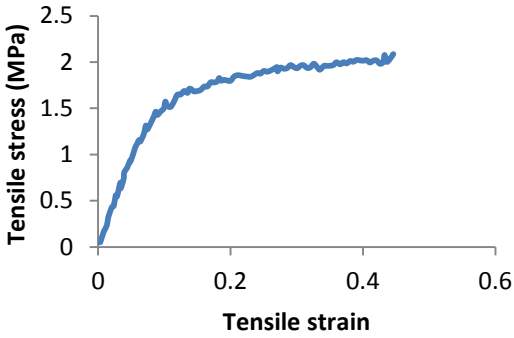
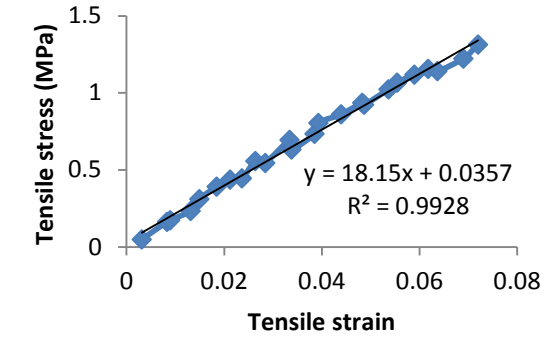
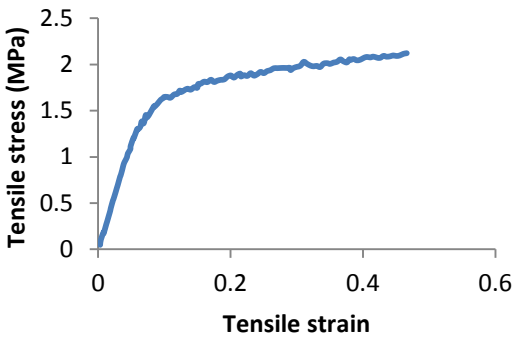
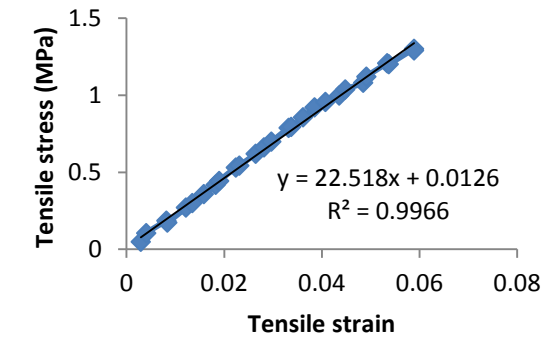
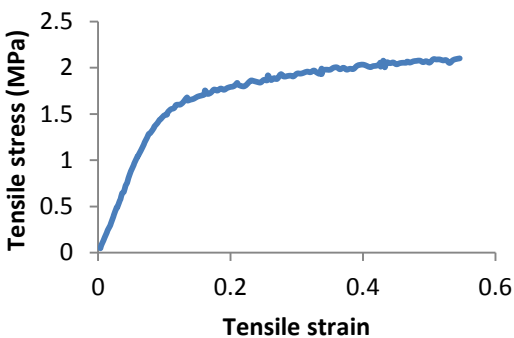
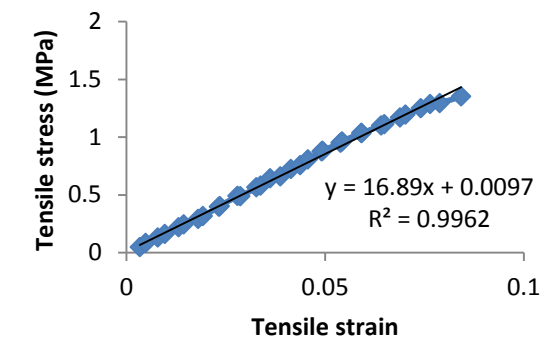
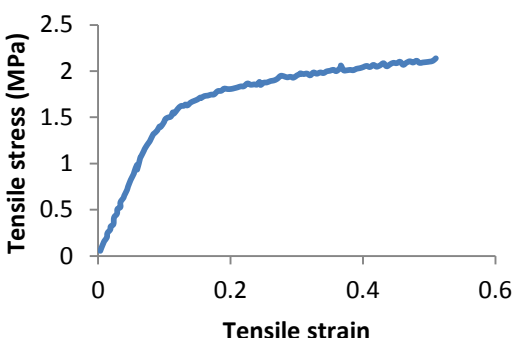
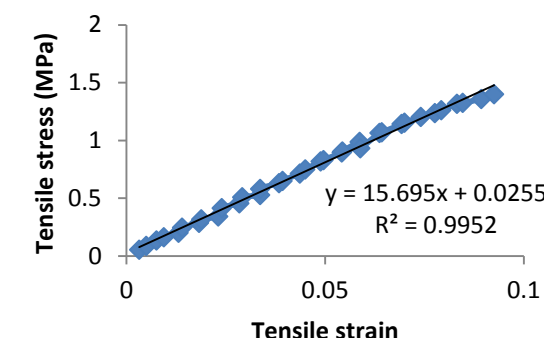










By4.3		 <p><math>y = 18.15x + 0.0357</math> <math>R^2 = 0.9928</math></p>
By4.4		 <p><math>y = 22.518x + 0.0126</math> <math>R^2 = 0.9966</math></p>
By4.5		 <p><math>y = 16.89x + 0.0097</math> <math>R^2 = 0.9962</math></p>
By4.6		 <p><math>y = 15.695x + 0.0255</math> <math>R^2 = 0.9952</math></p>

## Appendix B: Cell Attachment

### Appendix B.1: Standard curve data (7/25/12)

Table 16: Cell attachment measured by MTT. Standard curve data from 7/25/13 including cell seeding concentration, theoretical number of cells read, raw absorbance values, and back calculated cell number.

Seeding Concentration (cells/well)	Theoretical Cell Number (cells read)	Raw Value	Raw Average	Raw Std.Dev.	CV%	Back Calculated Cell Number (cells)
50000	33333	1.807	1.835	0.035	1.9	31910
		1.874				33112
		1.825				32233
25000	16667	1.083	1.060	0.058	5.5	18926
		1.104				19303
		0.994				17330
12500	8333	0.533	0.514	0.025	4.8	9063
		0.522				8865
		0.486				8220
6250	4167	0.227	0.238	0.016	6.7	3575
		0.230				3629
		0.256				4095
3125	2083	0.100	0.108	0.007	6.3	1297
		0.113				1530
		0.110				1477
1563	1042	0.059	0.062	0.005	8.4	562
		0.068				723
		0.059				562
782	521	0.041	0.043	0.002	4.8	239
		0.044				293
		0.045				311
0	0	0.075	0.050	0.023	45.3	849
		0.042				257
		0.032				78



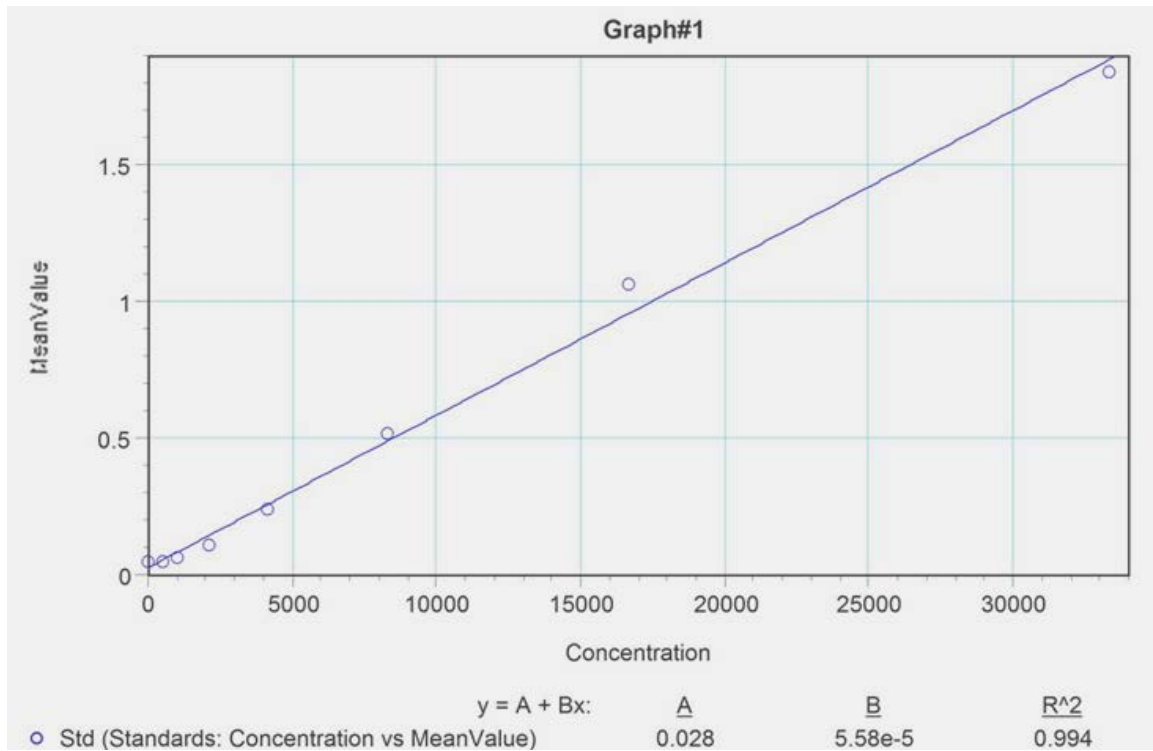


Figure 29: Graph showing linear curve fit used to generate equation (below) to calculate experimental sample cell number from raw absorbance values using a standard curve.

$$cell\ count = (0.028 + 5.58 \times 10^{-5}(x)) \times dilution\ factor$$

Dilution factor for all experimental samples = 5

## Appendix B.2: Standard curve data (7/26/12)

Table 17: Cell viability measured by MTT. Standard curve data from 7/26/13 including cell seeding concentration, theoretical number of cells read, raw absorbance values, and back calculated cell number.

Seeding Concentration (cells/well)	Theoretical Cell Number (cells read)	Raw Value	Raw Average	Raw Std.Dev.	CV%	Back Calculated Cell Number (cells)
50000	33333	1.694	1.813	0.108	6.0	29826
		1.906				33574
		1.838				32372
25000	16667	1.091	1.118	0.036	3.2	19168
		1.159				20370
		1.104				19398
12500	8333	0.436	0.497	0.053	10.6	7591
		0.527				9200
		0.527				9200
6250	4167	0.189	0.198	0.012	6.2	3226
		0.212				3632
		0.193				3296
3125	2083	0.086	0.082	0.003	3.9	1405
		0.080				1299
		0.081				1317
1563	1042	0.031	0.036	0.004	12.1	433
		0.039				575
		0.038				557
782	521	0.025	0.027	0.002	7.4	327
		0.029				398
		0.027				362
0	0	0.022	0.024	0.002	6.5	274
		0.024				309
		0.025				327

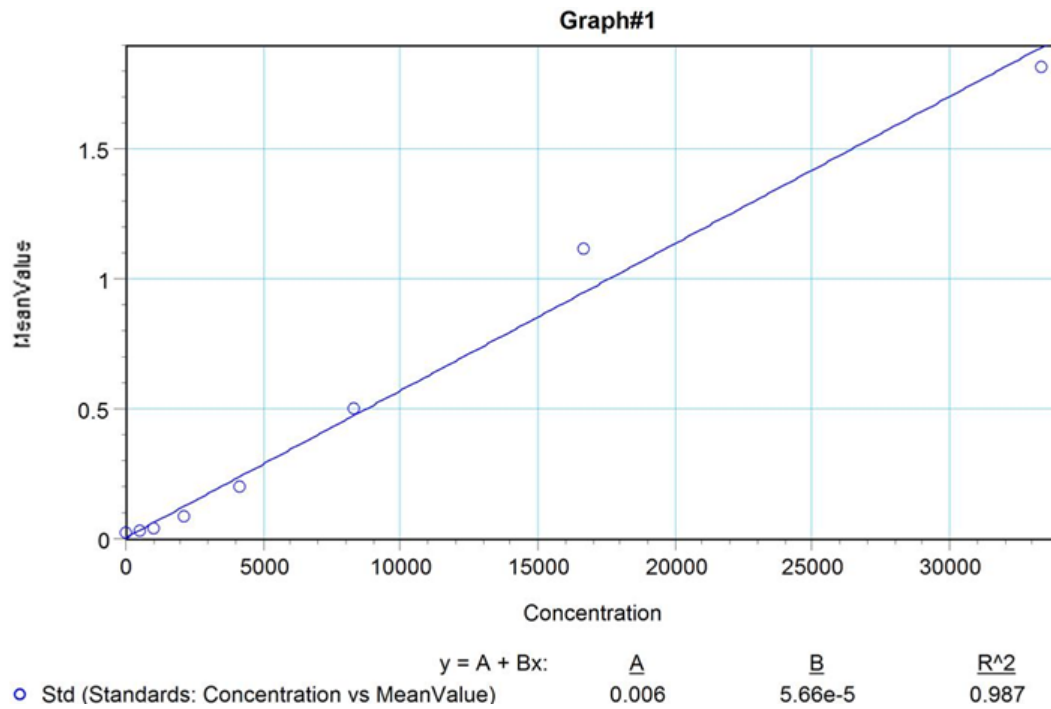


**Figure 30: Graph showing curve linear curve fit used to generate equation (below) to calculate experimental sample cell number from raw absorbance values using a standard curve.**

$$cell\ count = (0.006 + 5.66 \times 10^{-5}(x)) \times dilution\ factor$$

Dilution factor for all experimental samples = 5

### Appendix B.3: Cell Attachment Raw Data

Sample		Raw Absorbance	Calculated Cell Number
Blend A - barrier	7/25/13	0.181	13709.68
		0.13	9139.785
		0.086	5197.133
	7/26/13	0.204	17402.83
		0.155	13074.2
		0.066	5212.014
	Average		<b>10622.61</b>
	Std. Dev.		<b>4948.146</b>
	SEM		<b>2020.072</b>
	Blend A - dermal	7/25/13	0.179
0.179			13530.47
0.281			22670.25
7/26/13		0.196	16696.11
		0.056	4328.622
		0.183	15547.7
Average			<b>14383.94</b>
Std. Dev.			<b>5965.395</b>
SEM			<b>2435.362</b>
Blend B - barrier		7/25/13	0.192
	0.137		9767.025
	0.174		13082.44
	7/26/13	0.157	13250.88
		0.107	8833.922
		0.145	12190.81
	Average		<b>11970.07</b>
	Std. Dev.		<b>2237.968</b>
	SEM		<b>913.6465</b>
	Blend B - dermal	7/25/13	0.213
0.176			13261.65
0.231			18189.96
7/26/13		0.126	10512.37
		0.095	7773.852
		0.076	6095.406
Average			<b>12068.38</b>
Std. Dev.			<b>4811.787</b>
SEM			<b>1964.404</b>

Collagen-GAG sponge control	7/25/13	0.032	358.4229
		0.036	716.8459
		0.035	627.2401
	7/26/13	0.041	3003.534
		0.024	1501.767
		0.028	1855.124
	Average		<b>1343.822</b>
	Std. Dev.		<b>991.8285</b>
	SEM		<b>404.9123</b>
	TCPS control	7/25/13	0.23
0.219			17114.7
0.251			19982.08
7/26/13		0.225	19257.95
		0.212	18109.54
		0.206	17579.51
Average			<b>18357.35</b>
Std. Dev.			<b>1070.281</b>
SEM			<b>436.9406</b>

## Appendix C: Cellular Outgrowth Data

### Appendix C.1: Cellular Outgrowth Raw Data – Blend A

Green indicates sample used as the representative in 5.2.2 In Vitro Analysis of Cellular Outgrowth

		Time (days)	1-A1-1	1-A1-2	1-A1-3	1-A1-4	1-A2-1	1-A2-2	1-A2-3	1-A2-4
Experiment 1 – Blend A	1	257.992 9	278.119 4	265.686 3	311.855 6	973.600 7	151.798 6	464.074 9	46.8912 7	
	2	460.003 6	474.085 6	576.196 1	613.201 4	994.773 6	392.755 8	574.210 3	243.679 1	
	3	661.422 5	1078.51 9	674.014 3	974.618 5	1181.09 1	747.014 3	1457.29 1	618.648 8	
	4	882.019 6	1108.18 9	744.486 6	1027.23 9	1604.27 8	852.629 2	1364.88 6	779.601 6	
	5	992.119 4	1187.22 5	1520.07 1	1066.69 3	2022.18 9	876.780 7	1623.35 3	940.554 4	
	6	1150.14 1	1223.79 3	1644.00 9	1079.46	2052.33 7	913.101 6	1779.48 3	875.032 1	
	7	1437.33 9	1728.39 8	1623.02 9	1318.71 1	2183.86 1	1336.17 3	1843.72	988.449 2	
	8	1695.18 7	1915.12 8	1547.34	1438.51 3	1461.52 4	1482.16 6	1821.74 7	1334.13 9	
	9	1786.69 7	2101.85 7	1936.06 2	1923.56 5	2566.82 4	1628.15 9	1781.88 2	1619.32 8	
	10	1865.89 1	1888.75	1928.86 1	1964.30 7	2571.21	1857.40 1	1929.89 5	1561.82 7	
	11	2005.07 7	2125.21	1956.20 3	2214.06 4	2599.63 1	2204.07 3	2092.70 4	1815.12 1	
	12	2399.74 2	2563.31 9	2407.47 2	2603.20 1	2655.98	2246.85 2	2552.83 4	1935.36	
	13	2963.61	2872.14 4	2749.07	2829.01 1	2899.97 3	2583.96 6	2914.62 6	2272.55 6	
	14	2470.75	2849.08 2	3540.22 5	2905.80 4	2861.80 4	2641.82 9	2974.58 6	2349.41 9	
		Time (days)	2-A1-1	2-A1-2	2-A1-3	2-A1-4	2-A2-1	2-A2-2	2-A2-3	2-A2-4
Experiment 2 – Blend A	1	106.611 4	174.702 3	25.5668 4	276.966 1	64.3939 4	128.452 8	0	149.828 9	
	2	240.878 8	556.253 1	454.672	406.557 9	144.5	270.26	64.3939 4	176.550 8	
	3	529.654 2	673.244 2	686.181 8	659.925 1	224.598 9	412.076 6	251.393 9	276.418 9	
	4	1119.48 8	775.418 9	931.463 5	860.978 6	739.206 8	994.709 4	508.472 4	262.032 1	
	5	1097.31 2	802.299 5	1342.24 6	1422.46	989.666 7	866.574	620.689 8	283.623 9	
	6	1557.70 2	820.9	1611.36 5	2098	1621.03 6	894.984	920.035 7	445.008 9	

	7	1483.75 2	839.59	1692.28 3	2773.71 8	1546.04 6	1498.1	1203.22 1	438.796 8
	8	1173.86 6	797.240 6	1740.93 6	1958.02 3	1683.64 3	1191.06 2	735.426	466.008 9
	9	1321.12 7	1155.12 7	1813.22 1	2802.95 5	1921.24 6	925.689 8	851.342 2	604.656
	10	1455.34 2	1213.91 6	1786.10 3	2930.76 6	1850.46	1251.34 8	1000.22 8	995.012 5
	11	1759.35 8	1482.45 1	1860.99 3	3369.00 2	2119.16 6	1449.28 7	1053.49	1160.73 6
	12	1812.86 6	1562.41 4	2288.92 7	2813.20 3	2380.16 6	1328.02 3	1240.82 5	1198.15 9
	13	2390.66 7	1572.63 8	2321.89 7	3417.99 1	2801.23 5	2104.32 4	1696.94 1	1488.25 5
	14	2000.45 8	1850.27 5		3534.95 7	3075.03 6	2636.41 4	2643.30 5	1540.33 9
	<b>Time (days)</b>	<b>3-A1-1</b>	<b>3-A1-2</b>	<b>3-A1-3</b>	<b>3-A1-4</b>	<b>3-A2-1</b>	<b>3-A2-2</b>	<b>3-A2-3</b>	<b>3-A2-4</b>
Experiment 3 – Blend A	1	0	0	37.8128 3	235.536 5	219.251 3	155.172 9	139.037 4	171.456 3
	2	64.3939 4	345.613 2	80.3921 6	124.035 7	176.795	375.704 1	359.285 2	187.852
	3	294.117 6	363.989 3	360.834 2	208.830 7	326.597 1	476.417 1	722.242 4	240.878 8
	4	658.101 6	588.235 3	634.834 2	433.188 9	369.023 2	556.174 7	684.513 4	438.502 7
	5	1016.04 3	610	637.463 5	866.574	604.490 2	599.789 7	759.527 6	514.064 2
	6	1304.85 7	895.351 2	702.572 2	877.413 5	1214.09 3	701.534 8	818.811 1	797.939 4
	7	1267.50 4	1722.13 2	776.304 8	828.894 8	1199.87 7	1114.15	1176.57 9	1039.41 5
	8	1256.86 6	1440.73 8	866.721 9	914.688 1	1275.60 1	1771.21 6	1406.42 8	948.349 4
	9	1226.01 1	1692.00 4	1048.34 6	1105.80 2	1385.53 3	1582.88 8	2042.78 1	931.033 9
	10	1470.62 7	2117.88 9	1317.63 6	1139.48 8	2048.69 3	1579.07 1	2334.24 6	1807.51 9
	11	1572.92 9	2160.45 5	1886.85 2	1161.03 2	1788.14 4	1776.56	2556.15 7	1190.24 4
	12	1871.93 2	2882.51 2	2618.38 9	1315.92 2	3765.67 4	1841.09 4	2561.49 7	1623.17 8
	13	2114.73 4	3524.32 3	2212.92 9	1428.29 8	2850.28 7	2257.75 6	3046.59	2682.54
	14	2727.28 3	3155.61	3302.87	1923.06 8	3767.09 1	2412.48 1	3062.13 5	3556.76 1

Time (days)	AVERAG E	Std Dev	MAX	MIN	MEDIAN	25 <sup>th</sup> percentile	75 <sup>th</sup> percentile
----------------	-------------	---------	-----	-----	--------	--------------------------------	--------------------------------

Blend A results summary for all experiments	1	193.1171	202.734 6	973.600 7	0	153.485 7	60.01827	259.9162
	2	348.2101	220.495 5	994.773 6	64.3939 4	352.449 2	176.734	463.5241
	3	587.5008	328.806 2	1457.29 1	208.830 7	574.151 5	318.4773	695.197
	4	788.2364	314.708 5	1604.27 8	262.032 1	759.952 8	580.2201	947.275
	5	969.2421	399.498 5	2022.18 9	283.623 9	908.667 6	633.2701	1119.79
	6	1166.623	447.947	2098	445.008 9	999.747 8	861.4991	1571.118
	7	1377.502	491.828 2	2773.71 8	438.796 8	1327.44 2	1095.466	1640.342
	8	1346.773	399.999 5	1958.02 3	466.008 9	1422.47 1	1117.487	1686.529
	9	1573.089	540.533 1	2802.95 5	604.656	1623.74 3	1142.795	1921.826
	10	1744.437	478.236 1	2930.76 6	995.012 5	1828.98 9	1420.916	1938.498
	11	1889.956	524.959 7	3369.00 2	1053.49	1873.92 2	1550.309	2134.021
	12	2186.231	625.823 6	3765.67 4	1198.15 9	2334.54 6	1765.444	2573.29
	13	2499.848	571.751 1	3524.32 3	1428.29 8	2633.25 3	2188.38	2879.102
	14	2773.112	587.415	3767.09 1	1540.33 9	2849.08 2	2441.616	3115.323



## Appendix C.2: Cellular Outgrowth Raw Data – Blend B

Green indicates sample used as the representative in 5.2.2 In Vitro Analysis of Cellular Outgrowth

		Time (days)	1-B-1	1-B-2	1-B-3	1-B-4				
Experiment 1 – Blend B	1	762.957 2	367.201 4	424.303	429.290 6					
	2	778.784 3	443.502 7	451.962 6	446.203 2					
	3	779.534 8	966.873 4	878.554 4	825.247 8					
	4	793.311 9	1032.17 3	652.746 9	894.433 2					
	5	1153.34 6	1470.78 3	1069.15	1539.97 7					
	6	1287.28 3	1476.74	1121.63 1	2273.77					
	7	1543.07 8	2148.65 8	1373.04 1	2312.98 6					
	8	1677.94 5	2527.99 5	1864.93 9	2387.28 5					
	9	1977.38	2846.69 5	1933.57 9	2608.04 8					
	10	2001.14 6	3000.12 8	2114.09 4	2750.79 3					
	11	2327.46 3	2963.09 3	2253.19 1	2638.94 8					
	12	2788.51 5	3023.93 9	2584.59	3184.15 5					
	13	3365.02 3	3110.49 2	3060.11 8	3747.06 8					
	14	3351.22 3	3344.08 6	2954.56 1	3727.33 9					
		Time (days)	2-B1-1	2-B1-2	2-B1-3	2-B1-4	2-B2-1	2-B2-2	2-B2-3	2-B2-4
Experiment 2 – Blend B	1	69.7237 1	326.903 7	112.426	117.768 3	427.941 2	299.465 2	262.522 3	252.755 8	
	2	112.426	347.634 6	510.295 9	294.894 8	964.361 9	284.228 2	338.422 5	176.550 8	
	3	931.725 5	654.593 6	754.181 8	492.094 5	401.069 5	749.522 3	470.982 2	1582.67	
	4	829.721 9	610.212 1	756.736 2	815.802 1	810.032 1	1227.22 3	703.975	1722.33 2	
	5	775.935 8	625.8	777.629 2	1328.96 1	1568.15 9	1215.88 1	1328.02 3	1032.1	
	6	957.352 9	641.798 6	1295.70 8	1461.07 8	1577.86 6	1242.89 8	1289.16 9	1237.25	
	7	1262.44	920.035 7	1427.31 7	1627.72 5	1871.78 1	1465.71 8	1760.17 1	1638.59 9	

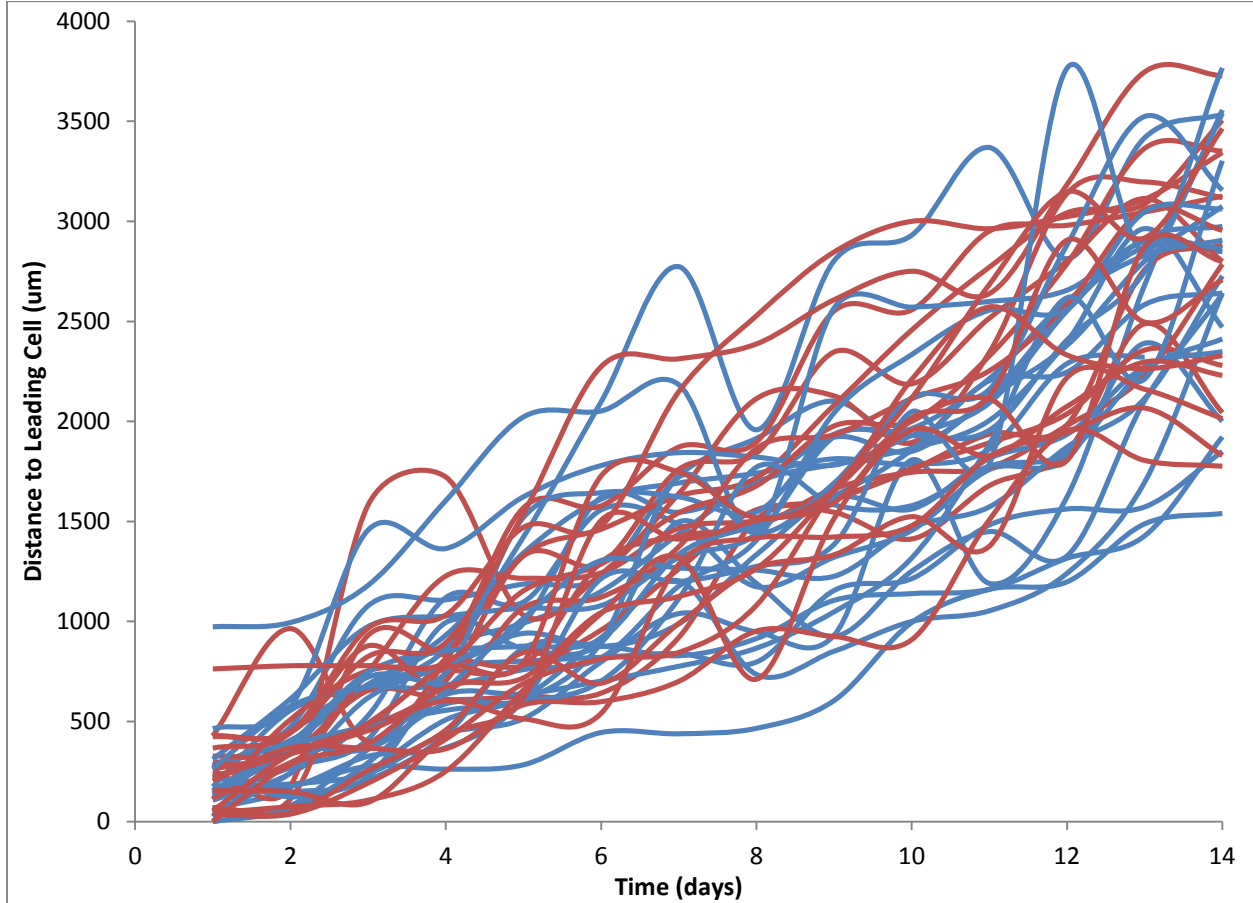
	8	1558.21 6	1509.62 2	1475.82 9	1718.24 2	1896.95 7	1504.04 3	1841.81 6	2113.62 6
	9	1545.68 6	1610.06 1	1663.79 9	2081.20 3	2551.38 7	1609.66 1	2347.02 7	2127.54 2
	10	1412.58 5	1765.68 6	1745.68 4	2456.87 5	2557.35 8	1757.60 2	2187.82	1894.52 8
	11	1679.15 3	1893.53 1	1770.18 4	2771.18	2951.22 6	1936.89 3	2516.37 8	2344.97 3
	12	1847.15 9	2038.00 2	1979.34 6	3042.57 2	2980.11 6	1984.02 1	2802.16 6	3139.33 3
	13	2487.93 6	2356.73 6	2230.26	3087.49 4	3046.40 6	2759.06 4	3114.08 9	3196.83 8
	14	2043.62 7	2279.48 7	2786.16 4	3505.67 7	3126.19 6	2882.57 2	2799.46 5	3118.42 8
	<b>Time (days)</b>	<b>3-B1-1</b>	<b>3-B1-2</b>	<b>3-B1-3</b>	<b>3-B1-4</b>	<b>3-B2-1</b>	<b>3-B2-2</b>	<b>3-B2-3</b>	<b>3-B2-4</b>
Experiment 3 – Blend B	1	204.331 6	42.7807 5	37.4331 6	53.4759 4	224.663 1	69.5187 2	0	154.340 5
	2	368.984	74.8663 1	37.4331 6	337.279 9	339.764 7	42.7807 5	286.632 8	149.732 6
	3	366.389	106.951 9	192.513 4	486.748 7	454.866 3	256.754	390.411 8	96.4046 3
	4	363.793 2	251.393 9	411.903 7	770.071 3	604.301 2	457.085 6	673.903 7	426.534 8
	5	583.279 9	658.101 6	689.861	796.809 3	513.369	845.342 2	718.570 4	619.882 4
	6	598.953 7	1040.13	813.274 5	1727.48	540.768 3	691.164	1044.43 9	1505.22 1
	7	700.861	1321.02 9	845.342 2	1747.28	1285.60 4	989.825 3	1125.14 4	1411.62 2
	8	952.247 8	711.249 6	1080.69	1518.80 2	1417.27 5	1266.55 6	1264.95 2	1504.34 8
	9	925.149 7	1514.51 2	1660.24 4	1658.79 7	1422.47 1	1333.36 4	1652.05 2	1593.91 4
	10	909.107	1957.48 3	2117.10 7	2210.01 2	1479.07 1	1524.07 3	2002.46	2017.92 5
	11	1508.02 1	1828.94 7	2685.03 6	2572.39 2	1823.81 1	1376.36 9	2111.92 7	2126.86 5
	12	1953.64 2	2074.97 1	3147.57	2331.80 4	1945.32 4	2219.25 8	1804.92 2	2906.04 1
	13	1805.00 2	2296.86 5	2917.60 8	2264.07 8	2066.83 6	2160.75 2	2874.81 5	2496.22 6
	14	1776.20 7	2229.97 1	3464.43 3	2329.27 6	1829.15 9	2014.06 2	2799.46 5	2708.43 1

	Time (days)	AVERAG E	Std Dev	MAX	MIN	MEDIAN	25 <sup>th</sup> percentile	75 <sup>th</sup> percentile
Ble	1	231.9901	188.581 8	762.957 2	0	214.497 3	69.67246	336.9782

2	339.3371	231.661	964.361 9	37.4331 6	337.851 2	169.8463	444.1778
3	591.9045	355.369 4	1582.67	96.4046 3	489.421 6	384.4061	790.963
4	740.3843	328.397 6	1722.33 2	251.393 9	730.355 6	567.4973	819.2821
5	965.5479	344.593 2	1568.15 9	513.369	821.075 8	681.9211	1243.916
6	1191.199	427.292 2	2273.77	540.768 3	1240.07 4	921.3333	1464.994
7	1438.913	415.532 5	2312.98 6	700.861	1419.47	1228.116	1665.769
8	1589.632	445.197 7	2527.99 5	711.249 6	1514.21 2	1379.595	1847.597
9	1833.129	475.314 6	2846.69 5	925.149 7	1659.52	1581.857	2092.788
10	1993.077	481.940 1	3000.12 8	909.107	2001.80 3	1754.623	2193.368
11	2203.979	472.844 7	2963.09 3	1376.36 9	2190.02 8	1827.663	2589.031
12	2488.872	512.665 2	3184.15 5	1804.92 2	2458.19 7	1982.852	2991.072
13	2722.185	506.123 2	3747.06 8	1805.00 2	2816.93 9	2288.668	3093.243
14	2753.492	589.426 1	3727.33 9	1776.20 7	2799.46 5	2267.108	3180.668

### Appendix C.3: Individual Outgrowth Traces

Outgrowth traces for each sample are shown below. Traces shown in blue are from Blend A, traces in red are from Blend B.



The slope of each trace was calculated using a linear regression (calculated slope and  $R^2$  values shown below) and a t-test was performed to determine if there was a statistical difference between the average migration rate (slope) for Blend A and for Blend B. The resulting p-value ( $p=0.129298$ ) indicates no significant difference.

Sample	Slope	R <sup>2</sup>	Sample	Slope	R <sup>2</sup>
1-A1-1	189.78	0.9643	1-B-1	213.98	0.9392
1-A1-2	190.36	0.9581	1-B-2	246.6	0.9448
1-A1-3	205.27	0.9149	1-B-3	211.63	0.9722
1-A1-4	193.85	0.9662	1-B-4	263.2	0.9508
1-A2-1	152.33	0.8542	2-B1-1	156.53	0.9008
1-A2-2	190.39	0.9838	2-B1-2	171.67	0.9469
1-A2-3	164.51	0.8898	2-B1-3	170.97	0.9568

